



This is to certify that the thesis entitled

## FLOW DISTRIBUTION OF NON-NEWTONIAN FLUIDS

FROM A MANIFOLD SYSTEM presented by

Walter F. Salas Valerio

has been accepted towards fulfillment of the requirements for

M.S. degree in Agricultural Engineering

Major professor

PLACE IN RETURN BOX to remove this checkout from your record. TO AVOID FINES return on or before date due.

DATE DUE	DATE DUE	DATE DUE
	·	

MSU Is An Affirmative Action/Equal Opportunity Institution

4

# FLOW DISTRIBUTION OF NON-NEWTONIAN FLUIDS FROM A MANIFOLD SYSTEM

BY

Walter F. Salas Valerio

Submitted to

Michigan State University

In partial fulfillment of the requirements

MASTER OF SCIENCE

for the degree of

in

Agricultural Engineering

Department of Agricultural Engineering
1988

#### **ABSTRACT**

# FLOW DISTRIBUTION OF NON-NEWTONIAN FLUIDS FROM A MANIFOLD SYSTEM

by

#### Walter Francisco Salas Valerio

The flow distribution in a manifold system using non-Newtonian fluids was investigated for different flow rates and different orifice and manifold diameters. Gelatinized corn starch solutions (5, 7.5 and 10%, wet basis) were used as test fluids. Power-law behavior was found for all the solutions. A theoretical model was developed based on the mass balance equation at each orifice and the mechanical energy balance equation between any two orifices in the manifold.

Orifice discharge coefficients, determined to be in the range of 0 - 0.5, were found to be a function of the rheological properties of the fluid (consistency coefficient and flow behavior index) and the orifice diameter. A mathematical expression that correlated the orifice discharge coefficient with the generalized Reynolds number was obtained. Using the theoretical model developed and experimental data, a correction factor for the orifice discharge coefficient was determined to account for flow past the orifice in an actual manifold system.

Since the pressure calculated by means of the mechanical energy balance equation was higher than the experimental pressure, it became necessary to include a parameter that accounts for the energy loss due to turbulence at the orifice. Calculated values indicate that

the energy loss coefficients due to turbulence increased significantly for decreasing values of the generalized Reynolds number.

The theoretical model developed for the manifold distribution was used in conjunction with the corrected orifice discharge coefficient and an energy loss coefficient due to turbulence to simulate fluid flow from a manifold under various conditions. The simulation model for the less viscous fluid (5% starch solution) was inaccurate for several reasons: experimental error in the determination of the flow rate and pressure, the effect of the consistency coefficient in the corrected orifice discharge coefficient, and the system complexity due to the large number of interactive variables present. For highly viscous fluids, the simulation was more accurate; therefore, the model was used to develop general design recommendations to obtain uniform manifold flow.

## ACKNOWLEDGMENTS

The author sincerely appreciates the counsel, encouragement and technical support of his major proffessor Dr. James F. Steffe and wishs to thank to Dr. Robert Ofoli and Dr. L. Segerlind, members of the committee, for their helpful suggestions.

Sincerely thanks also to Peruvian Government and Universidad Nacional Nacional Agraria -La Molina (Lima-Peru) for its financial support.

Thanks to all of those friends and fellows who offered their time and expertise.

Finally, thanks for the moral support and encouragement freely given by my wife Elba and my son Julio.

## TABLE OF CONTENTS

	Page
LIST OF TABLES	. viii
LIST OF FIGURES	. ix
NOMENCLATURE	. xiii
1. INTRODUCTION	. 1
2. LITERATURE REVIEW	. 3
2.1 Introduction	
2.2 Fluid Models	
2.3 The Manifold Problem	
2.4 Network System	. 8
3. THEORETICAL DEVELOPMENT	. 11
3.1 Mechanical Energy Balance	. 11
3.2 Energy Losses in the System	. 13
3.2.1 Energy Losses Due to Friction in Straight	
Pipes	13
3.2.1.1 Friction Factor (f)	14
3.2.1.2 Laminar Transition Criteria	15
3.2.2 Energy Losses Due to Turbulence Induced at	
the Orifice ( $h_{\hat{k}}$ )	. 16
3.3 Kinetic Energy Coefficient	. 17
3.4 Application of the Mechanical Energy Balance	
Equation to the Flow in a Manifold	. 18
3.5 Manifold and Orifice Equations	. 21

	3.5.1 Bulk Fluid Velocity in the Pipe	21
	3.5.2 Velocity at the Entrance (U)	23
	3.5.3 Orifice Flow Rate	23
	3.6 Orifice Discharge coefficient and the Orifice	
	Discharge Coefficient Correction Factor	25
4.	MATERIALS AND METHODS	27
	4.1 Experimental Materials	27
	4.2 Determination of the Orifice Discharge	
	Coefficient	28
	4.2.1 Experimental Orifice System and Data	
	Collection	28
	4.2.2 Calculation of the Orifice Discharge	
	Coefficient	31
	4.3 Manifold Distribution System	31
	4.3.1 Experimental Manifold and Data Collection	31
	4.3.2 Calculation of the Energy Loss Coefficient	
	Due to Turbulence at the Orifice	34
	4.3.3 Calculation of Orifice Discharge	
	Coefficient Correction Factor	36
	4.3.4 Comparison of Simulated and Actual Manifold	i
	Performance	39
5.	RESULTS AND DISCUSSION	42
	5.1 Fluid Properties	42
	5.2 Orifice Discharge Coefficient	42
	5.3 Manifold Flow Distribution	50
	5.4 Energy Loss Coefficient Due to Turbulence at the	
	Orifice	59

	5.5 Orifice Discharge Coefficient Correction Factor .	63
	5.6 Comparison of Simulated and Actual Manifold Flow	
	Distribution	68
	5.7 Simulation of the Manifold Flow Distribution	76
	5.8 Strategies for Achieving Uniform Flow	82
6.	SUMMARY AND CONCLUSIONS	84
7.	SUGGESTIONS FOR FUTURE RESEARCH	86
8.	REFERENCES	87
	APPENDICES	90
	Appendix A	91
	Appendix B	96
	Appendix C	108
	Appendix D	118

# List of Tables

<b>Cable</b>		Page
1.	Properties of gelatinized starch solutions	43
2.	Results of the non-linear regression analysis for	
	the orifice discharge coefficient data	49
3.	Results of the linear and non-linear regression	
	analysis for the pressure versus mass flow rate	
	data	60

## LIST OF FIGURES

	Title	Page
1.	Typical manifold system	6
2.	Tube with slit attached, functioning as a	
	distributor	9
3.	Sketch of manifold distribution system with	
	illustration of manifold and orifice flow	
	parameters	12
4.	Mechanical energy balance between two orifices	
	in the manifold	19
5.	Mass balance at a orifice in the manifold	22
6.	Definition sketches of the manifold dead end	
	to illustrate Equations (32) and (34)	24
7.	Experimental equipment used to measure the flow	
	rate in the orifice and obtain the orifice	
	discharge coefficient	29
8.	Experimental equipment used to obtain the	
	manifold flow distribution	33
9.	Procedure to calculate the energy loss coefficient	
	due to turbulence at the orifice	35
10.	Procedure to calculate the orifice discharge	
	coefficient correction factor	37
11.	Procedure to simulate the manifold flow	
	distribution	40
12	Orifice discharge coefficient as a function	

	of the fluid velocity in the orifice for a	
	5% corn starch solution	45
13.	Orifice discharge coefficient as a function	
	of the fluid velocity in the orifice for a	
	7.5% corn starch solution	46
14.	Orifice discharge coefficient as a function	
	of the fluid velocity in the orifice for a	
	10% corn starch solution	47
15.	Orifice discharge coefficient as a function	
	of the generalized Reynolds number	51
16.	Manifold flow distribution for a 5% corn starch	
	solution	52
17.	Manifold flow distribution for a 7.5% corn starch	
	solution	53
18	Manifold flow distribution for a 10% corn starch	
	solution	54
19.	Pressure as a function of the mass flow rate in	
	the orifice for a 5% starch solution	56
20.	Pressure as a function of the mass flow rate in	
	the orifice for a 7.5% starch solution	57
21.	Pressure as a function of the mass flow rate in	
	the orifice for a 10 % starch solution	58
22.	Energy loss coefficient due to turbulence	
	at the orifice as a function of the generalized	
	Reynolds number	62
23.	Corrected orifice discharge coefficient as a	
	function of the fluid velocity in the orifice	
	for a 5 % corn starch solution	64
24	Corrected orifice discharge coefficient as a	

	function of the fluid velocity in the orifice	
	for a 7.5% corn starch solution	65
25.	Corrected orifice discharge coefficient as a	
	function of the fluid velocity in the orifice	
	for a 10% corn starch solution	66
26	Corrected orifice discharge coefficient as a	
	function of the generalized Reynolds number	67
27.	Manifold flow distribution: Simulated versus	
	experimental results for a 5% corn starch	
	solution	69
28.	Manifold flow distribution: Simulated versus	
	experimental results for a 5% corn starch	
	solution	70
29.	Manifold flow distribution: Simulated versus	
	experimental results for a 7.5% corn starch	
	solution	71
30.	Manifold flow distribution: Simulated versus	
	experimental results for a 7.5% corn starch	
	solution	72
31.	Manifold flow distribution: Simulated versus	
	experimental results for a 10% corn starch	
	solution	73
32.	Manifold flow distribution: Simulated versus	
	experimental results for a 10% corn starch	
	solution	74
33.	Simualted manifold flow distribution for	
	different flow rates at the entrance	77
34.	Simualted manifold flow distribution for	
	different orifice diameters in the manifold	78

35.	Simulated manifold flow distribution for	
	different fluid consistency coefficients	79
36.	Simulated manifold flow distribution for	
	different manifold diameters	80

### **NOMENCLATURE**

- A crossectional area of the pipe,  $m^2$
- $A_0$  crossectional area of the orifice,  $m^2$
- B slit width, m
- C orifice discharge coefficient, dimensionless
- C' corrected orifice discharge coefficient, dimensionless
- D pipe diameter, m
- d orifice diameter, m
- E<sub>f</sub> energy losses due to friction, J/kg
- e length of the pipe portion in the manifold, m
- f Fanning friction factor, dimensionless
- g gravitational acceleration, 9.81 m/s<sup>2</sup>
- He Hedstrom number, dimensionless
- $h_{\mathbf{f}}$  energy losses due to friction in the pipe, J/kg
- h, energy losses due to fitting, J/kg
- I total number of orifices
- K fluid consistency coefficient, Pa s<sup>n</sup>
- KE average kinetic energy per unit of mass, J/kg
- k<sub>f</sub> energy loss coefficient due to the turbulence at the orifice, dimensionless
- expansion in the orifice, dimensionless.
- L total pipe length, m

- m number of portions of pipe
- n fluid flow behavior index, dimensionless
- p pressure at any point, Pa
- p = pressure at point "a" defined in Figure 6, Pa
- p<sub>b</sub> atmospheric pressure, Pa
- Q mass flow rate in the pipe, kg/s
- Q mass flow rate at the entrance, kg/s
- Q total mass flow rate, kg/s
- Q<sub>z</sub> = flow rate in z-direction, defined in Figure 2, kg/s
- q = mass flow rate at the orifice, kg/s
- R tube radius, m
- Re generalized Reynolds number, dimensionless
- Re critical generalized Reynolds number, dimensionless
- r radius, m
- u bulk or average velocity at any point in the pipe, m/s
- $\mathbf{u}_1$  bulk or average velocity at first portion of pipe, m/s
- u' local linear velocity in the x-direction at r, m/s
- v fluid velocity in the orifice, m/s
- U fluid velocity at pipe entrance, m/s
- x direction

## Greek Symbols

- α kinetic energy coefficient, dimensionless
- $\psi$  constant defined by Equation (9), dimensionless
- $\psi_c$  constant defined in Equation (17), dimensionless
- correction factor for the orifice discharge coefficient,
   dimensionless
- $\mu$  viscosity coefficient, Pa s
- $\xi_{o}$  plug radius, dimensionless
- $\xi_{\rm oc}$  critical plug radius, dimensionless
- $\rho$  fluid density, kg/m<sup>3</sup>
- $\sigma$  shear stress, Pa
- $\sigma_{\rm o}$  yield stress, Pa
- $\sigma_{-}$  = shear stress at the wall, Pa
- $\pi$  = constant equal to 3.1415...
- $\dot{\gamma}$  shear rate, 1/s

## Subscripts

- a assumed
- c calculated
- i orifice number

#### 1. INTRODUCTION

Pumping systems are used in many food processing operations and, in special cases, they pump a fluid into a manifold (perforated pipe with a closed end). Currently, food industries which works with non-Newtonian fluids flowing in a manifold system cannot predict the flow rate in the outlets (orifices) with accuracy, and this causes problems in process and product quality.

Little work has been done in the area of non-Newtonian manifold flow. Previous studies on manifold flow were performed primarily for application to irrigation (drip irrigation) which uses water, a Newtonian fluid. The study of non-Newtonian manifold flow will make an important contribution to the technological advancement of the food industry.

The overall focus of this study is to develop a theoretical model that can be used for the design of manifold systems for non-Newtonian fluids. To date, analytical expressions to determine flow rate distribution in a manifold system using non-Newtonian fluids are not available. Therefore, the objectives of this study are as follows:

- Develop a theoretical model to calculate the flow distribution in a horizontal, circular cross-sectional manifold system for non-Newtonian, non-time dependent, non-elastic fluids.
- 2. Determine the validity of the theoretical model by using data from an experimental manifold system.
- 3. Develop design strategies to achieve uniform flow distribution through a horizontal, circular cross-sectional

manifold system for non-Newtonian, non-time dependent, non-elastic fluids.

#### 2. LITERATURE REVIEW

#### 2.1 Introduction

In contrast to the concentration of effort on the problem of Newtonian fluid flow (e.g., water in a simple pipe or in network), the problem of non-Newtonian fluids flowing in a manifold system has been almost ignored. Few papers on this subject have been presented and those published deal only with part of the problem. Manifold flow analysis techniques for water systems have been available for many years. The implementation of these techniques by hydraulic engineers have brought improved speed and accuracy to the analysis of irrigation systems (Ramirez-Guzman and Manges, 1971).

This chapter will present a short discussion of fluid models and references on manifold systems found in the literature consulted.

#### 2.2 Fluid Models.

Newtonian Model.

For a Newtonian fluid, the viscosity ( $\mu$ ) is constant. It is convenient to represent the behavior of flowing materials by means of flow curves (shear stress against shear rate), thus the flow curve of a Newtonian fluid is a straight line through the origin, the slope being equal to the viscosity (Whorlow, 1980). The Newtonian fluid model is represented as

$$\sigma = \mu \dot{\gamma} \tag{1}$$

Non-Newtonian Model.

Non-Newtonian fluids are those for which the flow curve (shear stress versus shear rate) is not linear through the origin at a given temperature and pressure (Bird, et al. 1987). A great many empirical or semi-empirical equations have been proposed to represent the flow behavior of materials. The choice of an equation for a particular application is to some extent a matter of preference (Whorlow, 1980).

Non-Newtonian fluids are commonly divided into three broad groups:

- 1. Time-independent fluids are those for which the shear rate at a given point is solely dependent upon the instantaneous shear stress at that point. These materials are sometimes referred to as "non-Newtonian viscous fluids" or alternatively as "purely viscous fluids".
- 2. Time-dependent fluids are those for which the shear rate is a function of both the magnitude and the duration of the shear.
- 3. Viscoelastic fluids are those which show partial elastic recovery upon the removal of a deforming shear stress. Such materials have properties of both fluid materials and elastic solids (Skelland, 1967).

Some of the most common rheological models which have been used in axial laminar flow are the power law, Bingham plastic, and Herschel-Bulkley models.

The power-law model, usually attributed to Ostwald but proposed independently by de Waele and others, is used to represent the behavior of many polymer solutions. The equation for the model can be written as

$$\sigma = K \dot{\gamma}^{n} \tag{2}$$

Many non-Newtonian fluids are not well approximated by either the Bingham plastic or the power-law model. They are, however, well represented by a combination model known as the Herschel-Bulkley model (H-B) written as (Osorio and Steffe, 1984)

$$\sigma = \sigma_0 + K \dot{\gamma}^n \tag{3}$$

## 2.3. The Manifold problem.

A manifold system is a special kind of fluid transport system that is composed of a pump and a manifold as a main pipe (Figure 1). The distribution of flow in a horizontal manifold is determined by the inertia and friction forces (Keller, 1949). The inertia forces correspond to the change in velocity (kinetic energy). The velocity decreases in the direction of the flow as the fluid passes through each outlet (emitter or orifice).

The fluid in the manifold decelerates so it increases in pressure as predicted by the mechanical energy balance. On the other hand, there is a pressure drop along the line of the manifold; gaining pressure for down slopes and losing pressure for up slopes. Thus the relative magnitudes at these forces will determine whether the static pressure at the dead end of the manifold increases or decreases.

Meller (1949) was one of the first to publish a paper on the manifold problem. He took, as an example, a familiar pipe burner for gaseous fuels. Keller stated that there are only two important factors

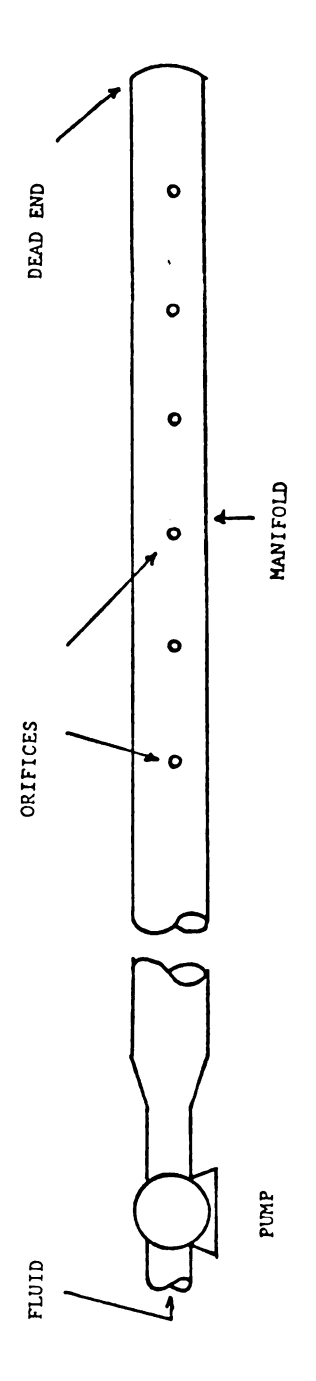


Fig 1. Typical manifold system.

which determine the distribution of the flow in a manifold: (1) inertia and (2) friction. In general, as the fluid flows along the manifold its longitudinal velocity decreases due to part of the fluid volume being discharged laterally through the openings. Therefore, the fluid in the manifold is being decelerated and, in accordance with Bernoulli's equation (mechanical energy balance equation), this tends to increase the fluid pressure. Friction on the other hand, results in loss of pressure along the length. The relative magnitude of the pressure is regained due to deceleration and the pressure loss due to the friction determines whether the pressure rises or falls from the inlet end to the closed or dead end of the manifold (Keller, 1949).

Ramirez-Guzman and Manges (1971) studied uniformity of discharge from equally spaced orifices in a long pipe. In their paper, they assumed the velocity in a pipe diminishes as the flow passes each orifice and, if an infinite number of orifices are considered, the velocity distribution for uniform orifice discharge could be a straight line. To calculate the flow rate at each orifice, Ramirez-Guzman and Manges (1971) applied the mechanical energy equation between the dead end of the pipe and any point along the pipe. The velocity of the fluid in the pipe was calculated using the Hazen-Williams formula, where the friction factor coefficient is kept constant.

Ramirez-Guzman and Manges (1971) used the following relationship to determine the flow in each orifice, assuming the value of the discharge coefficient was unity:

$$q - C A \left[2 \frac{P}{\rho}\right]^{1/2} \tag{4}$$

The results showed that the equation consistently overestimated the orifice discharge at the inlet to the pipeline and underestimated the discharge near the dead end. This indicated that the coefficient of discharge for the orifices varied in magnitude inversely with distance from the dead end. Differences between the calculated discharge and the measured discharge (assuming constant orifice coefficient) did not exceed 6.5% for a 6 in diameter aluminum pipe 60 ft long with 18 orifices.

Bird et al. (1987) reported a distribution design for a power-law fluid consisting of a tube of radius R with a thin slit of width B attached (Figure 2). The researchers assumed that the flow rate in the pipe is function of the distance "x". They applied the power-law result for a circular tube locally to obtain a differential equation for the pressure as a function of the flow rate and the rheological characteristics of the fluid.

## 2.4 Network Systems.

Bralts (1983) developed a theory to find the flow rate and pressure in a drip irrigation network. He applied the linear theory method, based on the continuity and the mechanical energy balance equation (Wood and Charles, 1972), to solve the hydraulic network problem. Under such circumstances, the friction drop is already a linear function of the flow velocity and can be analyzed using the nodal equation and the finite element method. In addition, the finite element method is simple to apply and results in an accurate solution. The major limitation of applying the finite element method in this system is the requirement of laminar flow throughout the hydraulic network (Bralts, 1983).

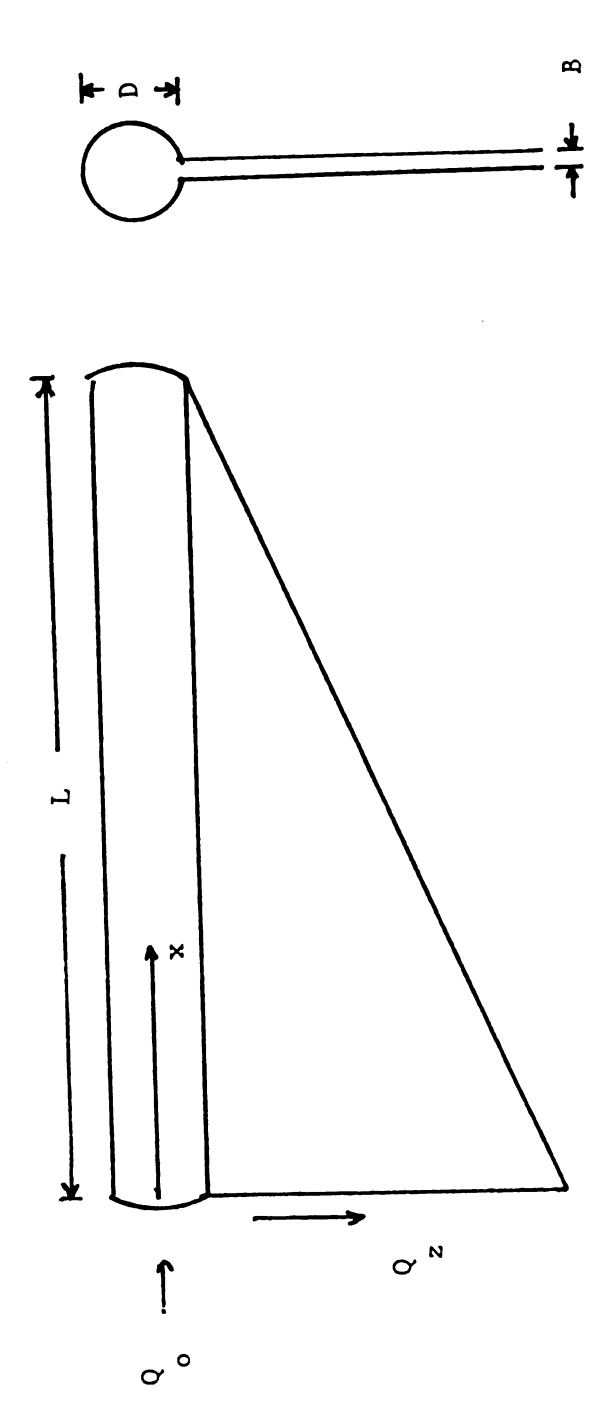


Fig 2. Tube with slit attached, functioning as a distribultor.

Segerlind et al. (1983) derived a solution for a pipe network operating with a non-Newtonian fluid using a network model and matrices components. The matrices can be used in a non-linear finite element program to obtain the junction pressure and the flow rate in the pipe network. The pressure at each node or junction in the pipe network is obtained by solving a system of linear equations in which the nodal pressures are the unknown values. The flow in each element is calculated once the pressure values are known. Since some coefficients must be calculated and the solution process repeated, the iterations are continued until the nodal pressure values do not change (Segerlind et al. 1983).

#### 3. THEORETICAL MODEL

The review of literature has shown that the theory of the flow of a non-Newtonian fluid in a manifold system is limited for several factors. First, the friction factor has never been adequately considered. Secondly, a method has not been proposed which allows one to obtain uniform distribution in the manifold system using a non-Newtonian fluid. Furthermore, none of the analytical methods utilized to date presents a comprehensive design procedure for this type of system.

The method proposed in this work is based on the mechanical energy balance and the mass balance equations. The mechanical energy balance equation is applied between orifices and the mass balance equation applied at the orifices to account for fluid discharge from the system.

## 3.1 Mechanical Energy Balance.

Applying the mechanical energy balance, in the system shown in Figure 3, between orifice number 1 and orifice number 2 gives

$$z_{1}g + \frac{u_{1}^{2}}{\alpha_{1}} + \frac{p_{1}}{\rho} - z_{2}g + \frac{u_{2}^{2}}{\alpha_{1}} + \frac{p_{2}}{\rho} + E_{f}$$
 (5)

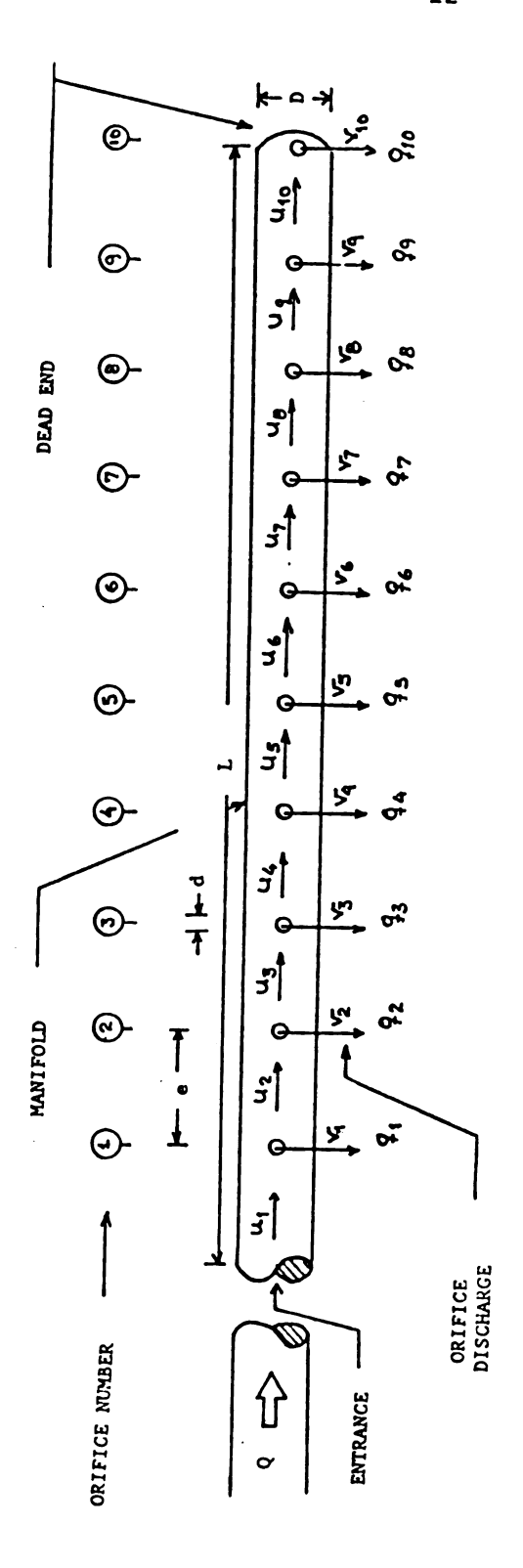


Fig 3. Sketch of manifold distribution system with illustration of manifold and orifice flow parameters.

## 3.2 Energy Losses in the System.

The energy losses in the system are divided into energy losses due to the friction of the fluid in the manifold and energy losses due to fittings. The total energy loss can be written as

$$E_f = h_f + h_k \tag{6}$$

where:

 $h_{\text{f}}$  - energy losses per unit mass due to friction, J/kg.

 $h_k$  - energy losses per unit mass due to valves and fittings in the system, J/kg.

## 3.2.1 Energy Losses Due to Friction in Straight Pipes.

The energy loss due to friction in a straight pipe can be written in terms of the Fanning equation as cited by Govier and Aziz (1972). If the manifold is divided into "m" portions, and each one has a length or space (e), the energy loss due to friction in each one is (Garcia and Steffe, 1986)

$$h_f = \frac{2 f e u^2}{D} \tag{7}$$

If the space between orifices is constant, the value of "e" in the Equation (7) will be the same for all portions of the manifold.

Notice that the velocity changes with respect to the length, so the energy loss will change accordingly.

#### 3.2.1.1 Friction Factor (f).

The friction factor depends on the fluid characteristic as well as the fluid properties. At slow flow, the fluid velocity is parallel to the tube axis and the pattern is smooth. This condition is known as laminar or streamline flow. As the velocity of the flow increases, there is a point where the fluid will swirl in all directions to the line of flow and turbulent conditions exist. The region from the end of laminar to turbulent flow is known as transitional region.

If the flow is laminar, the Fanning friction factor for a non-Newtonian fluid is given by (Garcia and Steffe, 1985)

$$f = \frac{16}{\psi \text{ Re}} \tag{8}$$

where:

Re 
$$-\frac{D^n u^{2-n} \rho}{8^{n-1} K} \left[ \frac{4n}{1+3n} \right]^n$$
 (9)

and

$$\psi = (1+3n)^{n} (1-\xi_{o})^{1+n} \left[ \frac{(1-\xi_{o})^{2}}{1+3n} + 2\xi_{o} \frac{1-\xi_{o}}{1+2n} + \frac{\xi_{o}^{2}}{1+n} \right]^{n}$$
 (10)

where:

$$\xi_{0} = \frac{\sigma_{0}}{\sigma_{W}} = \frac{2\sigma_{0}}{f_{0}u^{2}} \tag{11}$$

The variable  $\xi_0$  can also be written as an implicit function of Reynolds number and the Hedstrom number (He) as shown by Hanks (1978), cited by Garcia and Steffe (1985)

Re - 2 He 
$$\left[\frac{n}{1+3n}\right]^2 \left[\frac{\psi}{\xi_0}\right]^{(2/n)-1}$$
 (12)

where:

He - 
$$D^2 \frac{\rho}{K} \left[ \frac{\sigma_0}{K} \right]^{(2/n)-1}$$
 (13)

#### 3.2.1.2. Laminar Transition Criteria.

To determine if the flow in the manifold has a laminar condition, it is necessary to check the critical generalized Reynolds number for the manifold flow at any section in the pipe. From the use of stability theory developed by Hanks (1969), anks and Ricks (1974) developed a relation for the critical generalized Reynolds number, given by Steffe and Morgan (1986) as

$$Re_{c} = \frac{6464n (2+n)^{\frac{2+n}{1+n}} \psi_{c}^{2n}}{(1+3n)^{2} (1-\xi_{oc})^{(2/n)+1}}$$
(14)

where:  $\xi_{\rm UC}$  is

$$\frac{\xi_{\text{oc}}^{\frac{2}{n-1}}}{(1-\xi_{\text{oc}})^{(2/n)+1}} - \frac{n \text{ He } \left[\frac{1}{2+n}\right]^{\frac{2+n}{1+n}}}{3232}$$
(15)

and

$$\psi_{c} = (1 - \xi_{oc})^{1+n} \left[ (1 - \xi_{oc})^{2} + 2\xi_{oc} (1 - \xi_{oc}) \left( \frac{1+3n}{1+2n} \right) + \xi_{o}^{2} \left( \frac{1+3n}{1+n} \right) \right]$$
(16)

If Re is lower than Re<sub>c</sub>, then the flow is laminar and it can be used Equation (8) is used to calculate the Fanning friction factor in the manifold. Otherwise the relationship for turbulent flow must be used (Garcia and Steffe, 1986).

## 3.2.2. Energy Losses Due to Turbulence Induced at the Orifice $(h_{\scriptscriptstyle L})$

In each orifice there is a loss of energy due to the turbulence induced in the manifold. The energy loss is

$$h_k - k_f \frac{(u_1 - u_2)^2}{2}$$
 (17)

where  $\mathbf{u}_1$  and  $\mathbf{u}_2$  are the fluid velocities in the manifold before and after the orifice and  $\mathbf{k}_f$  is a energy loss coefficient due to turbulence. This term was not found in the reviewed literature and is introduced for the first time in this work. It represents a correction factor needed to fit the experimental values with the simulated values by means of a computational program. It also has a physical meaning because when a fluid is flowing in a manifold, then suddenly has two potential flow directions, a turbulence is induced around the orifice which causes a friction loss which must be taken into consideration. The  $\mathbf{h}_k$  could be interpreted as a loss of energy in a fitting like a tee. When the fluid in question is very viscous and has non-Newtonian behavior this value may be significant. The coefficient  $\mathbf{k}_f$  may be

function of the fluid properties (flow behavior index and consistency coefficient), orifice diameter and the velocity of the fluid in the orifice.

## 3.3 Kinetic Energy Coefficient $(\alpha)$ .

Solving design problems of non-Newtonian fluids flowing in circular tubes requires a knowledge of the energy requirements related to the changes in kinetic energy. An expression for kinetic energy is generally presented as a separate term in the mechanical energy balance equation. The average kinetic energy per unit mass (KE) of any fluid stream moving in a round pipe is (Skelland, 1967)

$$KE - \frac{1}{R^2 u} \int r u'^3 dr \qquad (18)$$

The KE in laminar flow can be expressed in terms of a kinetic energy correction factor as

$$KE - \frac{u^2}{\alpha}$$
 (19)

where  $\alpha$  is the kinetic energy correction factor. For non-Newtonian fluids (Herschel- Bulkley model) in laminar flow, Osorio and Steffe (1984) found  $\alpha$  as

$$\alpha = [(2 (1+3n+2n^2+2n^2\xi_0+2n\xi_0 +2n^2\xi_0^2)^3 (2+3n) (3+5n) 3+4n)]/$$

$$[((1+2n)^2(1+3n)^2) (18+n(105-66\xi_0) + n^2(243+306\xi_0+85\xi_0^2) +$$

$$n^3(279+522\xi_0+350\xi_0^2) + n^4(159+390\xi_0+477\xi_0^2)$$

$$+(n^5 (36+108\xi_0+216\xi_0^2)] (20)$$

# 3.4 Application of the Mechanical Energy Balance Equation to Flow in a Manifold.

Recalling Equation (5) and considering the assumptions made in Figure 3 (no difference in height between points 1 and 2, and equal bulk velocities between two orifices), Equation (6) may be written as

$$\frac{p_2}{\rho} - \frac{p_1}{\rho} - h_f - h_k \tag{21}$$

In this equation,  $h_f$  and  $h_k$  are functions of  $u_1$  and  $u_2$ , where  $u_1$  and  $u_2$  are the bulk average velocities of the fluid in the manifold. Equation (21) permits calculation of the pressure at orifice number 2 in the manifold, so it is possible to determine the mass flow rate in each orifice by this relationship. Equation (21) may be generalized as (Figure 4)

$$p_{i+1} - \rho \left[ \frac{p_i}{\rho} - h_{i+1} - h_{i+1} \right]$$
 (22)

where:

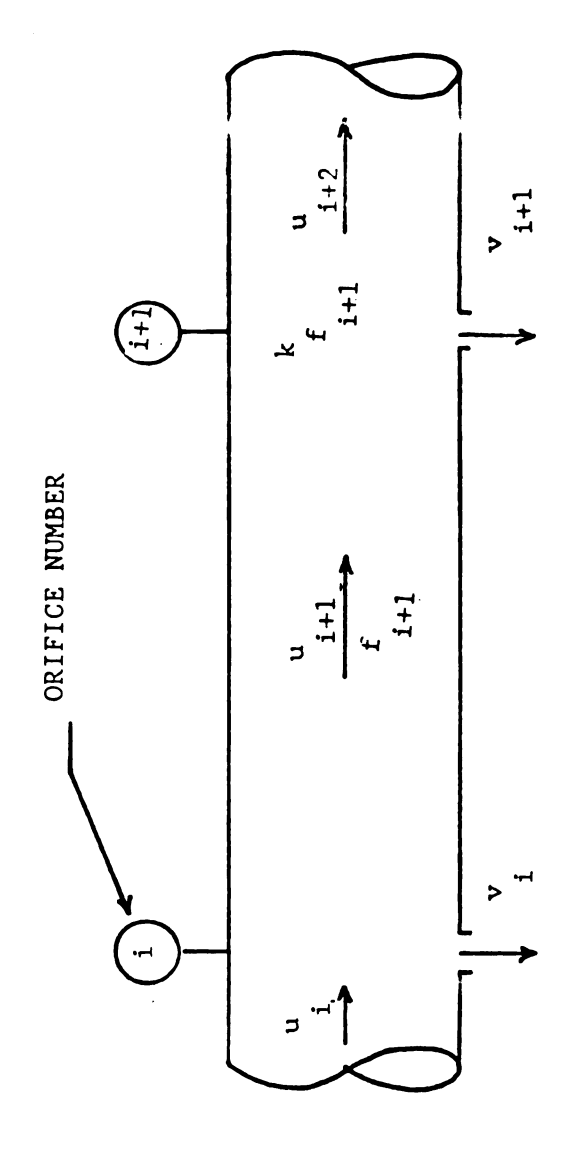


Fig 4. Mechanical energy balance between two orifices in the manifold.

$$h_{f_{i+1}} = \frac{2 f_{i+1} e u_{i+1}^2}{D}$$
 (23)

and

$$h_{k_{i+1}} - k_{f_{i+1}} \frac{(u_{i+1} - u_{i+2})^2}{2}$$
 (24)

A special case is when the mechanical energy balance is applied between the entrance and the first orifice (number 1) in this case the value of i equals zero, which represents the pressure and the velocity at the manifold entrance. Another special case is when the mechanical energy balance is applied in the last orifice where the fluid velocity is zero at the dead end of the system.

Substituting Equations (23) and (24) into Equation (22) gives

$$\frac{p_{i+1}}{\rho} - \frac{p_i}{\rho} - \frac{2 f_{i+1} e u_{i+1}^2}{D} - k_{f_{i+1}} \frac{(u_{i+1} - u_{i+2})^2}{2}$$
 (25)

Equation (25) gives the pressure at any orifice in the manifold as a function of fluid velocity in the manifold preceding the orifice (u), manifold diameter (D), Fanning friction factor, energy loss coefficient due to the turbulence induced by the orifice and the static pressure at the preceding orifice.

# 3.5 Manifold and Orifice Equations.

## 3.5.1 Fluid Bulk Velocity in the Manifold.

The velocity is maximum at the manifold entrance and zero at the dead end. Velocity in the manifold diminishes as the flow passes each orifice. If a uniform orifice distribution exists, then the velocity distribution will be a straight line; however, the form of this relationship for a non-Newtonian fluid is unknown. In this work the velocity distribution will be predicted by applying mass and mechanical energy balances in each orifice. The evaluation will be done using Equation (5) and the following relationship (Figure 5):

$$Q_{i+1} - Q_i - q_i \tag{26}$$

where:

$$q_i - \frac{\rho v_i d^2}{4} \tag{27}$$

or

$$\mathbf{u_{i+1}^- u_i} - \frac{\mathbf{A_o}}{\mathbf{A}} \mathbf{v_i} \tag{28}$$

If the value of i is equal to I (total number of orifices), then  $\mathbf{Q}_{I+1}$  is zero and the value of  $\mathbf{Q}_I$  should be equal to  $\mathbf{q}_I$  this case occurs in the last orifice.

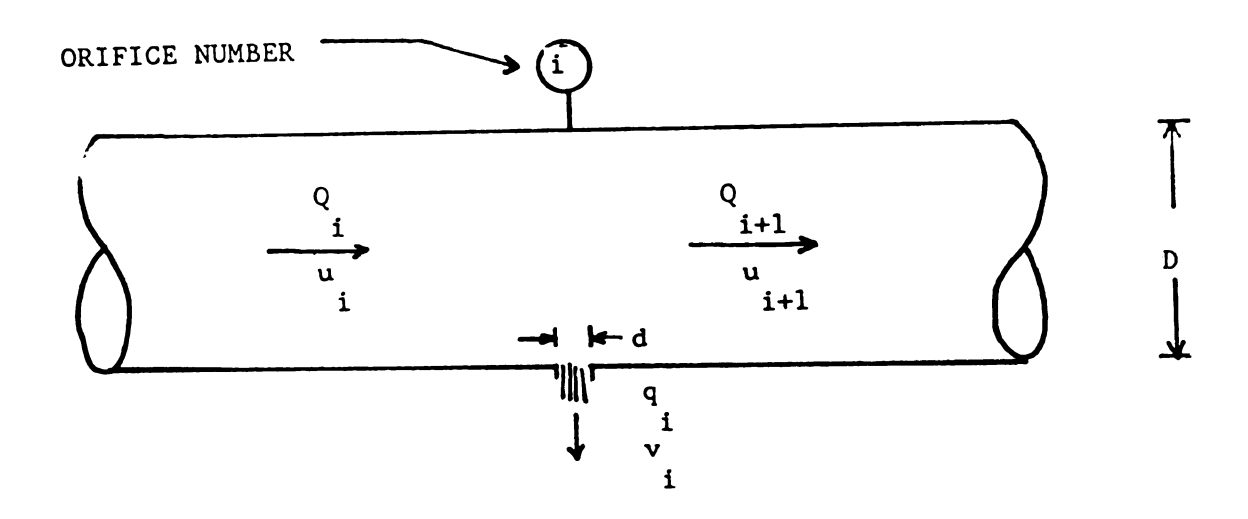


Fig 5. Mass Balance at an orifice in the manifold.

# 3.5.2 Velocity at the Entrance (U).

The average velocity at the entrance of the manifold is given by

$$U = \frac{4 Q_0}{\pi D^2 \rho} \tag{29}$$

#### 3.5.3 Orifice Flow Rate.

Consider a manifold as shown in the Figure 6-A under the conditions existing (single orifice pipe with dead end). Applying the mechanical energy balance between the point "a" and the point "b" gives the following relationship:

$$\frac{p_{a}}{\rho} + \frac{u_{a}^{2}}{\alpha_{a}} + Z_{a}g - \frac{p_{b}}{\rho} + \frac{v_{b}^{2}}{\alpha_{b}} + Z_{b}g + \frac{k_{o}v_{b}^{2}}{2}$$
 (30)

Rearranging terms and assuming that the distance  $\mathbf{Z}_{\mathbf{a}}$  is equal to  $\mathbf{Z}_{\mathbf{b}}$  , gives

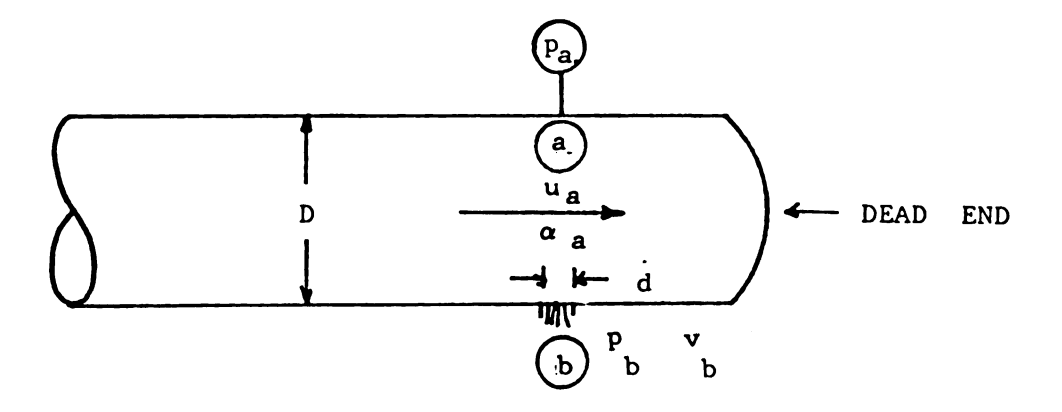
$$v_b^2 = \frac{(p_a/\rho + u_a^2/\alpha_a)}{(k_o/2 g + 1/\alpha_b)}$$
(31)

or

$$q_b = \rho A_o C \left[ \frac{p_a}{\rho} + \frac{u_a^2}{\alpha_a} \right]^{1/2}$$
 (32)

where:

$$c - \left[ \frac{k_o}{2 g} + \frac{1}{\alpha_h} \right]^{-1/2}$$
 (33)



(A)

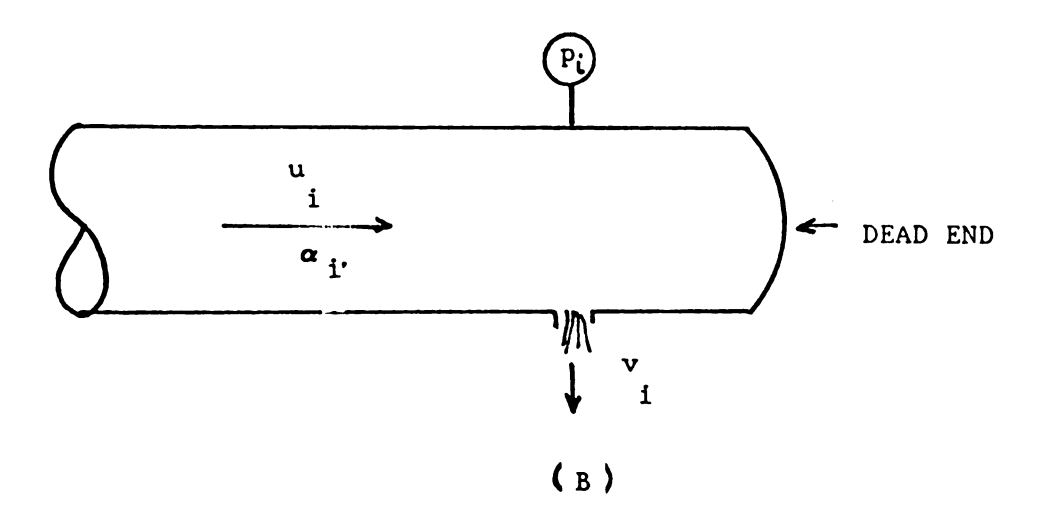


Fig 6. Definition sketches of the manifold dead end to illustrate Equations (32) and (34).

Generalizing this relationship for any orifice in the manifold, we have the following expression (Figure 6-B)

$$q_i = \rho A_o C_i \left[ \frac{P_i}{\rho} + \frac{u_i^2}{\alpha_i} \right]^{1/2}$$
(34)

This expression is for the discharge of a fluid through an orifice, where p<sub>i</sub> is the static pressure at orifice i. Notice that u<sub>i</sub> represents the fluid velocity in manifold section before the orifice. The coefficient of discharge represent the losses resulting from the friction in the orifice. The C values for water vary from 0.96 to 0.98 (Eskinazi, 1962). The discharge coefficient may be function of the fluid properties, velocity, orifice diameter, so on, then it is necessary to experimentally determine exact values.

# 3.6 Orifice Discharge Coefficient and the Orifice Discharge Coefficient Correction Factor.

To obtain the orifice discharge coefficient presented in Equation (34), it is necessary to collect experimental pressure data at different fluid velocities in the orifice. For this purpose, it is necessary to set up a manifold system and have a well defined fluid. The manifold and the orifice cross-sectional areas, length of the manifold, and fluid rheological properties are known. Using the pressure data obtained by experimentation the orifice discharge coefficient for a closed end system is calculated by means of Equation (34).

Since this experiment is not the same as the actual process in the manifold (except for the last orifice) it is necessary to introduce

a correction factor ( $\epsilon$ ) for the orifice discharge coefficient which accounts for energy losses due to the fluid flowing past a discharging orifice. This correction factor will modify the calculated flow rate using the orifice discharge coefficient obtained from Equation (34)

$$q_i - \rho A_0 C_i \left[ \frac{p_i}{\rho} + \frac{u_i^2}{\alpha_i} \right] \epsilon$$
 (35)

or

$$q_{i} - \rho A_{o}C'_{i} \left[ \frac{p_{i}}{\rho} + \frac{u_{i}^{2}}{\alpha_{i}} \right]$$
 (36)

where  $C'_i - C_i$ .  $\epsilon$ 

#### 4. MATERIALS AND METHODS

#### 4.1 Experimental Materials.

A modified waxy maize food starch (National 150: National Starch and Chemical Co., Bridgewater, New Jersey) containing erythorbic acid was used in the experiments. The starch is a white powder containing 11% moisture (wet basis). Tap water (pH = 7.5) was used to prepare aqueous solutions of 5, 7.5 and 10% (wet basis) starch.

A Haake RV-12 concentric cylinder viscometer was used to measure the rheological properties of the starch solution. The inner cylinder, the bob (MVI), was rotating, while the outer cylinder, the cup, was stationary. The height of the bob was 0.020 m and the cup radius was 0.021 m. The torque was measured and transformed into a proportional electrical signal by the measuring drive unit (M150). A Haake PG-12 was connected to the measuring drive unit to manually control the bob speed. Data were acquired using an HP-3497A data acquisition system, which was connected to a HP-85 computer via a 82937a HP-IB interface.

All samples were obtained directly from the orifice or manifold system. Once the product was in the cup, temperature control was established with a temperature vessel (Haake FC-3) built around the cup. Tests were performed at 22 ± 1 °C over a speed range of 10-150 rpm, resulting in a shear rate range of approximately 10 - 250 s<sup>-1</sup>, depending on the product and temperature. Twenty data points were taken in this range for each test. A computer program on the HP-85 calculated shear stress and shear rate values for each test; the Krieger method

(Krieger, 1968) was used to calculate the shear rate. A power-law model was then fitted to obtain the rheogram which gives the consistency coefficient, flow behavior index, correlation index of the regression analysis, and the data standard deviation.

The total solid contents (used to verify starch concentration) were determined with a drying oven at 103 °C for 24 hours. Fluid density was measured using a graduate cylinder and an analytical balance.

In this study, three different fluids with different rheological characteristics were examined. These fluids were prepared by first weighing the correct amount of water into the mixing tank, staring a mixer, and slowly adding starch until the required amount was added. The mixture was heated (68°C) until starch gelatinization was obtained, and the mixture had the appropriate thickness. After this period, the mixer was shut off and the solution was allowed to cool down to room temperature overnight.

# 4.2 Determination of the Orifice Discharge Coefficient.

#### 4.2.1 Experimental Orifice System and Data Collection.

Flow tests were carried out in an experimental manifold system (Figure 7). The experimental manifold system included a Waukesha Model 10 rotary drive with variable speed drive. The displacement of this pump was 0.0133 gal/rev with a pressure range of 0 - 200 psia. Two tanks made out of stainless steel were used. The bigger tank (diameter - 0.8 m and height - 0.7 m) contained the product was equipped with a mixer. The small tank (diameter - 0.7 m and height - 0.7 m) was used to hold water for cleaning purposes. A bypass was constructed, using an

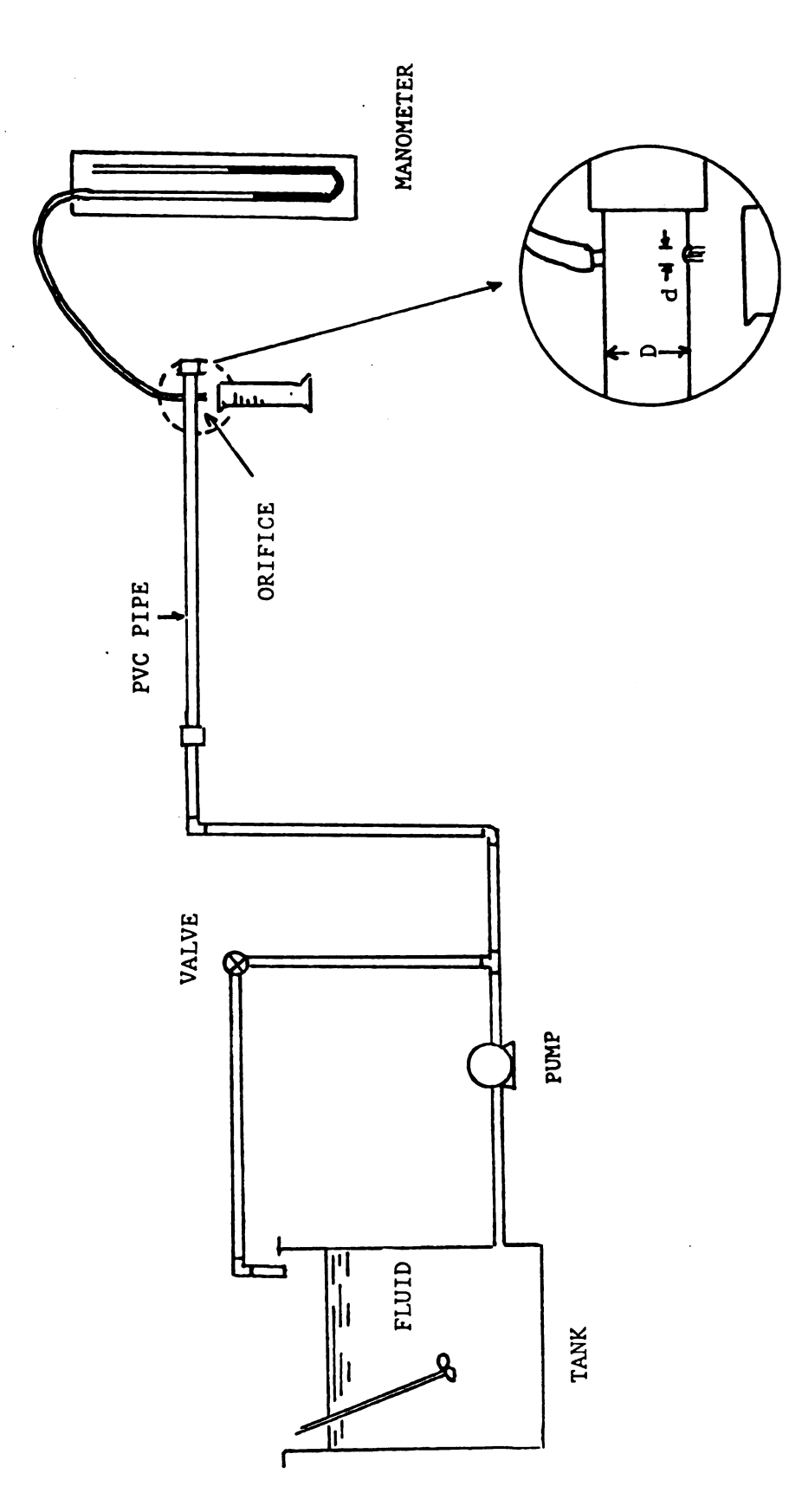


Fig 7. Experimental equipment used to measure the flow rate in the orifice and obtain the orifice discharge coefficient.

air-to-close valve, just after the pump to allow for a lower flow rate. When air was applied, the valve was physically more closed, allowing less fluid through the bypass.

Polyvinyl chloride (PVC) and stainless steel pipes were used to build the system. Threaded PVC pipes, schedule #40 (ASTM D17 85), with an inside diameter 0.0157, 0.0409 and 0.0525 m were used as a main pipe when taking single orifice measurements. The PVC pipe was 0.5 m long and the orifice was at the end of this pipe. Also, a manometer was installed opposite the orifice, on the wall, to measure the pressure at the orifice. Three orifice diameters (0.00318, 0.00476 and 0.07838 m) and different flow rates were used in the experiments. Tests were performed at room temperature (22 ± 1 °C).

According to the literature consulted, the orifice diameter, fluid velocity in the orifice and the fluid consistency coefficient are very important variables in the determination of the orifice discharge coefficient. To study the effect of orifice diameter, and the effect of flow rate on the orifice discharge coefficient, the following steps were performed:

- 1. A power-law fluid was selected and pumped through the experimental system.
- 2. An orifice diameter was selected and the mass flow rate was varied using the variable speed rotary pump.
- 3. The mass or volumetric flow rate in the orifice was measured by collecting and weighing samples after a fixed period of time. The pressure drop was collected by reading the manometer. The readings were in meters of mercury. Samples were taken at this point to measure the fluid rheological properties and fluid density.

Step three was repeated for different orifice flow rates.

#### 4.2.2 Calculation of the Orifice Discharge Coefficient.

The orifice discharge coefficient was calculated from Equation (34), using the data collected: mass flow rate, pressure, density, diameter of the orifice and kinetic energy coefficient. The values of the orifice discharge coefficients were plotted versus mass flow rate. A mathematical expression that fit the data was obtained. This results in the orifice discharge coefficient being a function of the mass flow rate in the orifice when the orifice diameter and the rheological properties of the fluid are kept constant. In this way, three mathematical functions for each orifice diameter and three mathematical functions for each fluid for a total of nine mathematical functions were obtained.

## 4.3 Manifold Distribution System.

## 4.3.1 Experimental Manifold and Data Collection.

Studying the theoretical model, it can be observed that the diameter of the manifold, orifice diameter, flow rate at the entrance and fluid properties are the most important variables in the flow distribution from a manifold system.

The same laboratory pump system (Figure 7) described previously was used to collect manifold data, but a longer PVC pipe with 10 orifices was used as the manifold. A schematic view of the total system is given in Figure 8. The main pipe was threaded and had fittings enabling the changing of manifold pipe diameters. In this part of the experiment, the same three fluids used in experimentation with the single orifice (Section 4.2) were tested. Since the objective was

to determine the response of the flow rate at each orifice in manifold, three orifice diameters (0.00318, 0.00476 and 0.00794 m) and two mass flow rates at the entrance of the manifold were tested.

Tests were performed at  $25 \pm 1$  °C. The PVC manifold pipe was 1 m long, and the space between each orifice was 0.1 m. All orifices were aligned on the manifold, and the wall thickness of the manifold pipe at each orifice was 0.0017 m; hence the effect of the pipe thickness was constant through the experiments. One manometer was installed at the end of the manifold beside the last orifice, and a second manometer was installed at the entrance of the manifold to measure the pressure at the first orifice.

To study the effect of the rheological characteristics of the fluid, orifice diameter and flow rate at the entrance of the manifold on the distribution of flow in the manifold, the following steps were performed:

- Power-law fluid with known rheological characteristics was selected.
- 2. A constant orifice diameter for all orifices in the manifold was selected.
- 3. Different flow rates, at the entrance, were obtained using the bypass valve and variable speed rotary pump.
- 4. The mass or volumetric flow rates were measured by collecting and weighing samples of fluid at each orifice after a fixed period of time. The flow rate at the entrance was kept constant during the collection of the data enabling measurement of the flow rate at each orifice under the same conditions.

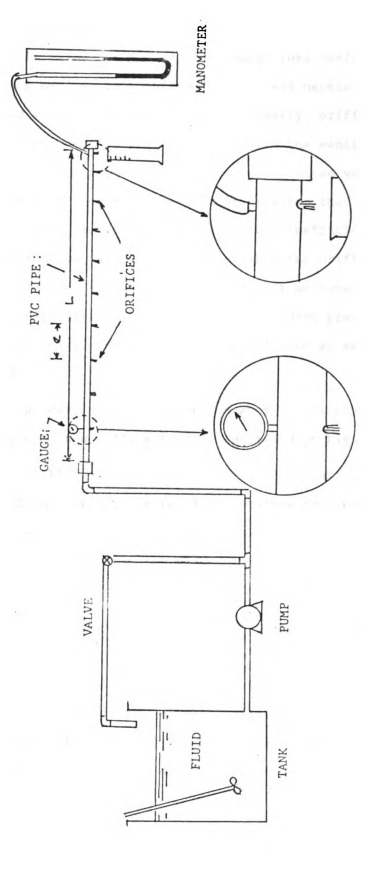


Fig 8. Experimental equipment used to obtain the manifold flow distribution.

# 4.3.2 Calculation of the Energy Loss Coefficient Due to Turbulence at the Orifice.

To calculate the orifice energy loss coefficient due to turbulence defined in Equation (17), it was necessary to use the data collected (mass flow rate, pressure, density, orifice and manifold diameter) to obtain a pressure profile in the manifold.

The experimental pressures were plotted versus mass flow rate in the orifice, and a mathematical expression that fit the data was obtained. This results in the energy loss coefficient being a function of the mass flow rate in the orifice when the orifice diameter and the fluid properties are constant. A different mathematical function for each manifold distribution was obtained. These pressure profiles were used to calculate the energy loss coefficient at each orifice in the manifold.

The procedure to calculate the energy loss coefficient due to the turbulence at the orifice  $(k_{\rm f})$ , illustrated in Figure 9, is

- 1. Fluid properties, manifold characteristics, experimental values of the pressure at the first orifice and the flow rates in the manifold are given.
- 2. Assume that the value of energy loss coefficient at the orifice  $(k_{\mbox{\scriptsize f}})$  is zero.
- 3. Calculate the pressure at orifice two by means of the empirical mathematical function (described above) giving pressure drop at the orifice as a function of mass flow rate and orifice diameter.
- 4. Apply the mechanical energy balance (Equation 25) and the mass balance (Equation 26) between orifice one and orifice two.

  Calculate the energy loss due to turbulence (Equation 17) and friction

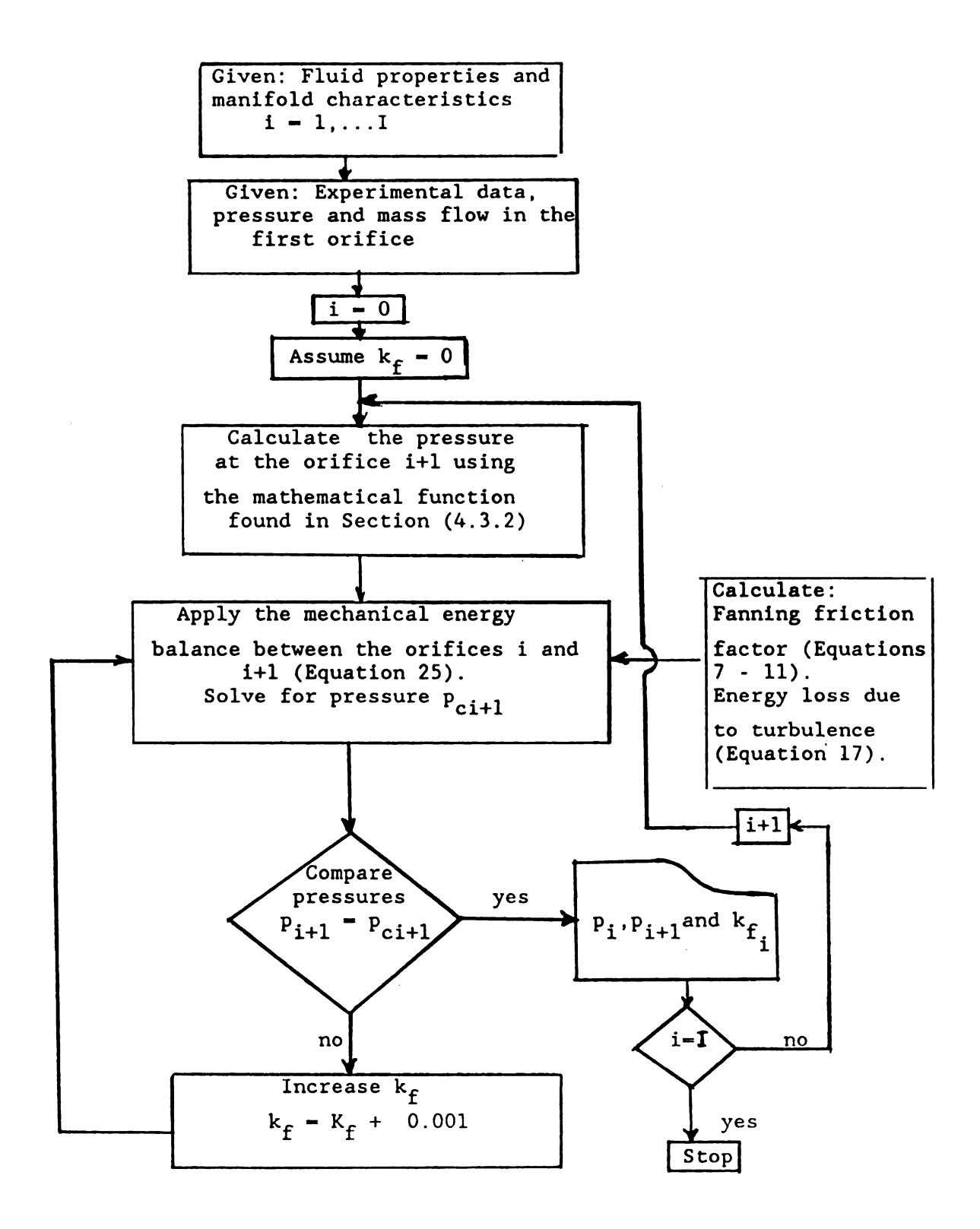


Fig 9. Procedure to estimate the energy loss coefficient due to turbulence at the orifice.

in the straight pipe by means of the Equations (7) - (12). Then solve for pressure at orifice two.

- 5. Compare the pressure calculated in step three with the pressure calculated in step four. If they are not the same increase the value of energy loss coefficient and repeat the steps four through five until both pressures are equal.
  - 6. Repeat steps two to five for the next orifices.
- 8. Assemble the calculated energy loss coefficient and find a relationship between them and the generalized Reynolds number based on the fluid velocity in the manifold.

# 4.3.3 Calculation of the Orifice Discharge Coefficient Correction Factor

Since the orifice discharge coefficient, calculated by means of the function found in Section 4.2.2, does not represent the actual process in the manifold, it is necessary to introduce a correction factor ( $\epsilon$ ) defined by Equation (35). The orifice discharge coefficient correction factor will be evaluated using flow rate data obtained from the manifold system and by the following procedure (illustrated in Figure 10),

- 1. Fluid properties, manifold and orifice physical dimensions, experimental values of pressure at the first orifice and fluid velocity in the manifold orifices are given.
- 2. Assume the value of the orifice discharge coefficient correction factor ( $\epsilon$ ) is 1.
- 3. Calculate the orifice discharge coefficient  $(C_i)$  using the experimental fluid velocity in the first orifice, static pressure at the orifice and the experimental correlation giving the discharge coefficient (calculated from Equation 34) as a function of the fluid

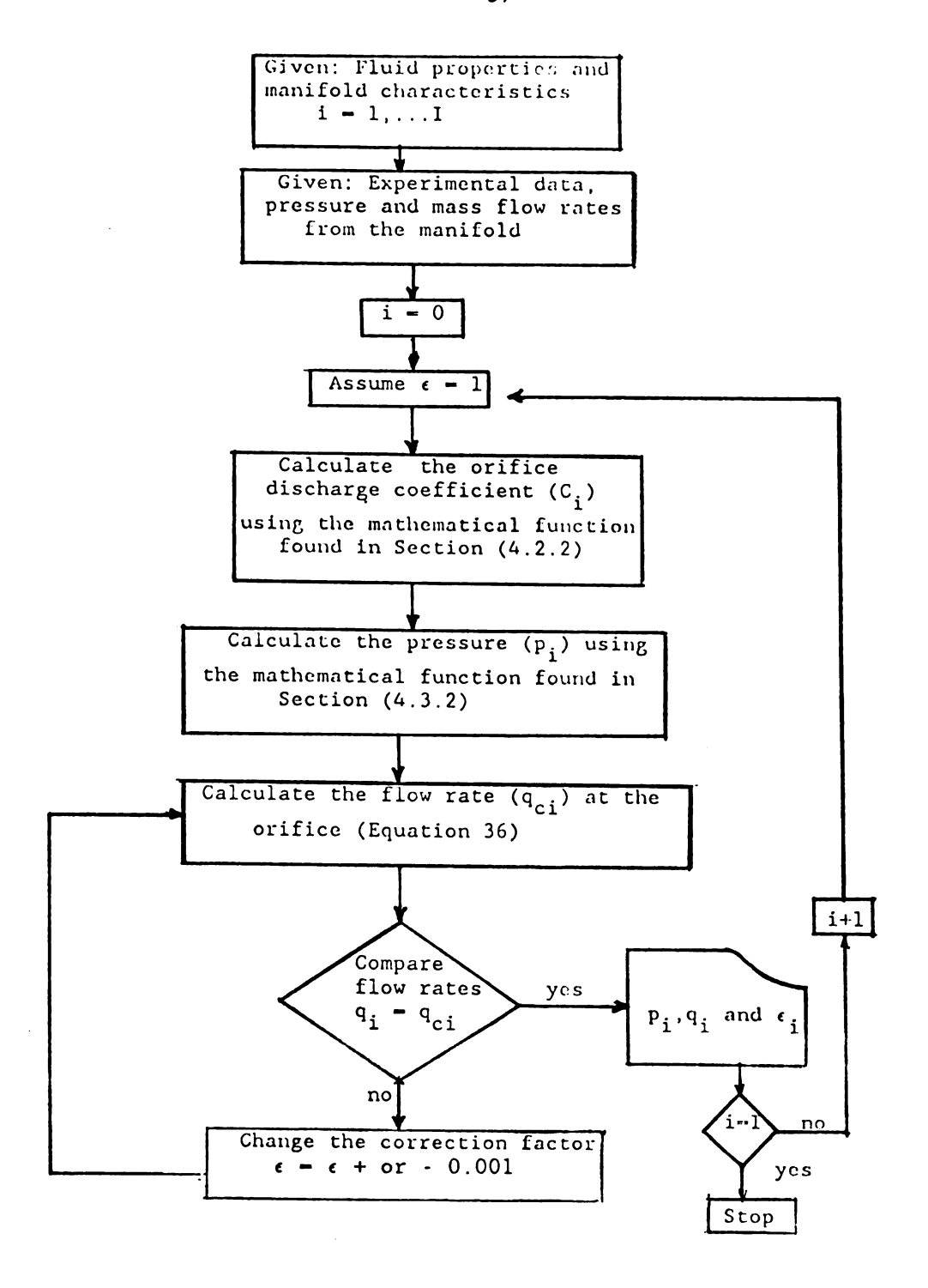


Fig 10. Procedure to estimate the orifice discharge coefficient correction factor.

velocity in the orifice for a closed end system.

- 4. Using the pressure profiles found in 4.3.2, the orifice discharge coefficient found in step three, fluid velocity in the manifold and the  $\alpha$  value using Equation (20), calculate the fluid velocity in the orifice by means of Equation (35).
- 5. Compare the calculated and experimental fluid velocity. If they are not the same, increase or decrease  $\epsilon$  in Equation (35).
- 6. Obtain a correction factor for the orifice discharge coefficient so that calculated and experimental fluid velocity in the orifice are equal.
- 7. Apply the mechanical energy balance equation (Equation 25) and mass balance (Equation 28) between the first and the second orifice. Find the energy loss in the straight manifold pipe by means of Equations (7) (11) and solve for the pressure at the second orifice.
- 8. Calculate the orifice discharge coefficient for the second orifice using the experimental correlation giving the discharge coefficient as a function of the velocity in the orifice for closed end system and the experimental fluid velocity in the orifice using the pressure calculated in step seven.
- 9. Again, compare the experimental fluid velocity with the calculate fluid velocity in the orifice. If they are not the same value, find a correction factor for the orifice discharge coefficient to make these fluid velocities equal.
- 10. Repeat step two to nine for the remaining orifice in the manifold system.

After the calculated correction factors are obtained, find a relationship between the correction factor or the product of the correction factor times the orifice discharge coefficient and the fluid velocity in the orifice.

#### 4.3.4 Comparison of the Simulated and Actual Manifold Performance.

Since the energy loss coefficient due to turbulence (Section 4.3.2), orifice discharge coefficient (Section 4.2.2) and its correction factor (Section 4.2.3) are known, it is possible to simulate the flow distribution in the manifold and compare it to the experimental data. Given fluid properties (consistency coefficient, flow behavior index and density), manifold characteristics (orifice and manifold diameter, total length, space between orifices and number of orifices), the flow rate at entrance and the pressure at the entrance, the flow rate at each orifice may be predicted using the following procedure (Figure 11):

- 1. Given: experimental mass flow rate and pressure at the entrance.
- 2. Apply the mechanical energy balance equation (Equation 25) between the entrance and the first orifice.
- 3. Calculate the fluid velocity in the manifold by means of the mass balance equation and the friction factor for the straight pipe using Equations (7) (11). Calculate the energy loss coefficient due to turbulence at the orifice (Equation 17).
- 4. Using the values found in step three and the mechanical energy balance equation, solve for the pressure at the first orifice in the manifold.
  - 5. Assume a flow rate in the first orifice.
- 6. Calculate the orifice discharge coefficient and its correction factor by means of the results found in Section 4.3.3
- 7. Using the calculated pressure in step four and the orifice discharge coefficient in step six find the fluid flow rate in the first orifice.

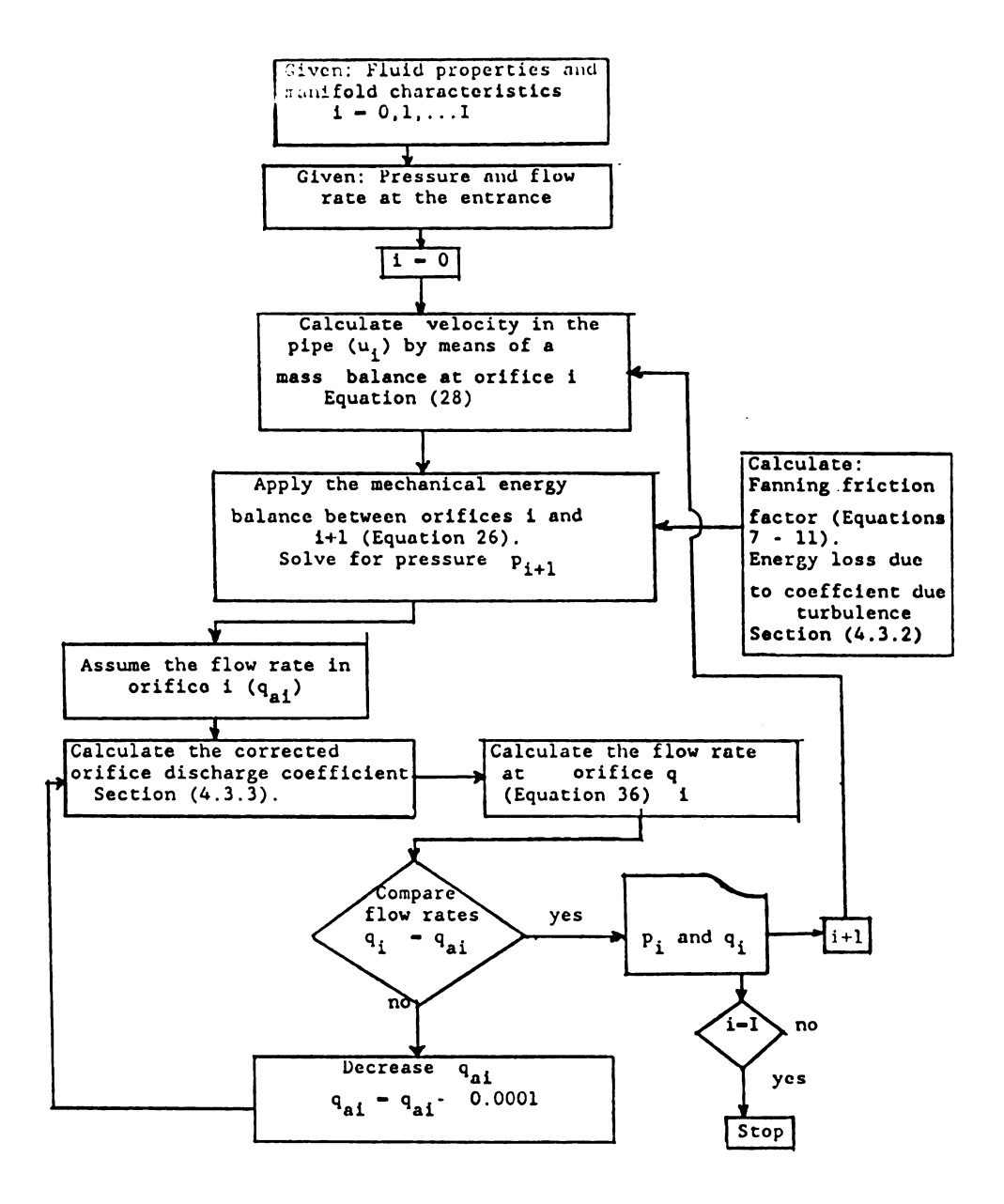


Fig 11. Procedure to simulate the manifold flow distribution.

- 8. Compare the assumed with the calculated fluid flow rate. If they are not equal assume another flow rate and repeat steps five to eight.
- 9. Apply the mass balance equation at the first orifice and the mechanical energy balance equation (Equation 25) between the first and the second orifice, and repeat the calculations in step three.
- 10. Solve the mechanical energy balance equation for the pressure in the second orifice.
- 11. Calculate the orifice discharge coefficient and its correction factor based on the pressure at the orifice calculated in step ten.
- 12. Calculate the fluid velocity in the second orifice (Equation 35).
- 13. Repeat steps five to eight until all the orifice fluid velocities in the manifold are obtained.

To perform this procedure, it was necessary to write a computer program with an iterative capacity so that the friction factor could be obtained for different conditions. The subroutine which calculates the friction factor is based on the computer program called "Friction" developed by Garcia (1985).

#### 5. RESULTS AND DISCUSSION

#### 5.1 Fluid Properties.

The properties of the gelatinized corn starch solutions used in the experiment are summarized in Table 1. The total solid content, density, and consistency coefficient decrease as the starch concentration decreases, but the flow behavior index increases. Similar results were reported by Steffe and Ford (1985) using hydroxypropyl methylcellulose at different concentrations. It was found that all fluids followed the power-law model over the shear rate range tested (20-250 s<sup>-1</sup>). In addition, rheological data collected showed no time-dependent behavior or the presence of a yield stress in the material.

## 5.2 Orifice Discharge Coefficient.

Orifice discharge coefficients were calculated using the appropriate fluid properties (Table 1), the fluid flow rate, and the pressure at the orifice recorded during the experiment. Orifice discharge coefficients were calculated using the fluid properties, the pressure at the orifice and the fluid flow rate recorded during the experiment. Tables Al to A3 of Appendix A present the experimental pressures and the mass flow rates in the orifice for different fluids, along with the calculated C values and generalized Reynolds numbers. In this case, the generalized Reynolds number is defined for the fluid flowing through the orifice based on the orifice diameter and the fluid velocity in the orifice

Table 1. Properties of gelatinized starch solutions.

Solid		Consistency	Flow Behavior
Content	Density	Coefficient	Index
8	kg/m <sup>3</sup>	Pa s <sup>n</sup>	dimensionless
wet basis			
5.0	1010	0.105	0.80
7.5	1021	1.300	0.77
10.0	1034	4.500	0.68

$$Re_{o} = \frac{d^{n} \rho v^{2-n}}{g^{1-n} \kappa} \left[ \frac{4n}{1+3n} \right]^{n}$$
 (37)

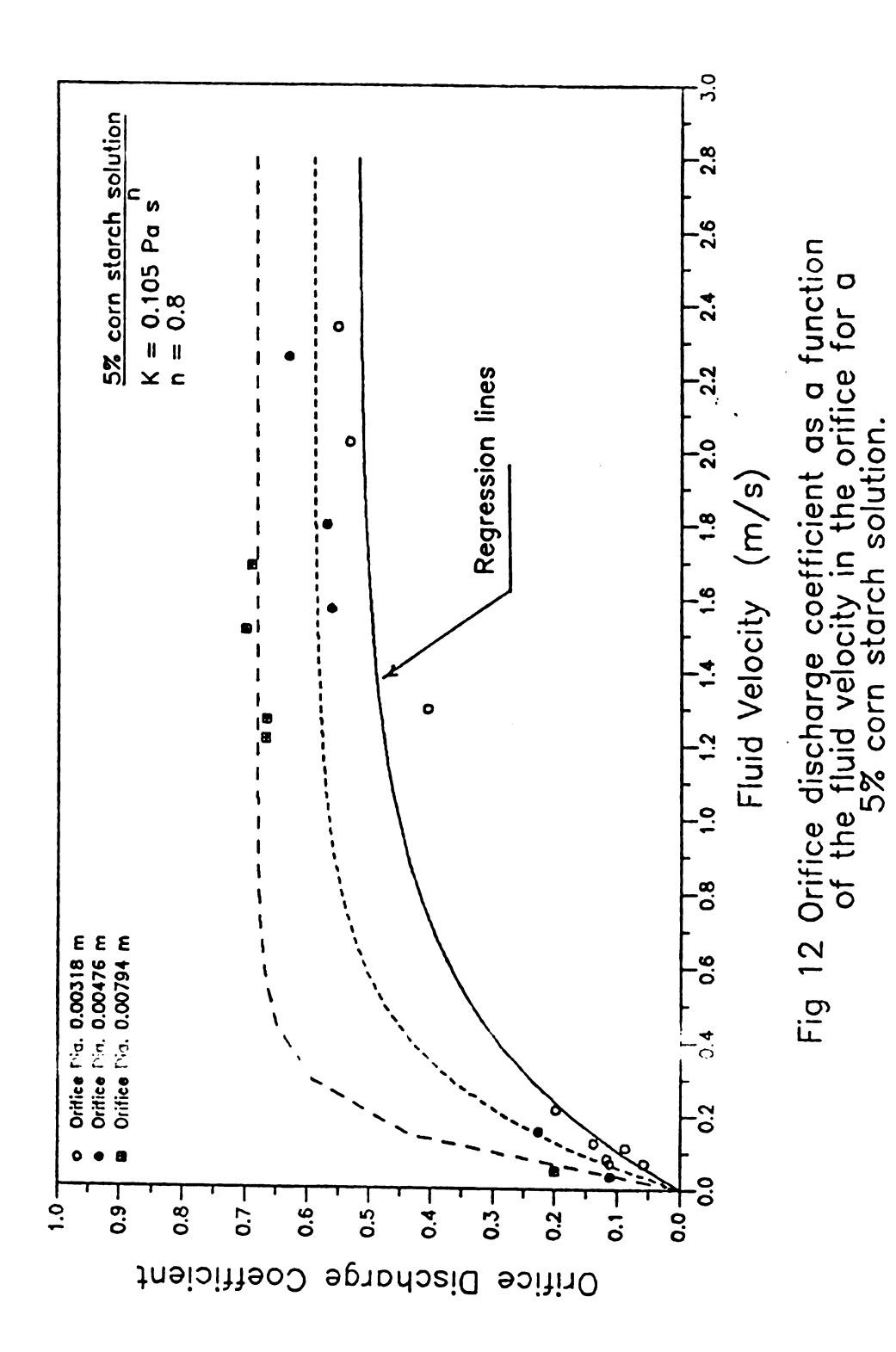
Also, the C values were calculated without including the  $\frac{u^2}{\alpha}$  term (Equation 34) to simplify the calculations. The results showed that the calculated C values with and without the  $\frac{u^2}{\alpha}$  term were almost the same (the difference was around 3%). For that reason it was decided to simplify Equation (34) and not include the  $\frac{u^2}{\alpha}$  term. Then, Equation (34) takes the following form

$$q_i - A_0 \rho C (2 p_i / \rho)^{\frac{1}{2}}$$
 (38)

Three separate sets of orifice discharge coefficient data for each starch solution concentration were generated using the simplified Equation (38). Figures 12, 13 and 14 show the results indicating that C values are a function of the orifice diameter, fluid velocity in the orifice and the fluid properties (consistency coefficient and flow behavior index).

It can be observed, that for a 0.00318 m orifice diameter, 0.105 Pa s<sup>n</sup> consistency coefficient and a 0.8 flow behavior index (Figure 12), the C values start from zero and increase with the fluid velocity. However, they tend to be a constant value in the range of 0.45 to 0.50. An examination of the data shown in Figure 12 indicates that experimental data for each orifice diameter follow the same pattern. Also, a comparison among Figures 12, 13 and 14 show that at relatively high velocities, the orifice discharge coefficient tends to be a constant which tends to decrease when the solid content of the solution is increasing.

A well defined value for this particular case of the orifice



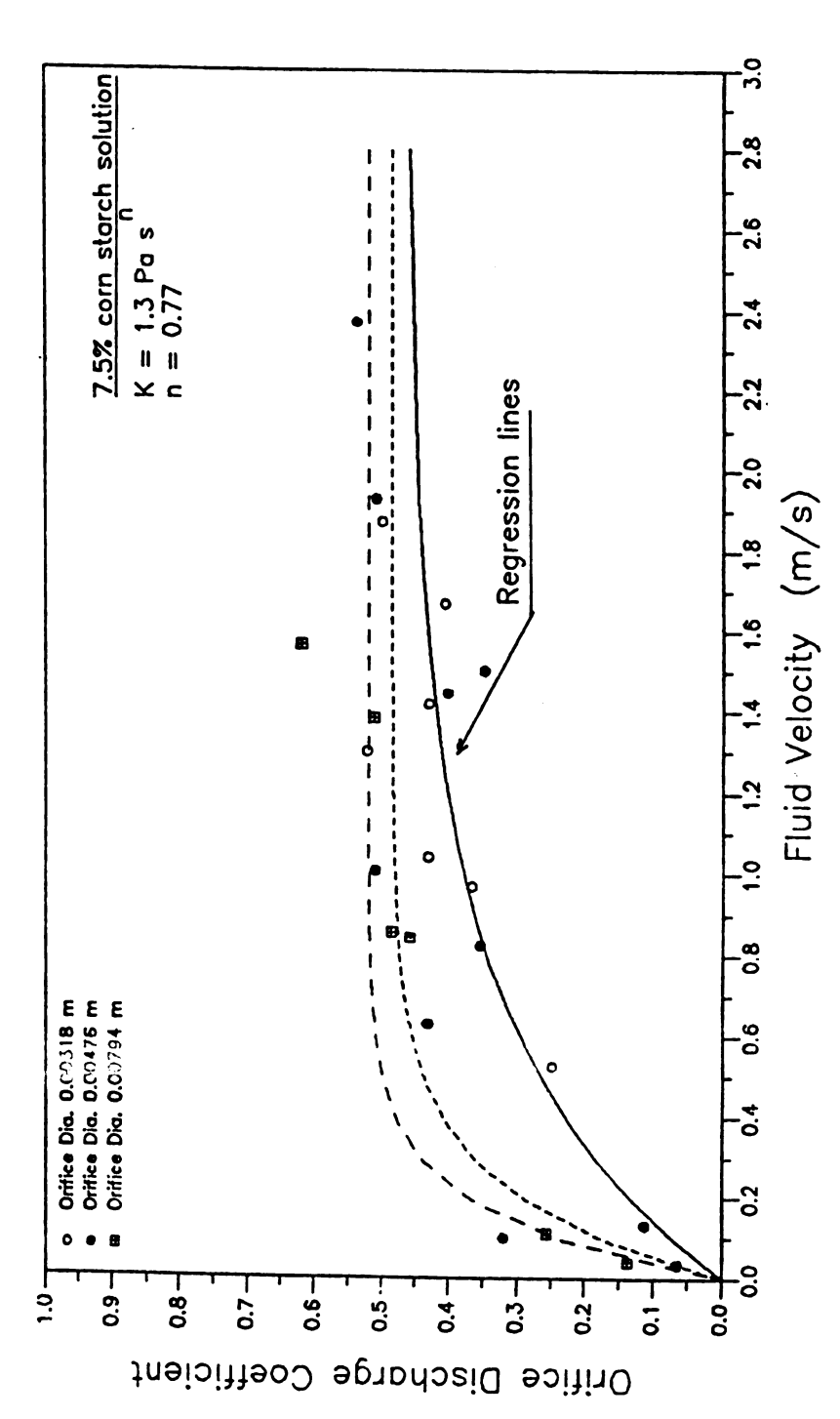


Fig 13 Orifice discharge coefficient as a function of the fluid velocity in the orifice for a 7.5% corn starch solution.

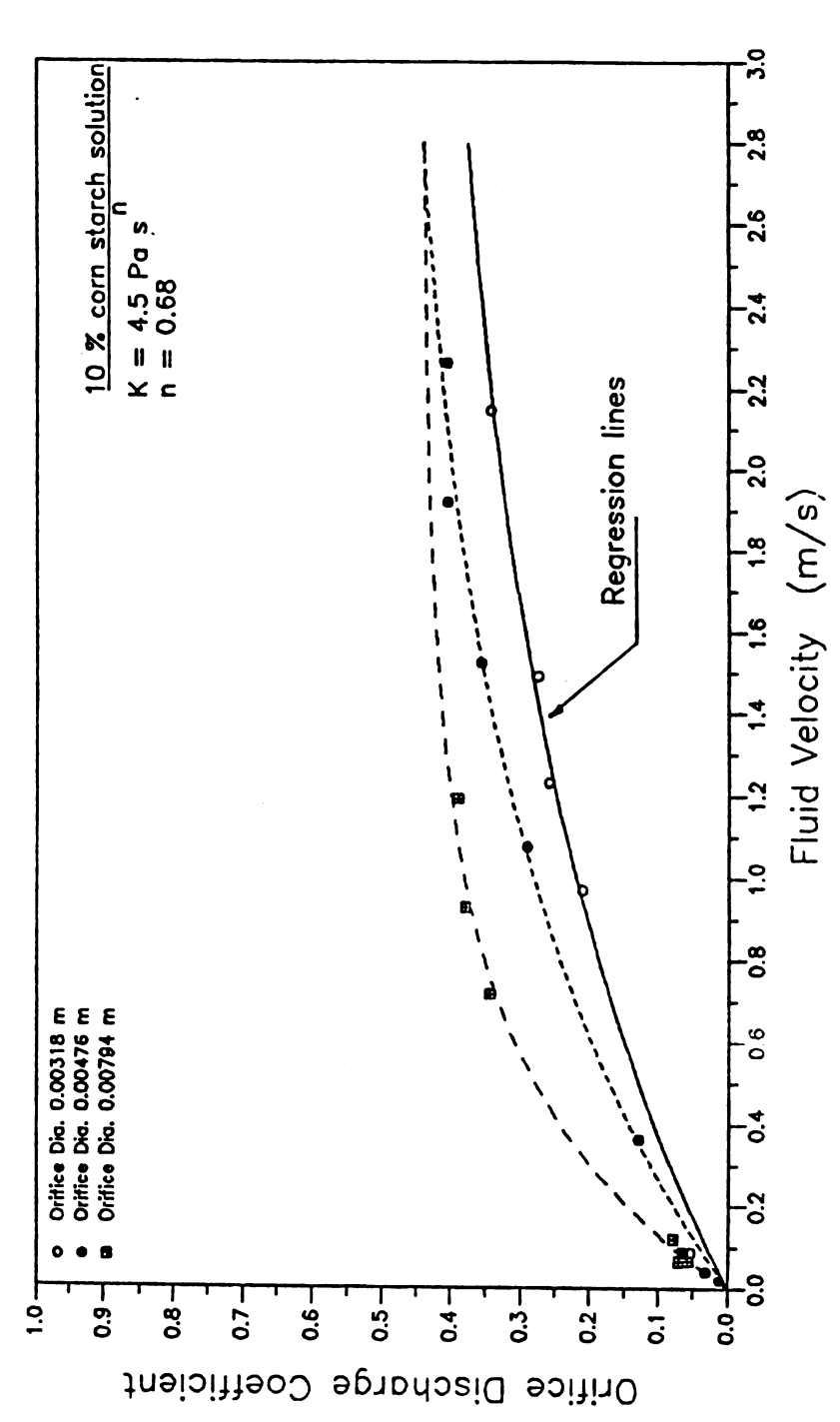


Fig 14 Orifice discharge coefficient as a function of the fluid velocity in the orifice for a 10 % corn starch solution.

discharge coefficient was not found in the published literature. Perry et al. (1963) mention that, for different fluids with discharge coefficients in the range of 0.6 to 0.95, C values increase as the orifice diameter increases and decreases as the fluid density decreases. This is consistent with the lower C values being found for the smallest orifice diameter and for more viscous fluids (see Figures 12, 13 and 14). No references for the orifice discharge coefficients for non-Newtonian fluids were found.

Each set of orifice discharge coefficient data was analyzed as a function of the fluid velocity in the orifice. Considering the distribution of the data in Figures 12, 13 and 14, it can be deduced that the data follows an exponential mathematical model. This mathematical model does not have any particular physical interpretation and is presented only as a compact representation of the experimental data. The orifice discharge coefficient versus the fluid velocity in the orifice were pooled and the following equation was found to fit the data:

$$C = B(1) (1 - \exp(-B(2) v))$$
 (39)

The coefficients B(1) and B(2) are parameters to be determined. Table 2 shows the parameter estimates found by means of non-linear regression analysis. A comparison of the experimental data and the regression curves shown in Figures 12, 13 and 14 indicates that the experimental orifice discharge coefficients fit well within the regression line in the range of fluid velocities studied.

Another way to analyze the data is to relate the calculated C values with Re<sub>o</sub> (Equation 37), Tables Al to A3 of Appendix A present the calculated values of Re<sub>o</sub>. If the orifice discharge coefficient is

Results of the non-linear regression analysis for data of orifice discharge coefficient. Model:  $C = B(1) \ (1.0 - \exp(-B(2) \ v))$ Table 2

nits for is B(2) Upper	2.8925 4.7646 8.3029	2.7763 8.3098 10.2341	1.1834 1.0682 2.5373
Confidence Limi Model Parameters B per Lower	1.2627 1.8423 5.5855	0.6412 0.9670 2.4174	0.3034 0.6939 1.5001
te Up	0.5763 0.6374 0.6975	0.5626 0.5686 0.5844	0.5580 0.5266 0.4833
Aproxima B(1) Lower	0.4612 0.5413 0.6651	0.3647 0.4041 0.4594	0.2876 0.4360 0.3062
Residual Sum Squares	0.1186E-1 0.4906E-2 0.7808E-3	0.3784E-2 0.4337E-1 0.1493E-1	0.8991E-3 0.4832E-3 0.7597E-3
r2	0.96 0.98 0.99	0.84 0.81 0.90	0.99 0.99 0.99
nmeters B(2) s/m	2.077 3.303 6.944	1.709 4.638 6.326	0.743 0.881 2.019
Param B(1)	0.5188 0.5894 0.6813	0.4636 0.4863 0.5219	0.4229 0.4308 0.4398
Starch Orifice solution Diameter % m	0.00318 0.00476 0.00794	0.00318 0.00476 0.00794	0.00318 0.00476 0.00794
Starch solution	8	7.5	10

plotted as a function of Re<sub>o</sub> (Figure 15), one finds that most of the Re<sub>o</sub> values are in the laminar region and C values increase with Re<sub>o</sub> until C is almost a constant. Results suggest an exponential relationship could exit between the orifice discharge coefficient and Re<sub>o</sub> that is similar to the relationship between C and the fluid velocity in the orifice. This mathematical expression was determined as

$$C = 0.494 (1 - \exp(-0.011 \text{ Re}_0)) + 0.086$$
 (40)

Equation (40) had an  $r^2$  value of 0.77 and represents the value of the coefficient that provides the best fit to the experimental data.

Equation (40) is very important for two reasons. First, the fact that the discharge orifice coefficient is a function of the generalized Reynolds number in the range studied means that it is possible to find the orifice discharge coefficient for a non-Newtonian fluid (power-law model) with any fluid property values (consistency coefficient and flow behavior index) and any orifice diameter. Second, and just as important, it enables one to transfer this model to analysis of manifold system subjected to the same or similar conditions.

## 5.3 Manifold Fluid Flow Distribution.

Using the manifold system (Figure 8), the data included in Tables B1 to B3 of Appendix B were obtained. These tables report the fluid flow rate at each orifice from the manifold for different orifice and pipe diameters for different fluids.

Figures 16, 17 and 18 are manifold flow distribution example for 5% starch solution (low viscous fluid), 7.5% starch solution

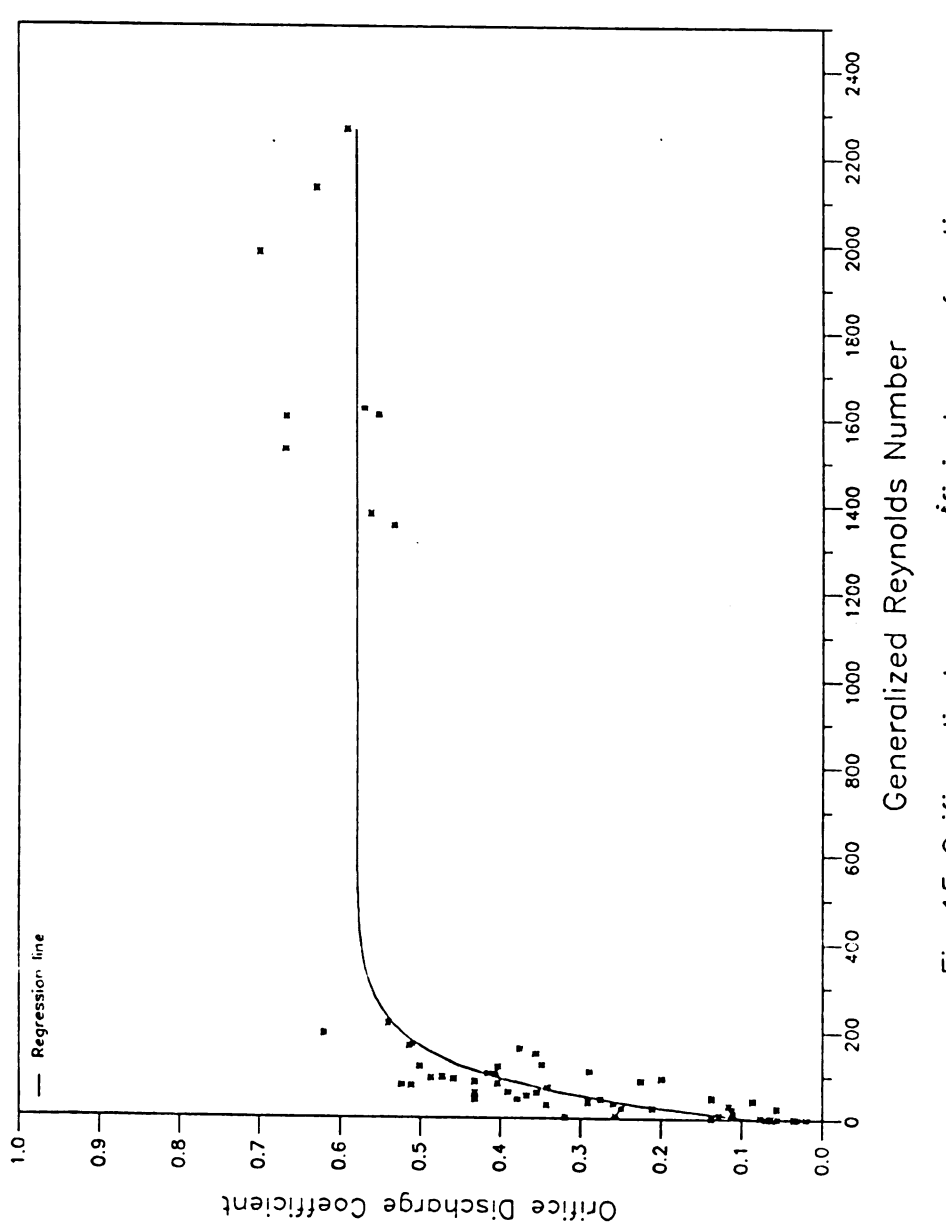
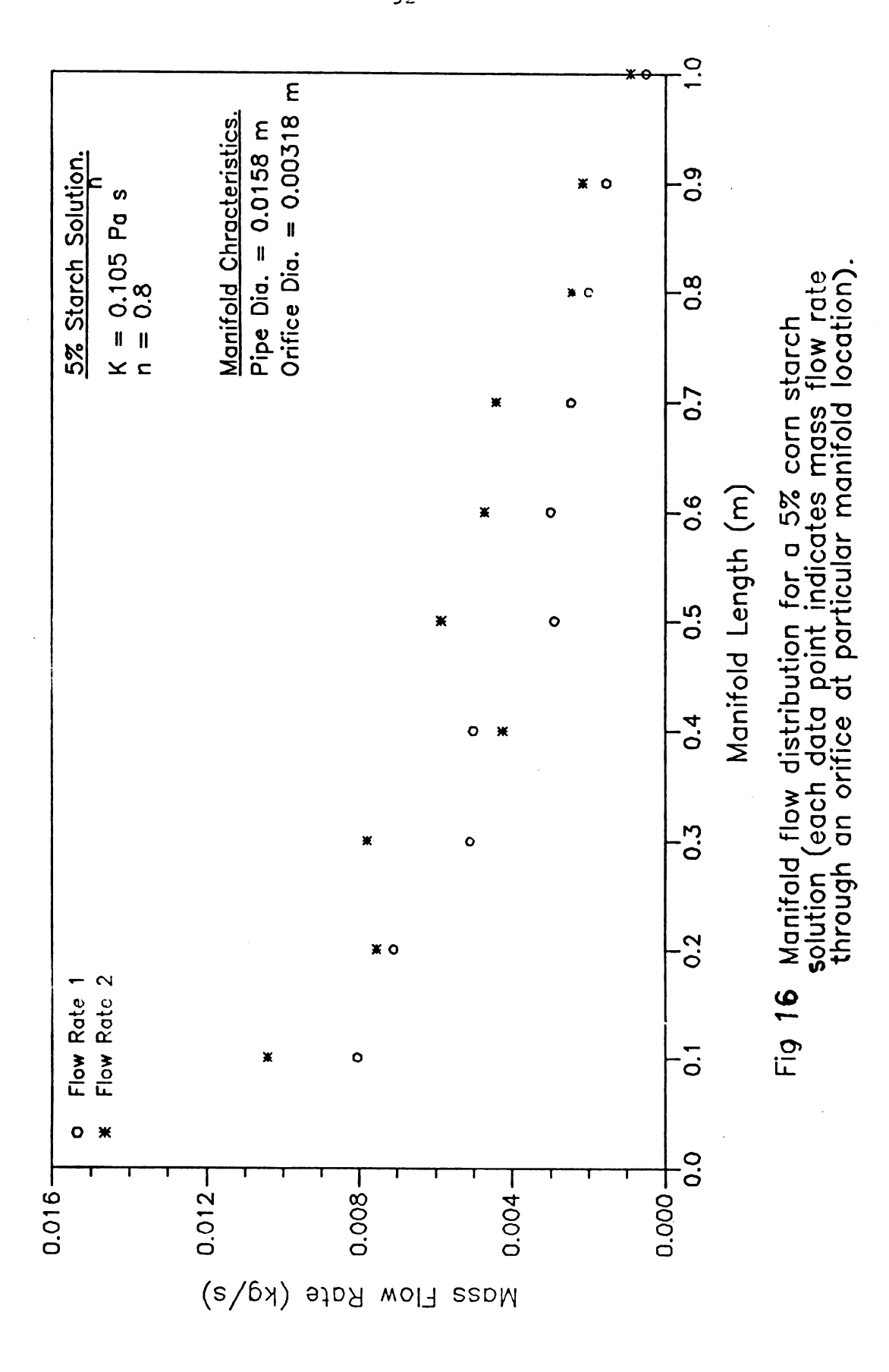
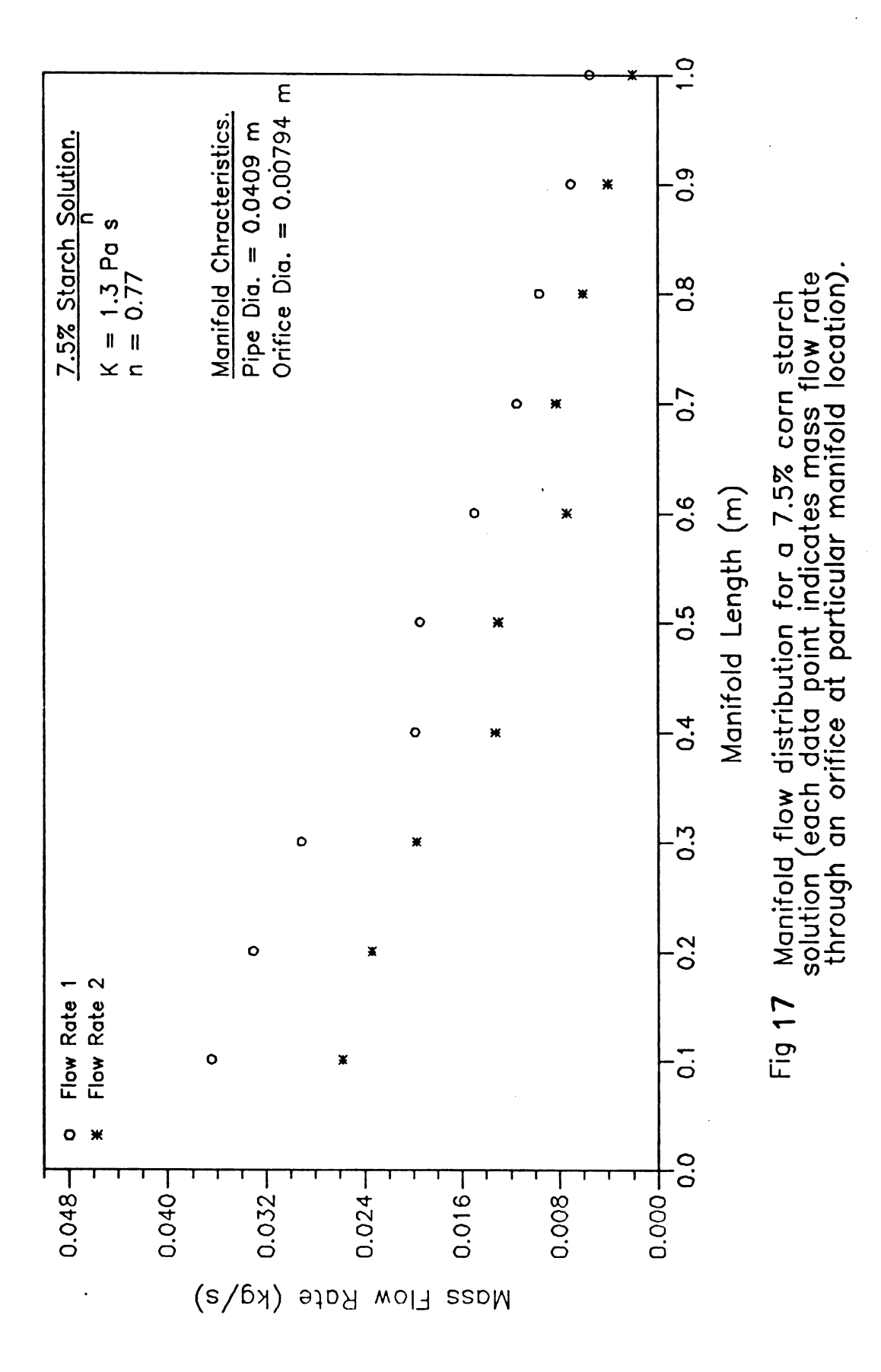
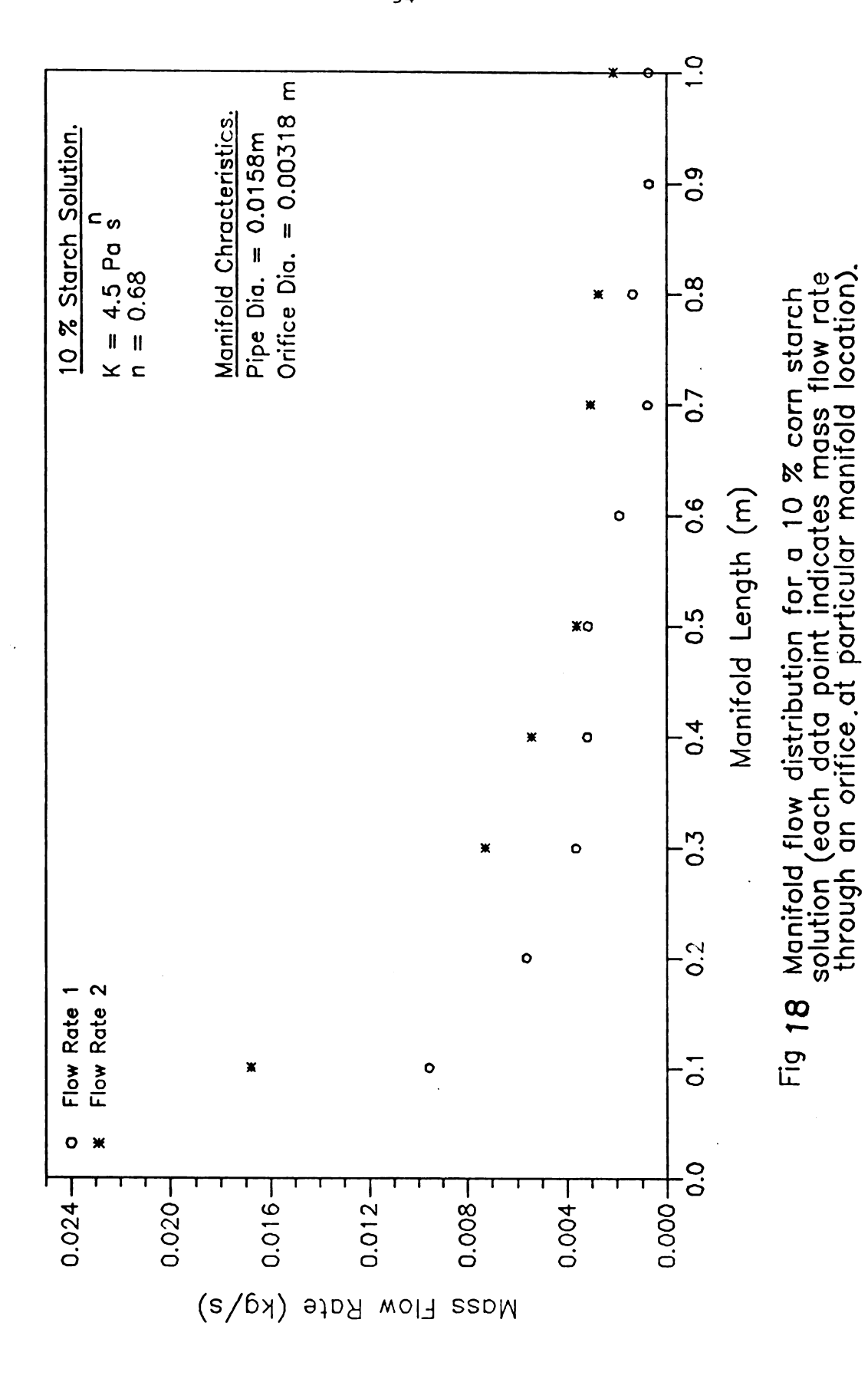


Fig 15 Orifice discharge coefficient as a function of the generalized Reynolds number.

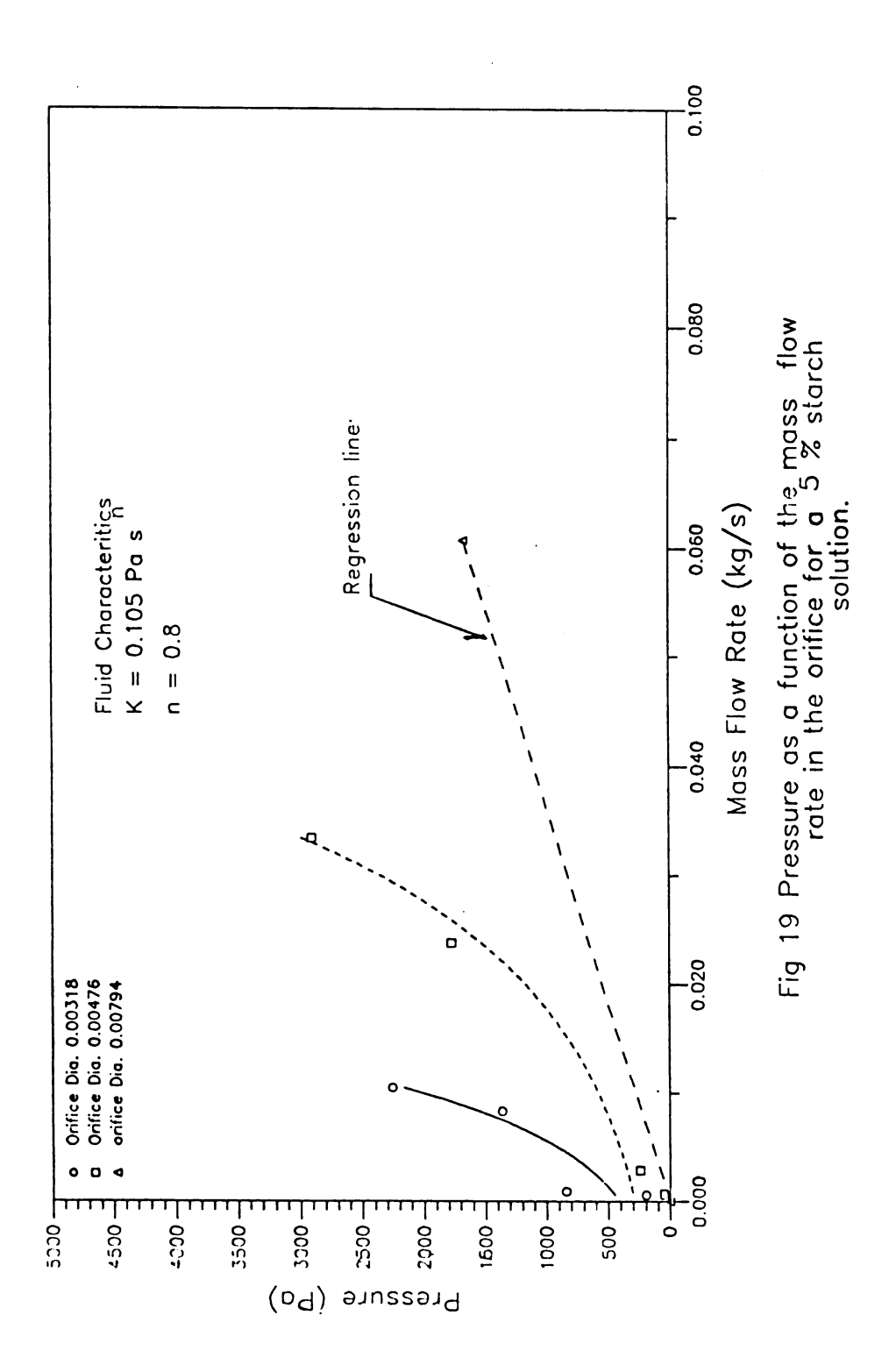


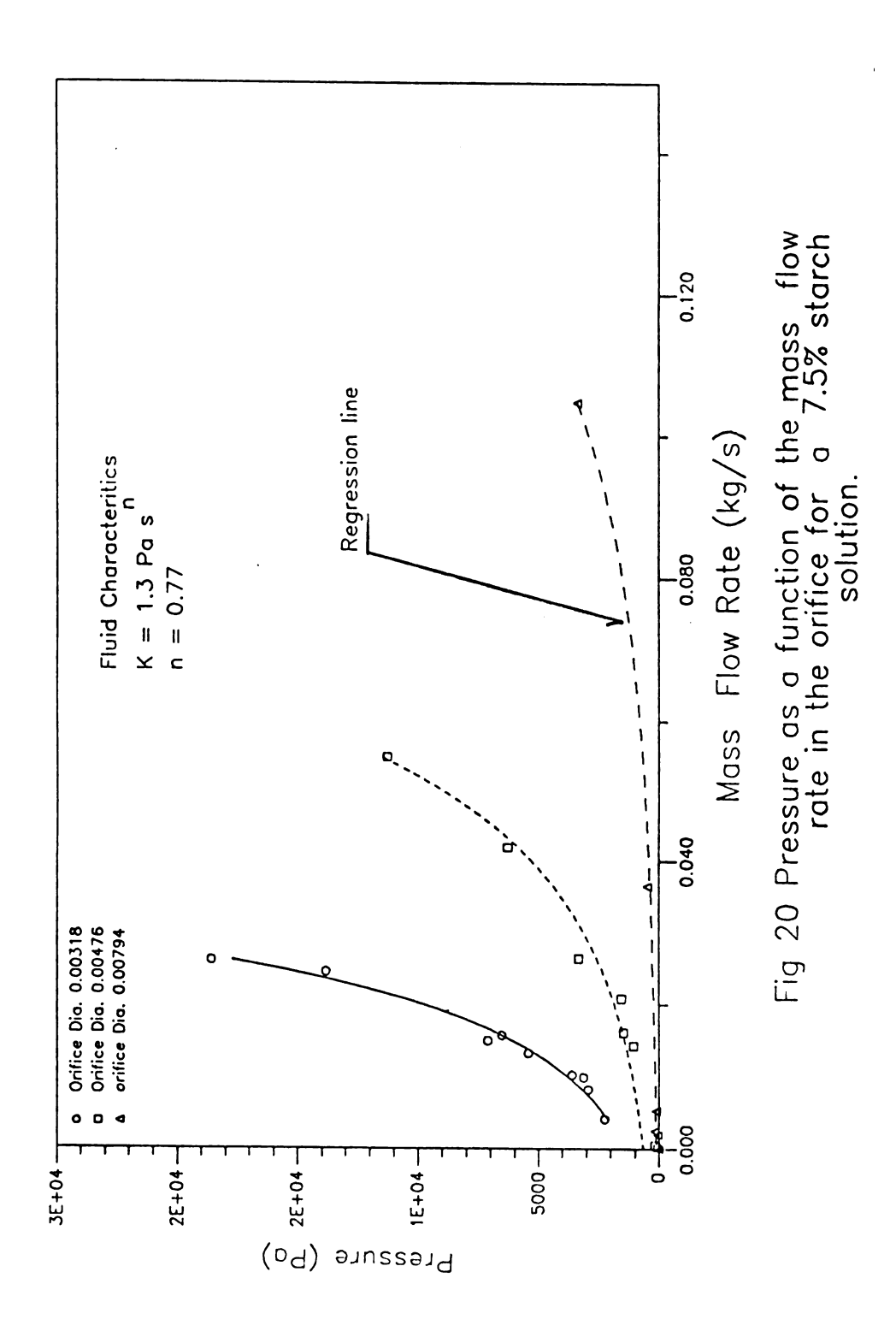


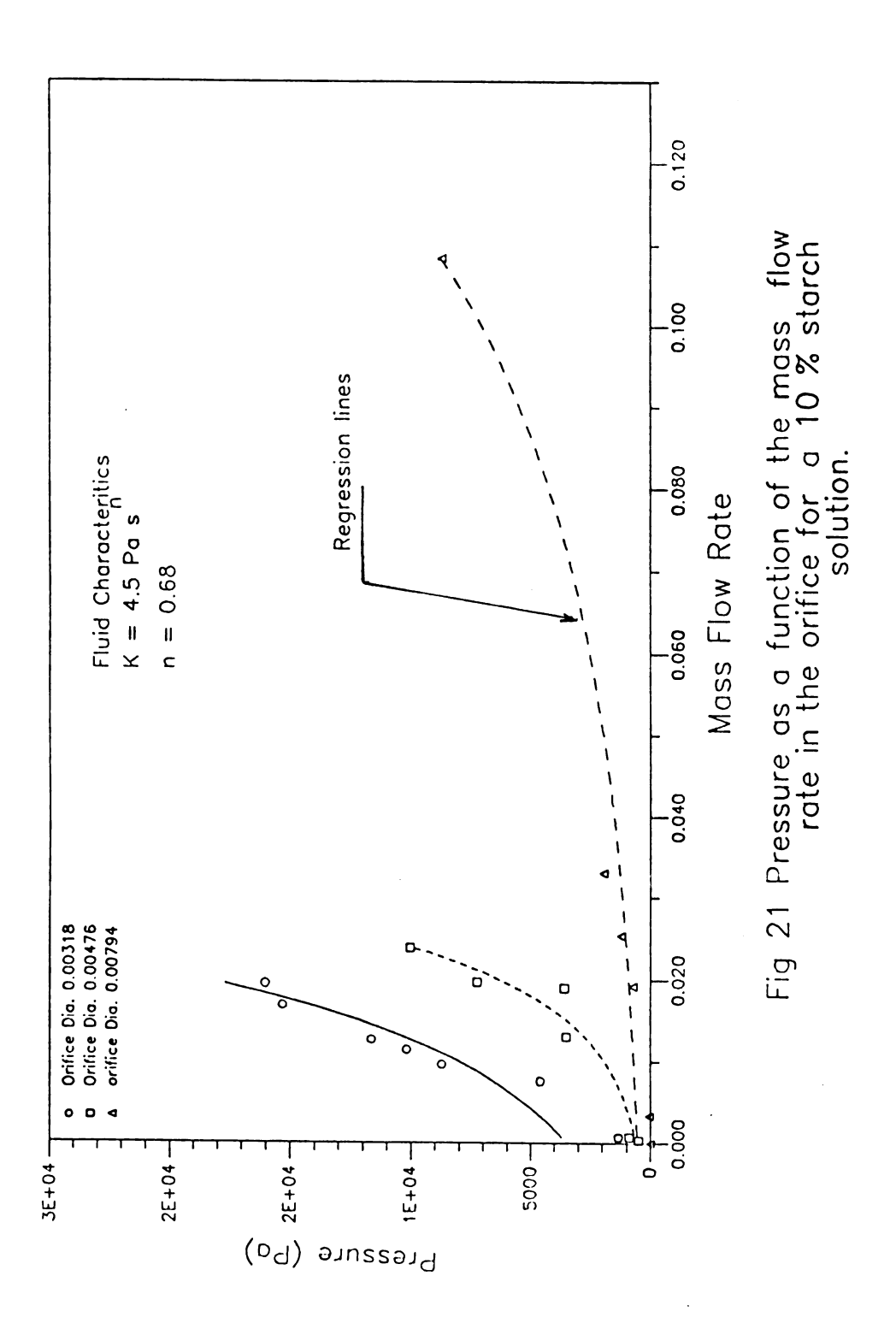


(medium viscous fluid) and 10% starch solution (high viscous fluid) and Figures 19, 20 and 21 are plots of pressure at the first orifice versus the mass flow rate for the same fluid at different orifice diameters. From the data and figures the following can be observed:

- 1. The fluid flow rate in each orifice decreases along the manifold. This can be observed at any fluid flow rate distribution reported in Tables B1 to B3 of the Appendix B. Even though most of the data follows this tendency, there are some data points which do not. One explanation for this is that fluids with high viscosity or high concentrations sometimes formed starch clumps which acted as plugs causing a reduction of the flow in the orifice, especially in the smaller orifices.
- 2. The discharge at any orifice in the manifold is controlled by the pressure at that orifice, and the orifice and pipe diameter. The pressure profiles are similar to the pressure profile along the manifold reported by Dow (1950) and Wu and Glitin (1974). The fluid flow rate in the orifice is function of the square root of the pressure (Equation 38) and the orifice discharge coefficient which depends on on fluid properties (consistency coefficient and flow behavior index) and flow rate in the orifice.
- 3. At constant fluid properties, pipe diameter and flow rate at the entrance, a manifold with a small orifice diameter required more pressure than the manifold with a bigger orifices diameter (see Figure 19). Also the flow distribution was different. This occurs because the energy loss in the small orifice diameter are larger and consequently larger pressure drop is needed to keep a







higher flow rate.

- 4. At constant pipe and orifice diameter but different fluid properties, the more viscous fluid requires more pressure at the manifold entrance than the less viscous fluid to produce the same flow rate (see Figures 19, 20 and 21). This occurs because the more viscous fluid produces more friction loss in the pipe and consequently it needs more pressure to produce the same manifold flow distribution.
- 5. At constant fluid properties and orifice diameter, the pressure needed to pump the same flow rate in the manifold is higher in the smaller pipe diameter than in the bigger one. This can be observed from the data when a flow rate of 0.1 kg/s of 10% corn starch solution was pump in manifold diameters 0.0158, 0.0409 and 0.0525 m. The pressures necessary were approximately 40000, 15000 and 11000 Pa, respectively. This is because in a small pipe diameter, the velocity was higher and the energy loss due to the friction in the straight pipe (Equation 7) is increased due to the fluid velocity that is proportional to the square of the pressure.

### 5.4 Energy Loss Coefficient Due to Turbulence at the Orifice.

Using the procedure described in Section 4.3.2 and the relationship between the mass flow rate and the pressure at the orifice shown in Figures 19, 20 and 21; the energy loss coefficient due to turbulence at the orifice  $(k_f)$  was calculated. Table 3 shows the mathematical model parameters used to calculated the pressure at the orifice as a function of the mass flow rate. Tables C1 and C2 of the

Table 3 Results of the non-linear regression analysis for data of pressure versus flow rate in the orifice. Model:  $p = B(1) \exp(B(2) q)$ 

Starch solution %	Orifice Diameter m	Parameters		
		B(1) Pa	B(2) m <sup>3</sup> /kg	r²
5.0	0.00318 0.00476	407.4 287.9	160.3 70.3	0.89
7.5	0.00318 0.00476 0.00794	1037.2 652.0 113.3	86.1 52.5 32.5	0.98 0.99 0.99
10.0	0.00318 0.00476 0.00794	1746.1 592.8 189.8	52.2 18.4 19.4	0.90 0.91 0.98

Appendix C present the calculated  $k_f$ . A comparison of the  $k_f$  calculated for different starch solutions indicates that  $k_f$  is consistently present in the less viscous fluid while in the higher viscous fluid did not follow a defined pattern.

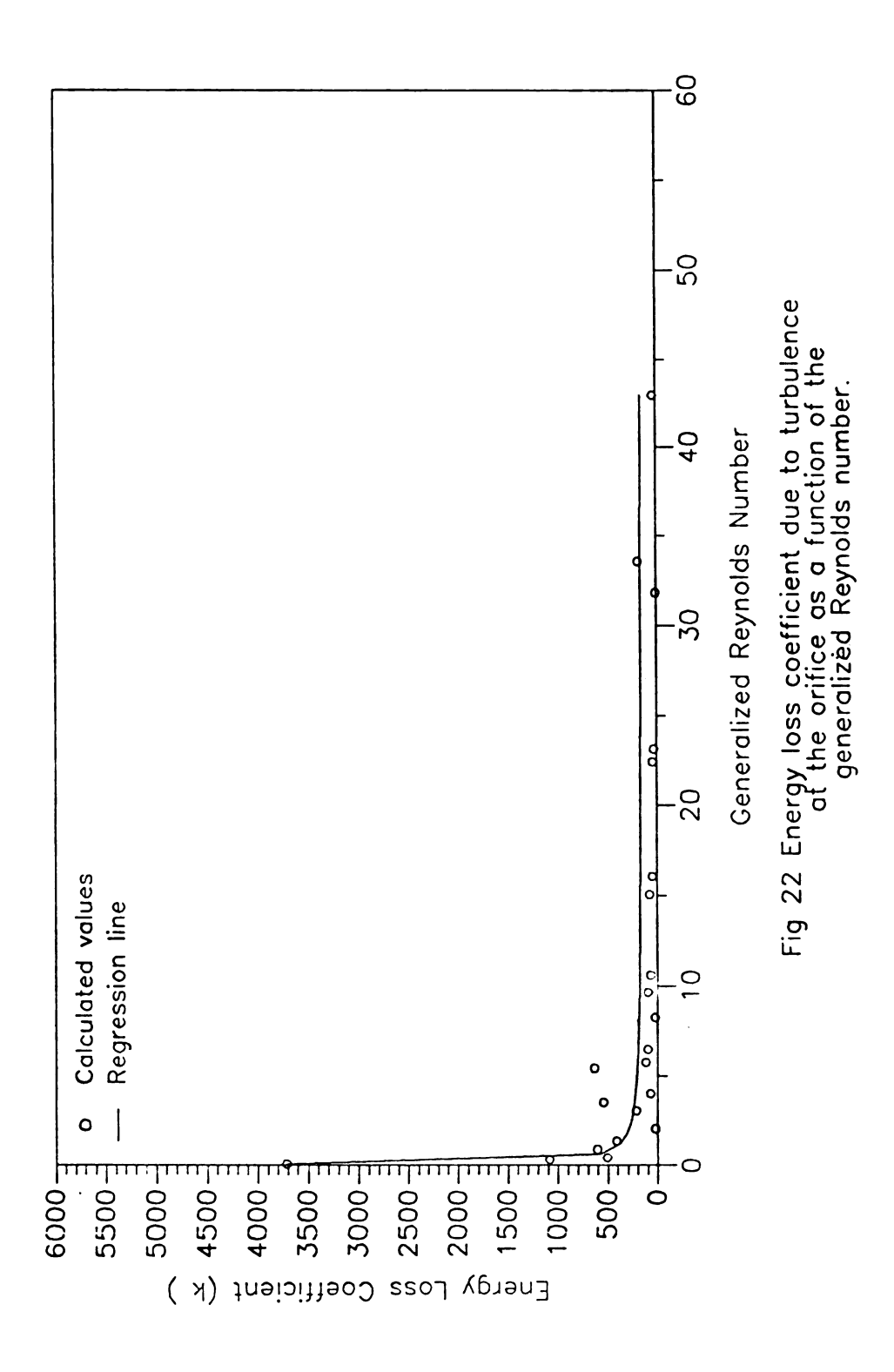
It is important to note, for 5% starch solution (low viscous fluid), the pressure calculated by means of the mechanical energy balance is larger than the calculated pressure using the mathematical model shown in Table 3. This means that the energy loss due to the turbulence at the orifice is important and it is necessary to consider in the simulation model to get the actual pressure at each orifice. For more viscous fluids, the data indicates that the friction loss due to turbulence was insignificant; because without using this factor it was possible to obtain good results for the pressure at the last orifice compared with the experimental data.

To include this coefficient into the model it is necessary to find a mathematical relationship between  $\mathbf{k_f}$  and the generalized Reynolds number for the fluid in the straight pipe (Figure 22). Considering the above, the energy loss coefficient  $\mathbf{k_f}$  versus the generalized Reynolds number data were pooled and the following equation (determined by non-linear regression) was found to fit the data:

$$k_f = 281.2 \text{ Re}^{-0.97} + 148.4$$
 (42)

Equation (42) had an  $r^2$  value of 0.77 and represent the value of the coefficient that provides the best fit to the data.

The equation has no particular theoretical significance and is present only as a representation of the data; however, it should be mentioned that a similar form of the equation was suggested by Steffe et al. (1984) and similar results were obtained for a tee, valve and



elbow.

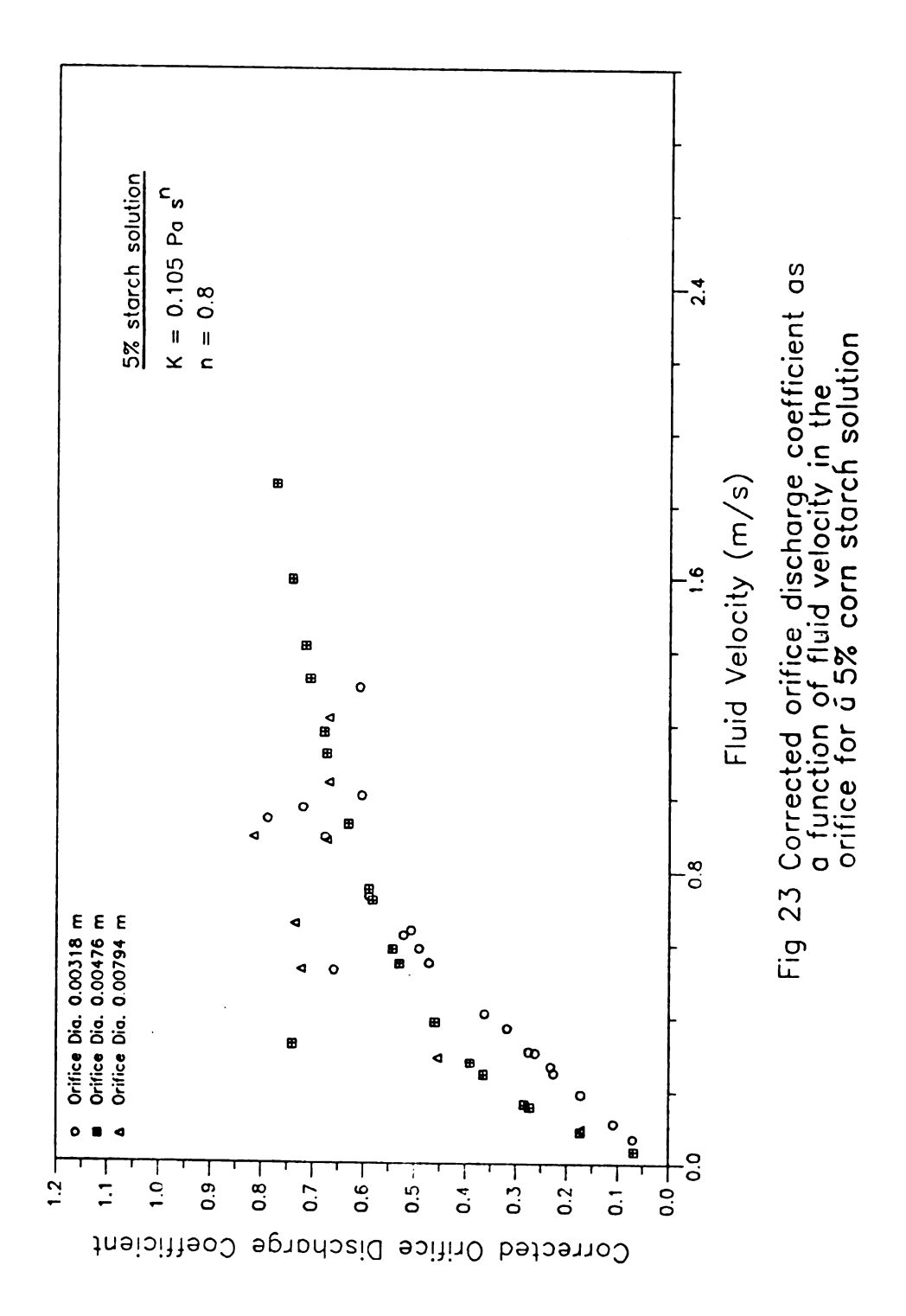
# 5.5 Orifice Discharge Coefficient Correction Factor.

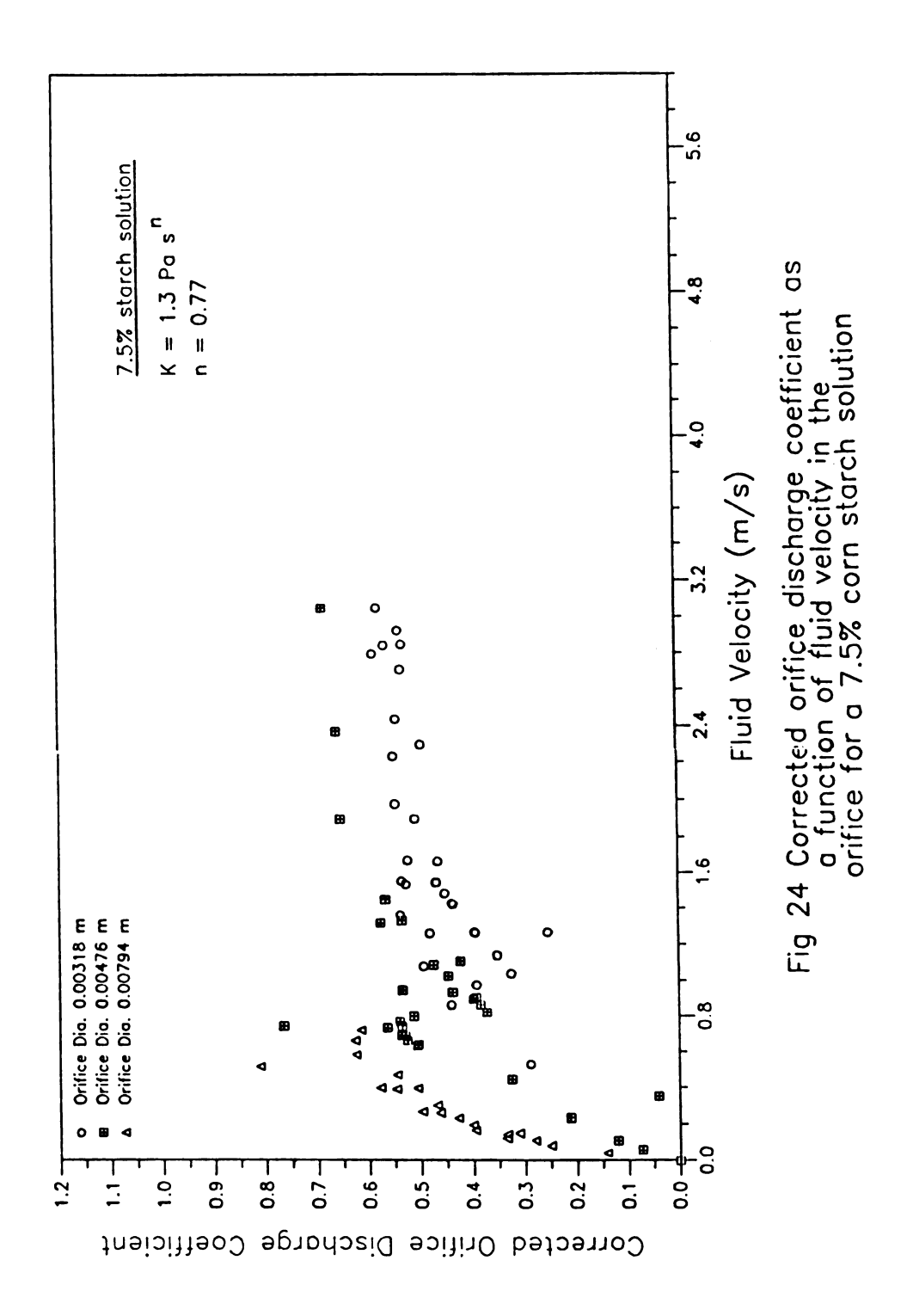
It was explained in Section 3.6 that the orifice discharge coefficient does not represent the actual coefficient present in the manifold orifice because there is a "pass by flow" (this is not present in the experiment to find the orifice discharge coefficient). This coefficient underestimates the discharge in the orifices.

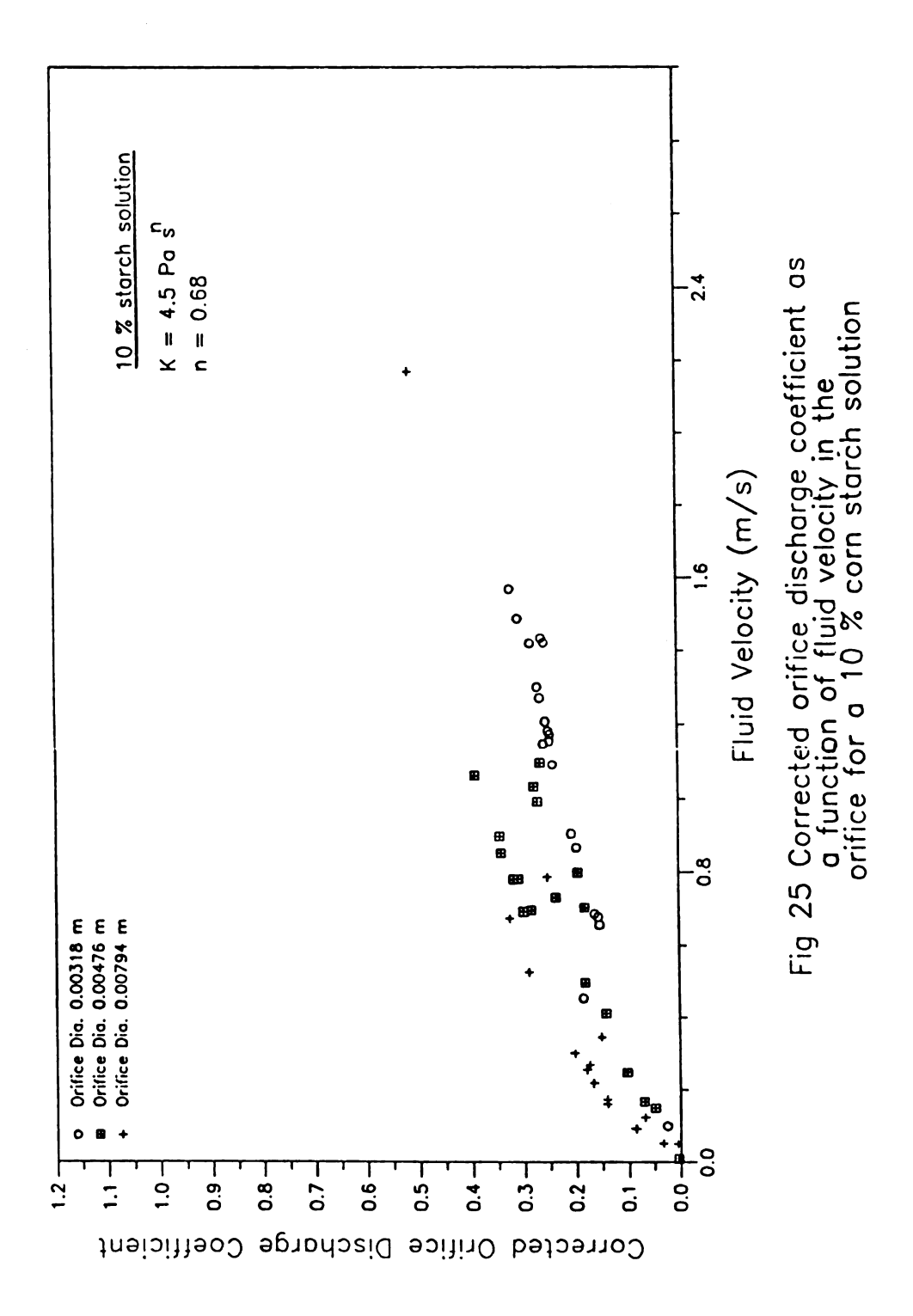
Using the manifold system, as explained in Section 4.3.1, the data included in Tables C1 to C3 of Appendix C were generated. The tables report the flow rate at each orifice from the manifold for different orifice and pipe diameters, and different fluid properties. Pressure drop at each orifice was calculated by means of mathematical function found in Section 5.4 (see Table 3) that related the pressure with the mass flow rate in the orifice.

Results indicate that the correction factor generally is larger than 1, and follows the same pattern as the orifice discharge coefficient versus fluid velocity in the orifice. This leads one to believe that the orifice discharge coefficient times its correction factor is another coefficient that can be called "the corrected orifice discharge coefficient, C' " defined in Equation (36). Figures 23, 24 and 25 show the relationship between the corrected orifice discharge coefficient and fluid velocity in the orifice for different orifice diameters and fluid properties.

The calculated corrected orifice discharge coefficient (C') may be considered a function of the generalized Reynolds number ( $Re_o$ ). Tables C1 to C3 of Appendix C present the calculated values of  $Re_o$ . If the C' values are plotted as a function of the  $Re_o$  (Figure 26), it can







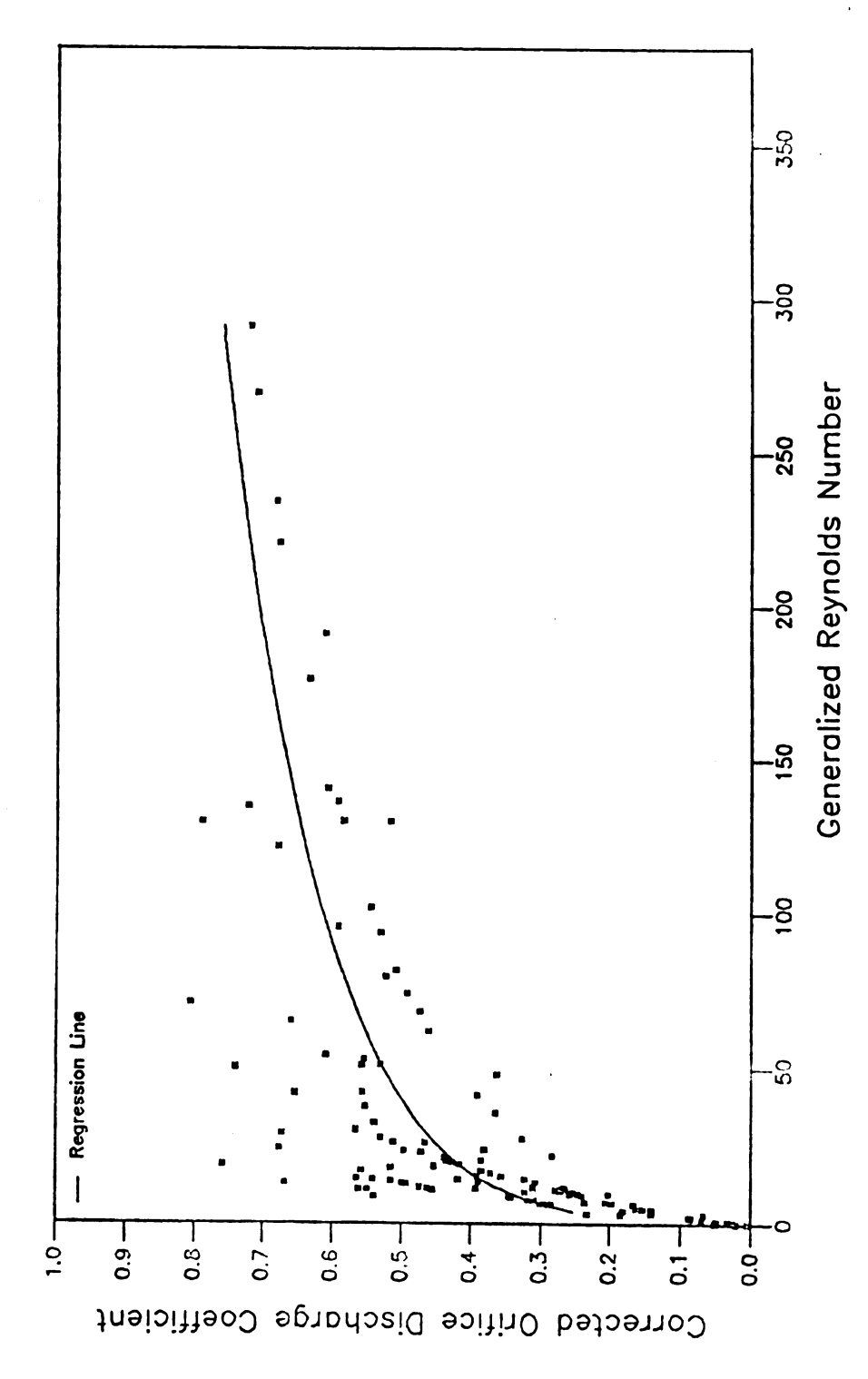


Fig 26 Corrected orifice discharge coefficient as function of the generalized Reynolds number

be observed that C' values increase with Re<sub>o</sub> until C' is almost a constant. Results suggest an exponential relationship between the corrected orifice discharge coefficient and the generalized Reynolds number. Similar results were obtained between the orifice discharge coefficient (C) and the generalized Reynolds number (Re<sub>o</sub>). The mathematical model that best fit the data points was determined as

$$C' = 0.905 \text{ Re}_0^{0.093} - 0.7742$$
 (43)

with an  $r^2$  value of 0.77. The low correlation index is due to variation of the C' values which may depend on the fluid rheological properties. Equation (43) is important because this is going to be used in the simulation of the flow distribution in the manifold for different conditions.

### 5.6 Comparison of Simulated and Actual Manifold Distribution.

Using the theoretical model, the energy loss coefficient due to the turbulence at the orifice (Section 5.4) and the corrected orifice discharge coefficient developed in Section 5.5, the manifold flow distribution at any fluid flow rate at the entrance may be predicted. To test the theoretical model, two sets of experimental flow rates for each type of fluid were plotted with the simulated flow rates. Figures 27, 28, 29, 30, 31 and 32 show the experimental and the simulated manifold flow distribution predicted by the theoretical model for 5% (low viscosity), 7.55 (medium viscosity) and 10% corn starch solutions (high viscosity).

The theoretical model underestimated the flow rate in the first orifices and then overestimated the flow rate in the last ones

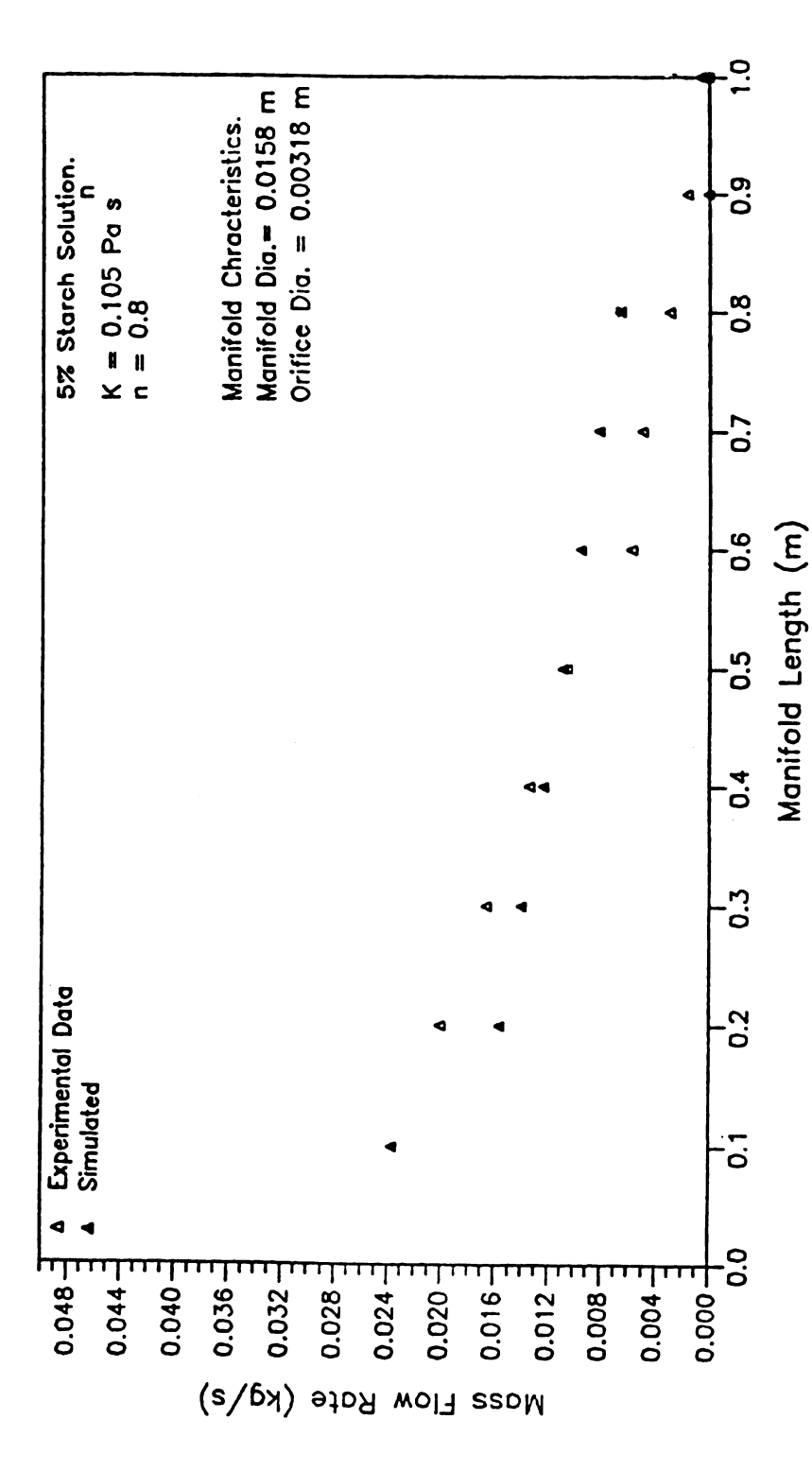


Fig 27 Manifold flow distribution: Simulated versus experimental results for a 5% corn starch solution

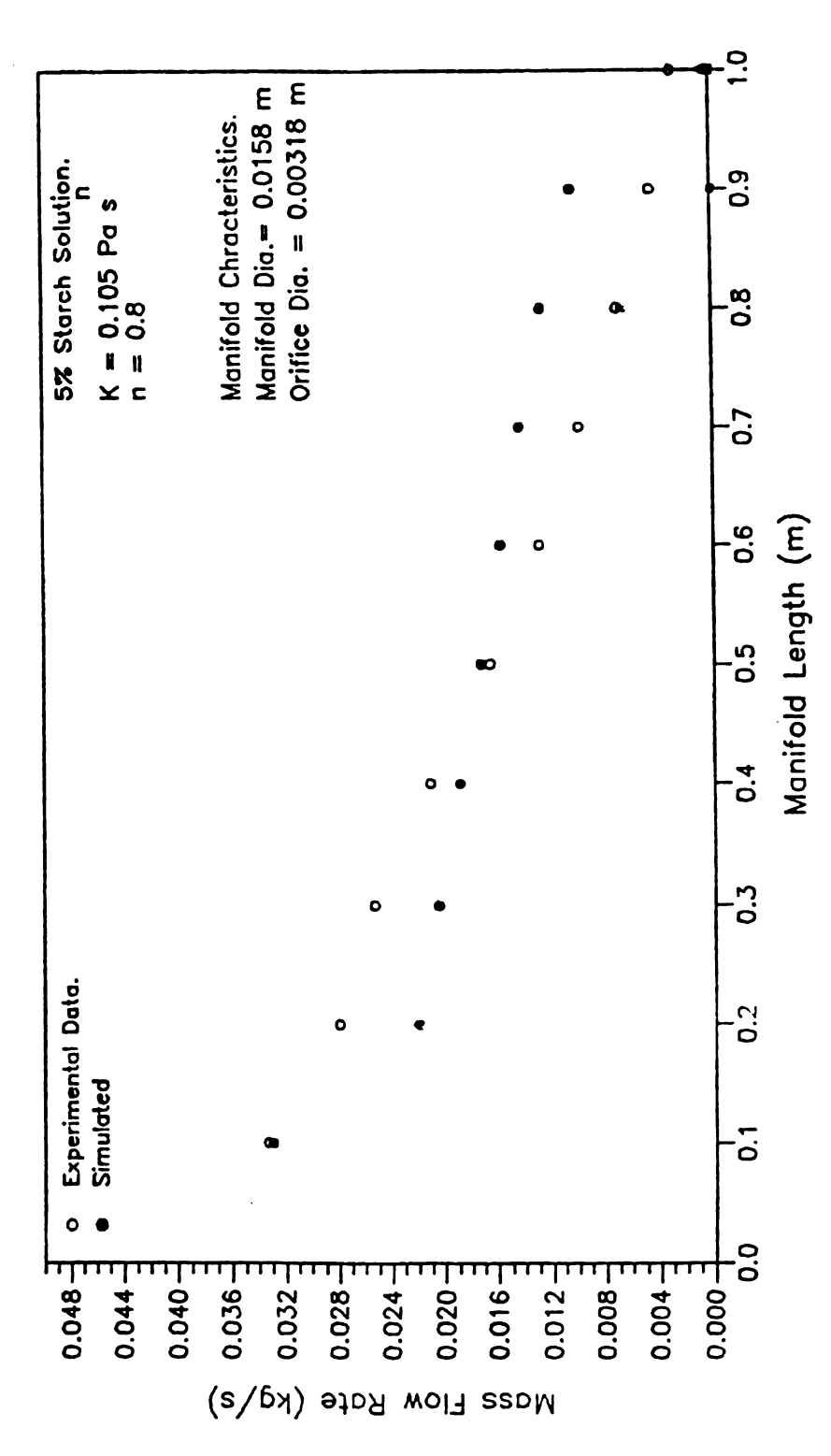
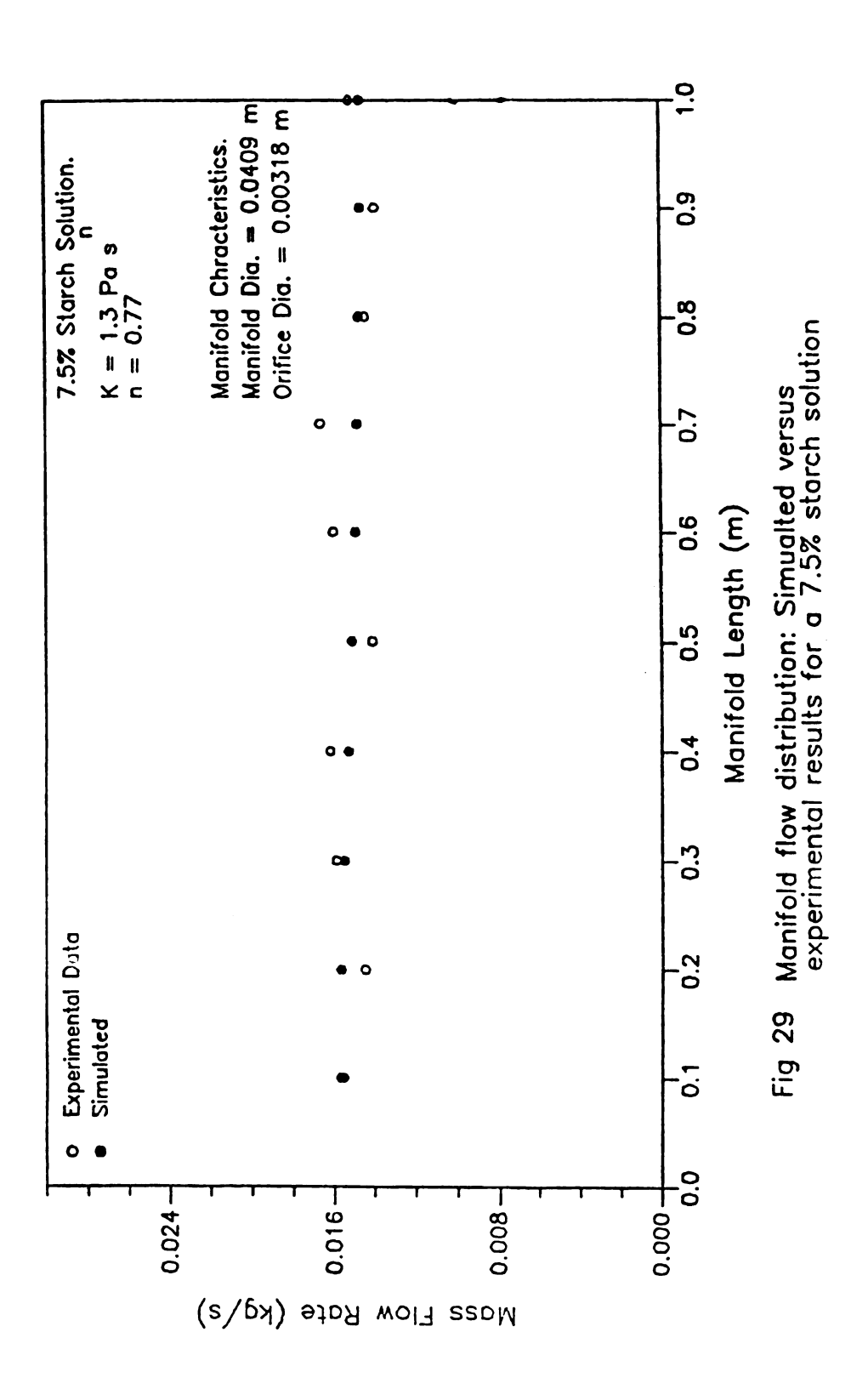
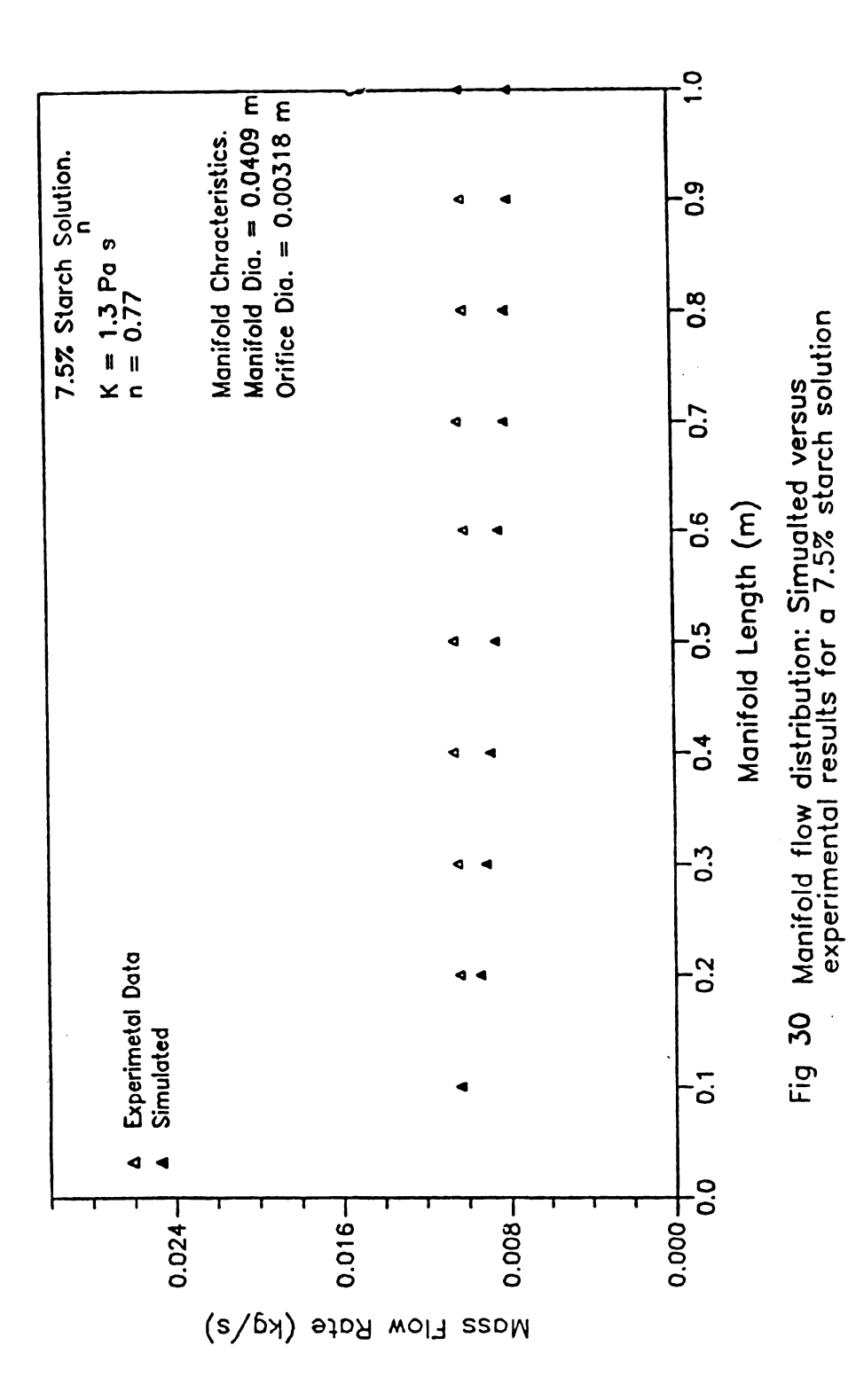
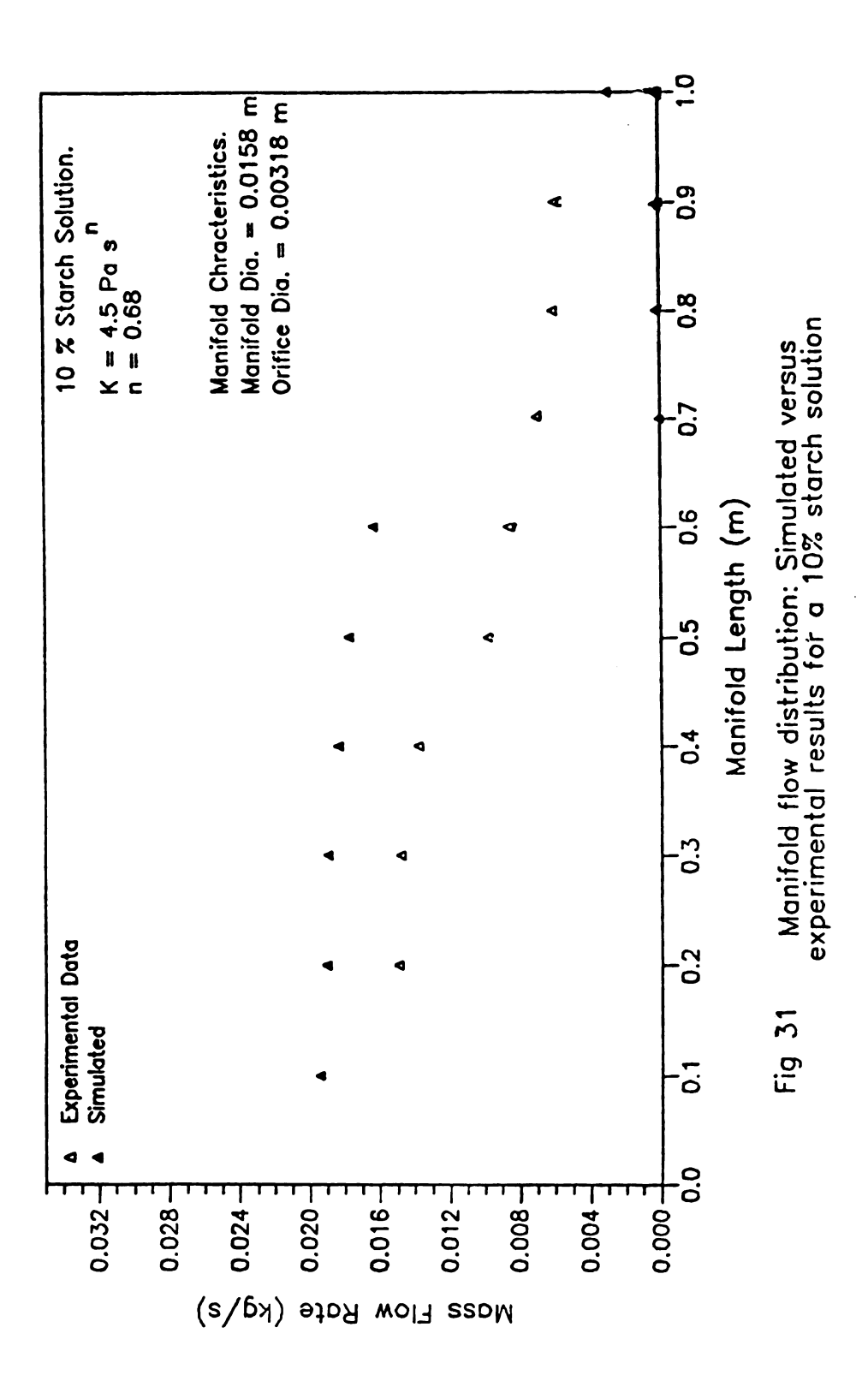
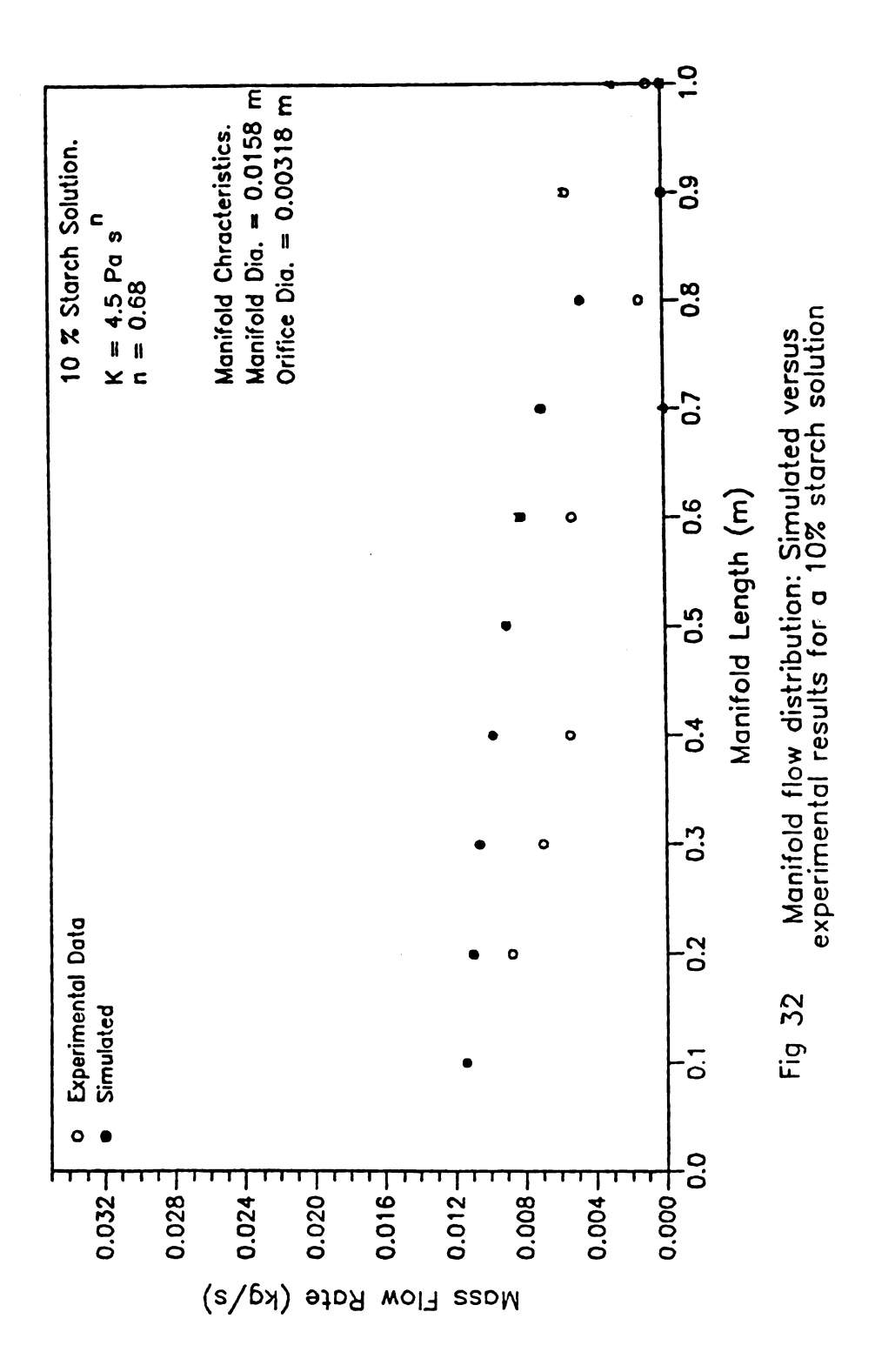


Fig 28 Manifold flow distribution: Simulated versus experimental results for a 5% corn starch solution









for the 5% solution (Figures 27 and 28). This behavior is repeated in each case. However, the simulated flow rates followed the trend of the experimental data. It is important to note that experimental flow rate and pressure at the first orifice of the manifold were used to initiate the simulation procedure and, for that reason the predicted and the experimental data are always the same for the first orifice.

The model also predicted flow rates that were lower and higher than the experimental values. A good agreement between the experimental predicted values for the 10% solution (Figures 31 and 32). A good agreement, however, between the experimental and predicted values was obtained. The error between the estimated and the experimental flow rate in the orifices ranges from 0 to 15%. The flow rate distribution was overestimated in both cases for the 10% solution and agreement was poor between the simulated and the experimental values.

As showed in Figures 27 to 32 the theoretical model does not always accurately predict the experimental data. The inaccuracy of the model may be related to many factors:

- a. The effect of the experimental errors in the determination of the flow rate in each orifice and the determination of the pressure at the first and last orifices in the manifold.
- b. The effect of the consistency coefficient appears to be important in the determination of the corrected orifice discharge coefficient and this means that there is not a single mathematical expression to obtain this coefficient.
- c. The energy loss coefficient due to turbulence does not have a well defined pattern in the highly viscous fluids, and this does not always allow it to be incorporated into the simulation model.

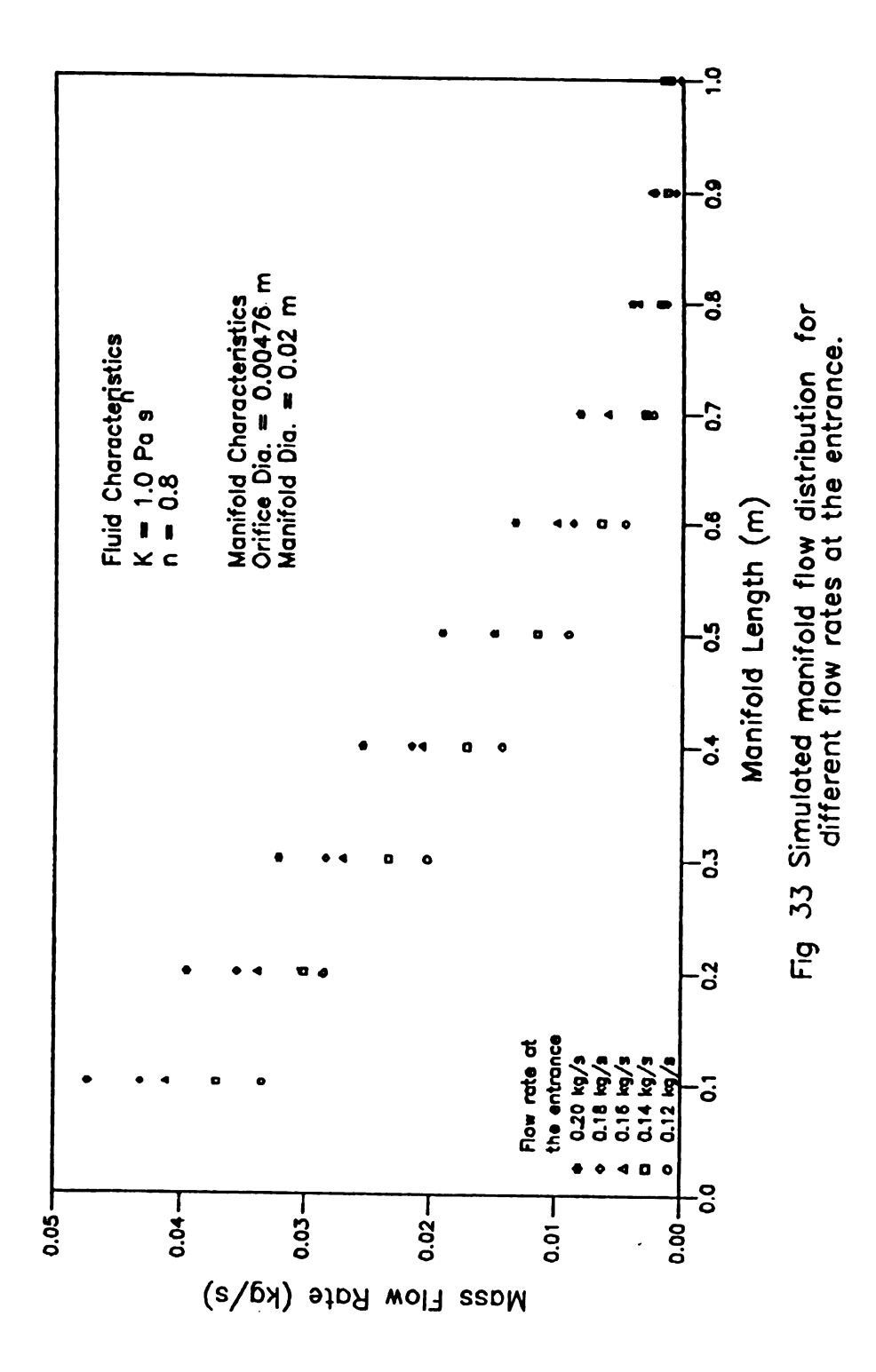
d. One of the major factors which causes the model inaccuracy is the system complexity due to the large number of interacting variables presented.

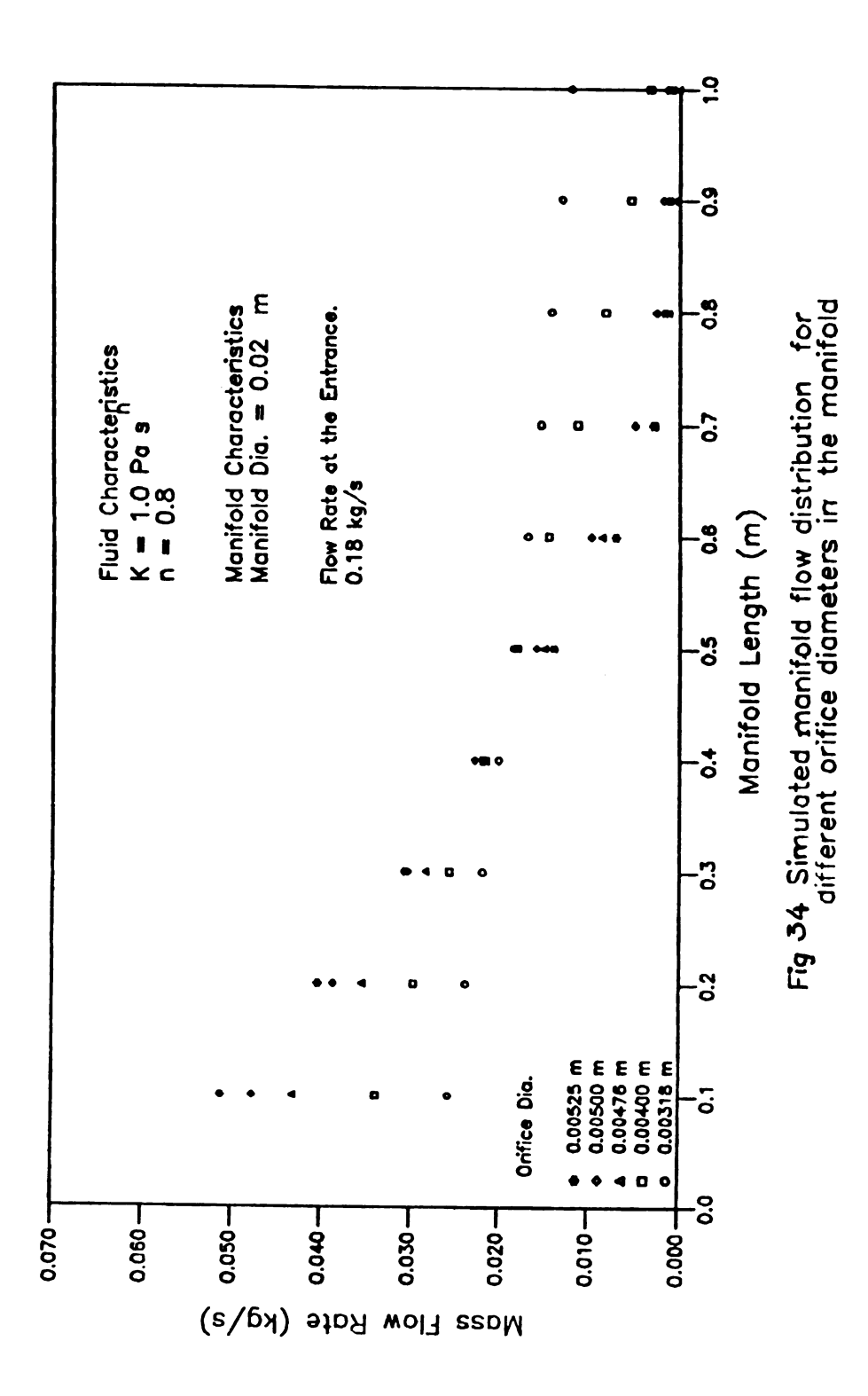
#### 5.7 Simulation of the Manifold Flow Distribution.

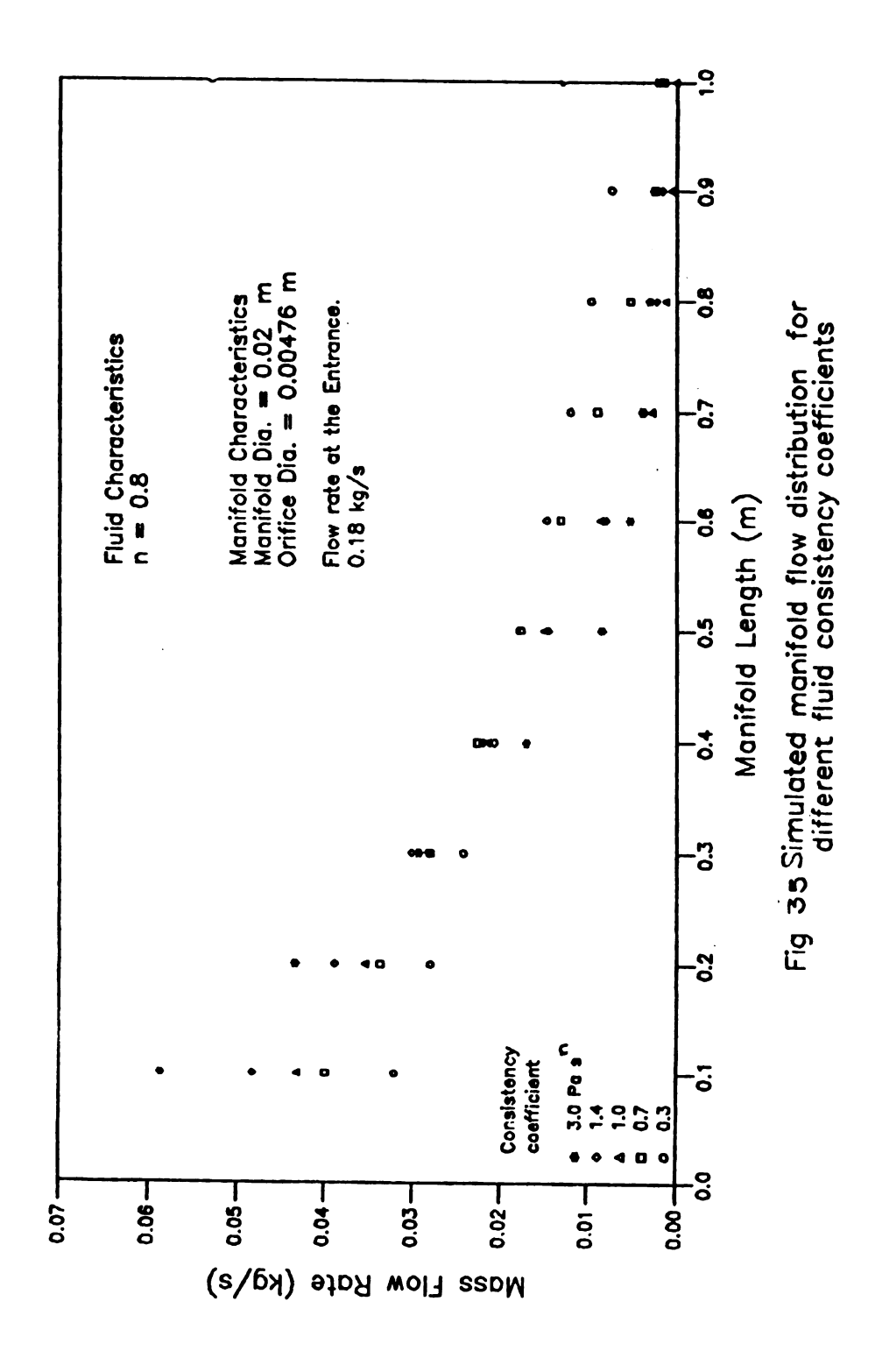
As shown in Section 5.6 the theoretical model, using the coefficients found in Section 5.4 and 5.5, fit the experimental data in same cases; hence it is instructional to simulate the manifold distribution for different conditions to observe the behavior of the manifold when different parameters are varied: the flow rate at the entrance, manifold diameter, orifice diameter, fluid consistency coefficient and so on.

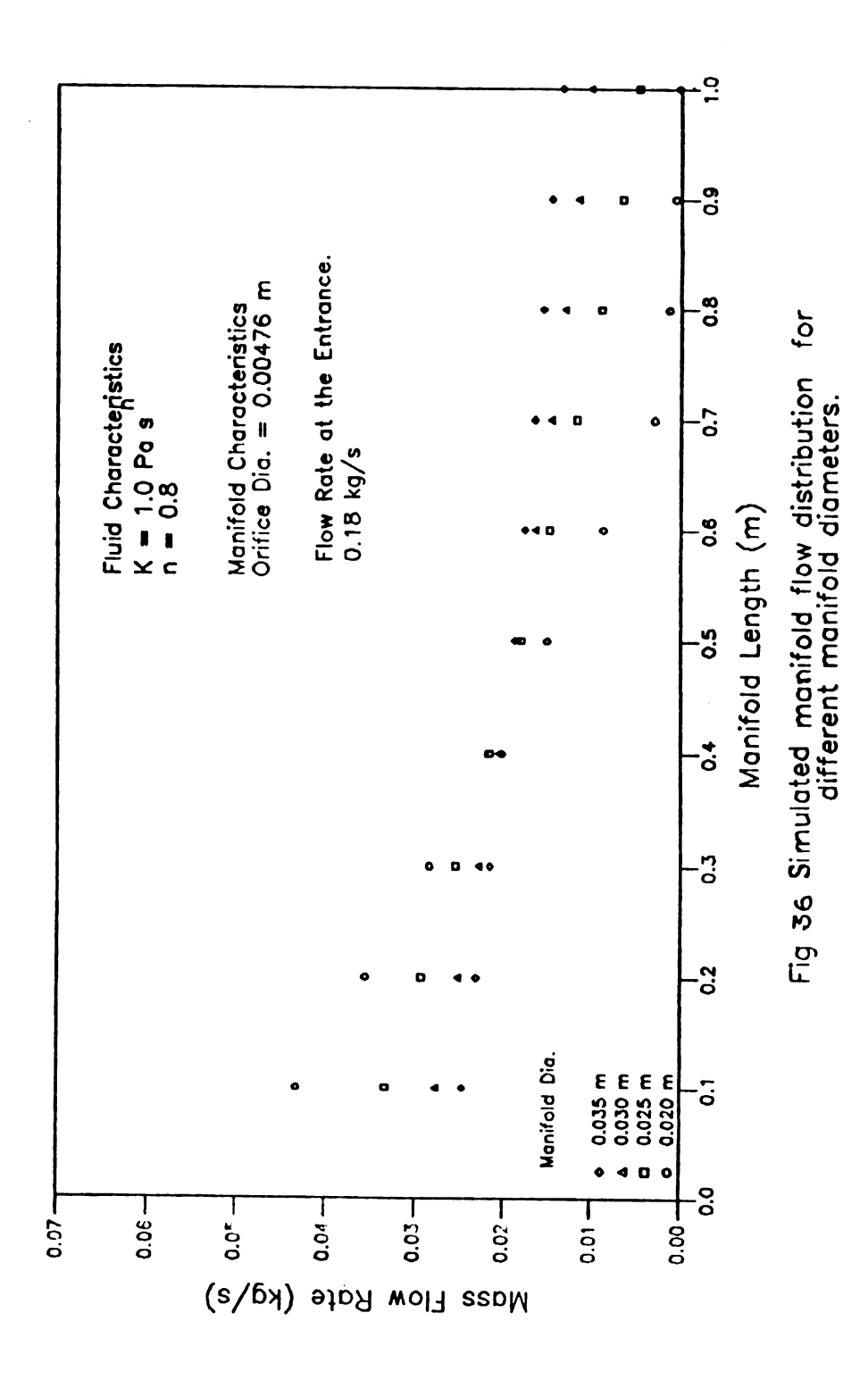
To simulate the manifold flow distribution using the theoretical model and the coefficients found above, a manifold system with a manifold length of 1 m and with 10 orifices was selected. The simulation was done for different flow rates at the entrance (0.12, 0.14, 0.16, 0.18 and 0.20 kg/s), manifold diameters (0.020, 0.025, 0.030 and 0.035 m), orifice diameters (0.00318, 0.004, 0.00476, 0.005 and 0.00525 m) and consistency coefficients (0.3, 0.7, 1.0, 1.4 and 3.0 Pa s<sup>n</sup>). Figures 33, 34, 35 and 36 show the simulation values of the flow rate in each particular orifice.

When the flow rate at the entrance is 0.2 kg/s, the difference between the flow rate in the first orifice and the last orifice is larger than for the case when the flow rate at the entrance is 0.12 kg/s (Figure 33). This means that when everything is constant and the flow rate at the entrance decreases the flow rate value for each orifice tend to be closer. This behavior is due to the energy loss due to the friction along the manifold which decreases when the flow rate









at the entrance is lower and, therefore, the pressure in the manifold tends to be constant. It is almost impossible to have a uniform flow distribution by decreasing the flow rate at the entrance (Figure 33). It is important to notice that the pressure at the entrance changed along with the flow rate at the entrance because there is a equilibrium between parameters that is required for any simulation.

In Figure 34, the orifice diameter was varied while everything was kept constant. When the orifice diameter decreases the orifice flow rate tend to constant value. Hence, it may be possible to obtain a uniform manifold distribution by decreasing the orifice diameter. The same pattern is found in Figure 35 where the fluid consistency coefficient took different values. When the fluid consistency coefficient is 0.3 Pa s<sup>n</sup> the difference between the flow rate in the first orifice with the last orifice is less than that found when the fluid consistency coefficient is 3.0 Pa s<sup>n</sup>. This behavior is present because the more viscous fluid produces higher energy loss due to friction causing the pressure along the manifold decrease rapidly. We can conclude that using water (less viscous fluid) it would be possible to obtain almost a uniform flow distribution in a manifold with these characteristics.

Figure 36 shows the simulated orifice flow rates when the manifold diameter was varied and everything was kept constant. When the manifold diameter is increased the difference between the flow rate in the first orifice and the last one is decreased. This means that manifold flow distribution tends to be uniform when the manifold diameter is increased. This is because the energy loss due to the friction is related to the surface area (diameter) of the manifold and when the manifold diameter is increased the surface area increases and, therefore, the energy loss due to the friction is decreased.

# 5.8 Strategies for Achieving Uniform Flow.

The strategies consist of developing the necessary conditions to insure that static pressure remains constant along the entire length of the manifold which will insure a uniform flow distribution from the manifold. It must be noted that the pressure drop is due to friction losses from flow through the pipe and the orifice; therefore, pressure drop is related to the orifice diameter, pipe diameter, space between orifices, and fluid properties (consistency coefficient and flow behavior index).

means, such as increasing the pipe diameter to have less pressure drop due to friction, decreasing the orifice diameter or both. The fluid properties play a very important role in the uniformity of the flow from a manifold. When the fluid has a high consistency coefficient, the pressure drop in the pipe and in the orifice is larger and the static pressure is significantly decreased. In some cases this static pressure can be zero (no flow in the orifice). If one have a very viscous fluid (power-law model) and the orifices are the same size, uniform flow distribution can be accomplish by increasing the pipe diameter and decreasing the flow rate at the entrance.

According to Dow (1950), uniform distribution in the manifold is achieved when the necessary conditions to insure that the pressure drop due to friction losses from flow through the pipe and the orifice are exactly balanced by the pressure due to the deceleration of the flow in the pipe which necessarily occurs when part of the fluid escapes through the orifices. Wu and Gitlin (1974) said that if the pressure distribution along the pipe can be determined, uniform flow can be achieved by adjusting size of the orifices, length and size of

the microtube (a special type of emitter) and slightly adjusting the spacing between orifices. The microtube idea may have excellent potential for fluid foods.

#### 6. SUMMARY AND CONCLUSIONS.

- 1. A laboratory manifold system was successfully designed and tested in the collection of the fluid flow rate at each orifice for different orifice diameters, pipe diameters and fluid properties (consistency coefficient, flow behavior index and density).
- 2. The rheological properties of the non-Newtonian fluid (consistency coefficient and flow behavior index) and the orifice diameter affect the orifice discharge coefficient. The orifice discharge coefficient for a non-Newtonian fluid is in the range of 0 - 0.5.
- A mathematical expression that correlate the orifice discharge coefficient with generalized Reynolds number of the fluid in the orifice was obtained.
- 4. The pressure calculated by means of the mechanical energy balance is higher than the experimental pressure, therefore it is necessary to include a parameter that accounts for energy loss due to turbulence at the orifice. Calculated values indicate that the energy loss coefficients due to turbulence increase significantly for decreasing values of the generalized Reynolds number.
- 5. Using the theoretical model developed, it is possible to determine a correction factor for the orifice discharge coefficient and also the corrected orifice discharge coefficient for the flow distribution from a manifold. This corrected orifice discharge coefficient (C') can be expressed as a function of the generalized Reynolds number

for the fluid in the orifice.

- 6. The theoretical model developed for the manifold in conjunction with the mathematical model for corrected orifice discharge coefficient simulate the fluid flow rate distribution from a manifold under the conditions studied.
- 7. The use of the simulation model for less viscous fluids (5% starch solution) caused significant errors in the flow distribution from the manifold due to the experimental error in the determination of the flow rate in the orifice and the pressure, the effect of the consistency coefficient in the correct orifice discharge coefficient and the system complexity due to large number of interactive variables presented.

## 7. SUGGESTIONS FOR FUTURE RESEARCH.

- 1. Investigate the importance of energy loss due to turbulence at the orifice by measuring the pressure drop at each orifice and comparing this with the pressure calculated by means of the mechanical energy balance equation.
- Validate the theoretical model developed in this study for a non-Newtonian fluid having a yield stress, i.e.
   Herschel-Bulkley or Bingham plastic materials.
- 3. Investigate the effect of the flow behavior index on the orifice discharge coefficient for a non-Newtonian fluid.
- 4. Evaluate the theoretical model developed in this research to network systems using non-Newtonian fluids.

### 8. REFERENCES

Bird, R. B., Armtrong, R. C. and Hassanger O. 1987. "Dynamics of Polymeric Liquids.". Vol 1. Wiley-Interscience Publication. John Wiley and Sons, New York, NY.

Bralts, V. 1983. Hydraulic design and field evaluation of drip irrigation submain units. Ph. D. Thesis, Michigan State University, East Lansing, MI.

Dow, W. M. 1950. The uniform distribution of a fluid flowing through a perforated pipe. J. of Appl. Mech. 431 -438.

Eskinazi, S. 1962. "Principles of Fluid Mechanics." Allyn and Bacon, Inc., Boston.

Garcia, E. J. and Steffe, J. F. 1986. Optimum economic pipe diameter for pumping Herschel-Bulkley fluids in a laminar flow. J. of Food Process Eng. 8, 117-136.

Garcia, E. J. 1985. Optimum economic tube diameter for pumping

Herschel-Bulkley fluids, M.S. Thesis. Michigan State University, East

Lansing, MI.

Govier, G. W. and Aziz, K. 1972. "The Flow of Complex Mixtures in Pipe." Van Nostrannd Reinhold Co., New York, NY.

Hanks, R. W. 1978. Low Reynolds number turbulent pipeline flow of pseudohomogeneous slurries. In Proceedings of the Fifth International Conference on the Hydraulic Transport of Solids in Pipe.

(Hydrotransport) May 8-11 Paper C2 p. C2-23 to C2-34. Hannover, Federal Republic of Germany. BHRA Fluid Engineering, Cranfild, Bedford, England.

Hanks, R. W. and Ricks, B. L. 1974. Laminar turbulent transition in flow of pseudoplastics fluid with yield stress. J. Hydronautic 8(4):163-166.

Hanks, R. W. 1969. A theory of laminar flow stability. AIChE Journal 15(1):25-27.

Keller, J. D. 1949. The manifold problem. J. of Appl. Mech. 16, 77-85. Krieger, I. M. 1968. Shear rate in the Couette viscometer. Trans. of the Soc. of Rheology 12(1):5-11.

Osorio, F. and Steffe, J. F. 1984. Kinetic energy calculation for non-Newtonian fluids in circular tubes. J. of Food Sci. 49(5):1295-1296, 1315.

Perry, R. H. and Chilton, C. H. 1963. "Chemical Engineers' Handbook."

MacGraw-Hill Book Co., New York, NY

Ramirez-Guzman, H. and Manges, H. 1971. Uniform flow from orifices in irrigation pipe. Transactions of the ASAE. 14(1):127-129.

Segerlind, L., Steffe, J. F. and Bralts, V. 1985. Network analysis for

non-Newtonian fluid foods. ASAE paper No 83-6005. Am. Soc. Agr. Eng., St. Joseph, Michigan.

Skelland, A. H. P. 1967. "Non-Newtonian Flow and Heat Transfer". John Wiley and Sons, Inc., New York, NY.

Steffe, J. F., Mohamed, I. O. and Ford, E. W. 1984. Pressure drop acrooss valves and fittings for pseudoplastic fluids in laminar flow. Transactions of the ASAE. 27(2):616-619.

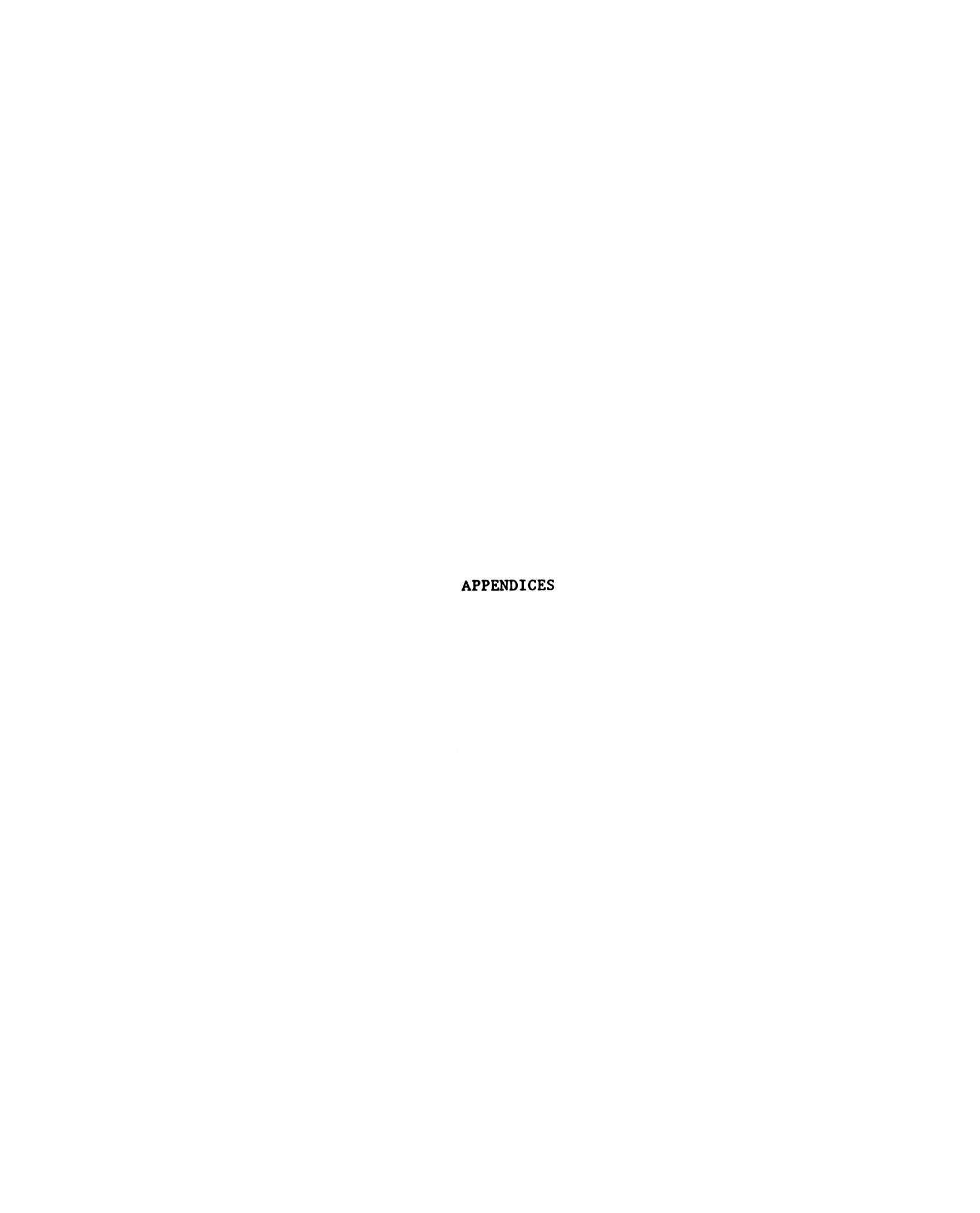
Steffe, J. F. and Ford, E. 1985. Rheological techniques to evaluate the shelf-stability of starch-thickened strained apricots. J. of Texture Studies 16, 179-192.

Steffe, J. F. and Morgan, R. G. 1986. Pipeline design and pump selection for non-Newtonian fluid foods. Food Technology 40(12):78-85.

Whorlow, R. W. 1980. "Rheological Techniques," Halstead Press, New York, NY.

Wood, I. and Charles, C. 1972. Hydraulic network analysis using linear theory. J. Hydraulic Div. Am. Soc. Civ. Eng. 98, 1157-1170.

Wu, I. and Gitlin, H. M. 1974. Drip irrigation design based on uniformity. Transactions of the ASAE 17(3):429-432.



### APPENDIX A

Pressure and Fluid Flow Rate in the Orifice for 5, 7.5 and 10% Corn Starch Solutions and Different Orifice Diameters

Table Al. Pressure and fluid flow rate in the orifice for a 5% starch solution and different orifice diameters

Experiment: Starch solution at 23°C 1010 kg/m<sup>3</sup> Density: 0.8

Flow behavior index:

0.105 Pa s<sup>n</sup> Consistency Coefficient:

Orifice Diameter:

0.00318 m.

Pressure Pa	Flow Rate kg/s	Velocity m/s	Orifice Discharge Coefficient	Generalized Reynolds Number
196.2	0.0005	0.07	0.112	23.8
264.9	0.0087	0.08	0.116	29.7
421.8	0.0010	0.12	0.137	48.2
598.5	0.0017	0.21	0.198	92.5
784.9	0.0005	0.07	0.057	24.4
843.7	0.0008	0.11	0.086	42.1
5141.2	0.0103	1.29	0.406	792.5
7260.5	0.0161	2.02	0.533	1351.0
9026.5	0.0186	2.33	0.552	1605.8

Orifice Diameter:

0.00476 m.

Pressure Pa	Flow Rate kg/s	Velocity m/s	Orifice Discharge Coefficient	Generalized Reynolds Number
49.0	0.0006	0.03	0.111	14.1
245.2	0.0028	0.15	0.225	87.3
3924.6	0.0282	1.56	0.562	1378.3
5003.8	0.0323	1.79	0.570	1620.5
6475.5	0.0405	2.25	0.629	2129.3

Orifice Diameter:

0.0079375 m.

Pressure Pa	Flow Rate kg/s	Velocity m/s	Orifice Discharge Coefficient	Generalized Reynolds Number
1667.9	0.0606	1.21	0.668	1524.3
1815.1	0.0632	1.26	0.667	1600.9
2354.7	0.0754	1.50	0.699	1980.4
4120.8	0.0943	1.68	0.690	2262.7

Table A2. Pressure and fluid flow rate in the orifice for a 5% starch solution and different orifice diameters

Experiment: Starch solution at  $23^{\circ}$ C Density:  $1021 \text{ kg/m}^3$ Flow behavior index: 0.77

1.3 Pa s<sup>n</sup> Consistency Coefficient:

Orifice Diameter: 0.00318 m.

Pressure Pa	Flow Rate kg/s	Velocity m/s	Orifice Discharge Coefficient	Generalized Reynolds Number
2256.6	0.0042	0.52	0.249	24.9
2943.4	0.0083	1.03	0.431	57.8
3139.6	0.0104	1.29	0.523	76.2
3532.1	0.0078	0.96	0.367	52.9
5494.4	0.0114	1.41	0.431	84.7
7113.3	0.0151	1.87	0.500	119.2
8192.6	0.0134	1.66	0.416	103.5
8506.2	0.0134	1.66	0.408	103.5
18221.4	0.0139	1.72	0.289	108.1
20047.6	0.0180	2.23	0.356	148.2
20412.8	0.0192	2.38	0.376	160.4

0.00476 m. Orifice Diameter:

Pressure Pa	Flow Rate kg/s	Velocity m/s	Orifice Discharge Coefficient	Generalized Reynolds Number
49.0	0.0018	0.09	0.319	4.3
147.1	0.0006	0.03	0.064	1.2
690.2	0.0023	0.13	0.112	6.1
1079.2	0.0114	0.62	0.432	42.6
1962.3	0.0182	1.00	0.511	75.7
2747.2	0.0149	0.82	0.354	59.3
6533.9	0.0262	1.44	0.403	118.6
7264.4	0.0350	1.92	0.510	169.0
9455.8	0.0272	1.50	0.348	124.3
9821.0	0.0430	2.36	0.539	217.8

Table A2. (Cont'd.)

Orifice Diameter: 0.00794 m.

Pressure Pa	Flow Rate kg/s	Velocity m/s	Orifice Discharge Coefficient	Generalized Reynolds Number
44.1	0.0020	0.04	0.137	2.2
93.2	0.0055	0.10	0.256	7.4
1569.8	0.0435	0.85	0.486	92.1
1717.0	0.0424	0.84	0.458	90.4
3237.7	0.0789	1.56	0.620	193.7
3685.1	0.0697	1.38	0.513	166.2

Table A3. Pressure and fluid flow rate in the orifice for a 10 % starch solution and different orifice diameters

Experiment: Starch solution at  $23^{\circ}$ C Density:  $1034 \text{ kg/m}^3$ Flow behavior index: 0.68

Consistency Coefficient: 4.5 Pa s<sup>n</sup>

Orifice Diameter:

0.00318 m.

Pressure	Flow Rate	Velocity	Orifice Generalized Discharge Reynolds
Pa	kg/s	m/s	Coefficient Number
1344.1	0.0004	0.05	0.035 0.6
10916.7	0.0079	0.96	0.211 24.8
11647.2	0.0100	1.23	0.259 34.0
15153.4	0.0122	1.49	0.275 43.7
20412.8	0.0175	2.14	0.341 70.7

### Orifice Diameter: 0.00476 m.

Pressure Pa	Flow Rate kg/s	Velocity m/s	Orifice Discharge Coefficient	Generalized Reynolds Number
490.5	0.0003	0.019	0.019	0.2
883.0	0.0007	0.041	0.031	0.5
4169.8	0.0067	0.365	0.128	9.0
7064.2	0.0197	1.074	0.290	37.4
9455.8	0.0280	1.522	0.356	59.3
11647.2	0.0353	1.919	0.404	80.4
16030.0	0.0416	2.260	0.405	99.8

### Orifice Diameter:

0.00794 m.

Pressure Pa	Flow Rate kg/s	Velocity m/s	Orifice Discharge Coefficient	Generalized Reynolds Number
461.1	0.003	0.06	0.069	1.3
735.8	0.003	0.06	0.056	1.3
981.1	0.004	0.08	0.063	1.9
1226.4	0.006	0.11	0.077	2.8
2256.6	0.036	0.71	0.342	30.9
3090.6	0.047	0.92	0.379	43.5
4807.6	0.060	1.19	0.390	60.6
6426.5	0.085	1.66	0.472	94.5

# APPENDIX B

Manifold Flow Distribution: Experimental Data

Table B1. Manifold flow distribution for a 5% starch solution

Experiment: Starch solution at 23°C 1010 kg/m<sup>3</sup> Density: Flow behavior index: 0.8

 $0.105 \text{ Pa s}^{n}$ Consistency Coefficient:

0.00318 m. Orifice Diameter:

Pipe Diameter: Orifice Diameter: 0.0158 m. 0.00318 m.

Orifice Number	Mass Flow Rate kg/s	Pressure Pa	Mass Flow Rate kg/s	Pressure Pa
1	0.00805	1363.8	0.01041	2256.6
2	0.00715		0.00910	
3	0.00512		0.00779	
4	0.00501		0.00680	
5	0.00298		0.00585	
6	0.00330		0.00472	
7	0.00246		0.00441	
8	0.00201		0.00244	
9	0.00154		0.00215	
10	0.00056	196.2	0.00089	843.8
Total	0.03820		0.05014	

Pipe Diameter: Orifice Diameter: 0.0158 m. 0.00476 m.

Orifice Number	Mass Flow Rate kg/s	Pressure Pa	Mass Flow Rate kg/s	Pressure Pa
1	0.03333	2904.2	0.02374	1775.0
2	0.02860		0.02009	
3	0.02533		0.01665	
4	0.02113		0.01346	
5	0.01666		0.01055	
6	0.01293		0.00587	
7	0.00986		0.00499	
8	0.00697		0.00296	
9	0.00442		0.00159	
10	0.00283	245.2	0.00632	49.0
Total	0.16210		0.10276	

Table B1. Cont'd.

Pipe Diameter: 0.0158 m. Orifice Diameter: 0.00794 m.

Orifice Number	Mass Flow Rate kg/s	Pressure Pa
1	0.06067	1667.9
2	0.05196	
3	0.04410	
4	0.04456	
5	0.03276	
6	0.02660	
7	0.01454	
8	0.00478	
9	no flow	
10	no flow	0
Total	0.27997	

Table B2. Manifold flow Distribution for a 7.5 % starch solution

Experiment: Starch solution at  $23^{\circ}$ C Density:  $1021 \text{ kg/m}^3$ Flow behavior index: 0.77

Flow behavior index: 0.77

Consistency Coefficient: 1.3 Pa s<sup>n</sup>

Pipe Diameter: 0.0158 m. Orifice Diameter: 0.00318 m.

Orifice Number	Mass Flow Rate kg/s	Pressure Pa	Mass Flow Rate kg/s	Pressure Pa
1	0.02443	13838.8	0.02282	18586.9
2	0.02239		0.02342	
3	0.02170		0.02278	
4	0.01518		0.01953	
5	0.01840		0.01786	
6	0.01242		0.01584	
7	0.01091		0.01336	
8	0.00864		0.01228	
9	0.00692		0.01011	
10	0.00424	2256.7	0.00781	3532.2
Total	0.14526		0.16581	

Pipe Diameter: 0.0158 m. Orifice Diameter: 0.00476 m.

Orifice Number	Mass Flow Rate kg/s	Pressure Pa	Mass Flow Rate kg/s	Pressure Pa
1	0.04181	6279.5	0.05472	11282.1
2	0.02541		0.04255	
3	0.02195		0.03401	
4	0.01335		0.02368	
5	0.00737		0.01700	
6	0.00327		0.00800	
7	0.00136		0.00418	
8	0.00074		0.00196	
9	0.00044		0.00102	
10	0.00018	49.0	0.00063	147.1
Total	0.11589		0.19342	

Table B2. Cont'd.

Pipe Diameter: 0.0158 m. Orifice Diameter: 0.00794 m.

Orifice Number	Mass Flow Rate kg/s	Pressure Pa
1 2 3 4 5 6 7 8	0.10478 0.06844 0.03450 0.00853 0.00172 no flow	3385.0
9 10 Total	0.21797	. 0

Pipe Diameter: 0.0409 m. Orifice Diameter: 0.00318 m.

Orifice Number	Mass Flow Rate kg/s	Pressure Pa	Mass Flow Rate kg/s	Pressure Pa
1	0.01572	6534.0	0.01038	3612.1
2	0.01456		0.01048	
3	0.01592		0.01065	
4	0.01619		0.01059	
5	0.01412		0.01007	
6	0.01605		0.01032	
7	0.01661		0.01001	
8	0.01445		0.01001	
9	0.01394		0.01001	
10	0.01510	7113.4	0.01004	3139.7
	0.15267		0.10259	

Table B2. Cent'd.

Pipe Diameter: 0.0409 m. Orifice Diameter: 0.00476 m.

Orifice Number	Mass Flow Rate kg/s	Pressure Pa	Mass Flow Rate kg/s	Pressure Pa
1 2 3 4 5 6 7 8 9	0.01615 0.01477 0.01190 0.00916 0.01101 0.00858 0.01041 0.00977 0.00875 0.00237 0.10290	1471.7	0.02632 0.02420 0.01970 0.01696 0.02009 0.01643 0.01861 0.01569 0.01626 0.01494 0.18920	3335.9 2747.2

Pipe Diameter: Orifice Diameter: 0.0409 m. 0.0079375 m.

Orifice Number	Mass Flow Rate kg/s	Pressure Pa	Mass Flow Rate kg/s	Pressure Pa
1	0.03645	461.1	0.02580	166.8
2 3	0.03309 0.02916		0.02341 0.01974	
4	0.02916		0.01974	
5	0.01988		0.01328	
6	0.01500		0.00741	
7	0.01152		0.00825	
8	0.00967		0.00606	
9	0.00710		0.00406	
10	0.00554	93.2	0.00204	44.1
Total	0.18686		0.123088	

Table B2. Cont'd.

Pipe Diameter: Orifice Diameter:

0.0525 m. 0.00318 m.

Orifice Number	Mass Flow Rate kg/s	Pressure Pa	Mass Flow Rate kg/s	Pressure Pa
1 2 3 4 5 6 7 8 9	0.01332 0.01139 0.00912 0.01237 0.01188 0.01014 0.01012 0.01015 0.00831 0.01144 0.10828	5438.4	0.00865 0.00859 0.00687 0.00584 0.00644 0.00787 0.00794 0.00807 0.00625 0.00838	3246.9 2943.4

Pipe Diameter: 0.0525 m. Orifice Diameter: 0.00476 m.

Orifice Number	Mass Flow Rate kg/s	Pressure Pa	Mass Flow Rate kg/s	Pressure Pa
1 2 3 4 5 6 7 8 9 10 Total	0.01437 0.01382 0.01341 0.01337 0.01243 0.01320 0.01242 0.01153 0.01192 0.01142 0.12793	1049.8	0.02077 0.01971 0.01956 0.02084 0.02078 0.02012 0.01989 0.01812 0.01846 0.01823 0.19648	1962.3

Table B3. Manifold flow distribution for a 10% starch solution: Experimental results.

Experiment: Starch solution at 23°C Density: 1034 kg/m<sup>3</sup> 0.68

Flow behavior index:

4.5 Pa s<sup>n</sup> Consistency Coefficient:

Pipe Diameter: 0.0158 m. Orifice Diameter: 0.00318 m.

Orifice Number	Mass Flow Rate kg/s	Pressure Pa	Mass Flow Rate kg/s	Pressure Pa
1	0.09575	8275.5	0.01681	15229.8
2	0.00563		0.00709	
3	0.00365		0.00728	
4	0.00320		0.00543	
5	0.03165		0.00359	
6	0.00190		0.00189	
7	0.00075		0.00304	
8	0.00135		0.00272	
9	0.00070		0.00100	
10	0.00071	1344.2	0.00214	n. d.*
Total	0.05911		0.05099	•

Pipe Diameter: 0.0158 m. Orifice Diameter: 0.00476 m.

Orifice Number	Mass Flow Rate kg/s	Pressure Pa	Mass Flow Rate kg/s	Pressure Pa
1 2 3 4 5 6 7 8 9 10 Total	0.04380 0.02596 0.02149 0.01091 0.00523 0.00608 0.00368 0.00240 0.00153 0.00035 0.12144	31954.6 490.5	0.03139 0.03581 0.02868 0.01856 0.00734 0.00718 0.00387 0.00276 0.00980 0.00076 0.14615	24796.0 883.0

<sup>\*</sup> no data.

Table B3. Cont'd.

Pipe Diameter: 0.0158 m.
Orifice Diameter: 0.0079375 m.

Orifice Number	Mass Flow Rate kg/s	Pressure Pa
1 2 3 4 5 6 7	0.10834 0.03924 0.01732 0.00623 0.00263 0.00040 no flow	8725.5
9 10 Total	0.17417	0

Pipe Diameter: 0.0409 m. Orifice Diameter: 0.00318 m.

Orifice Number	Mass Flow Rate kg/s	Pressure Pa	Mass Flow Rate kg/s	Pressure Pa
1 2 3 4 5 6 7 8 9 10 Total	0.01137 0.00875 0.00946 0.00543 0.00526 0.00526 0.00694 0.00724 0.00550 0.00080 0.06995	n. d.*	0.01945 0.01498 0.01480 0.01386 0.00974 0.00856 0.01296 0.00936 0.00595 0.00297 0.11265	16030.3 n. d.*

<sup>\*</sup> no data

Table B3. Cont'd.

Pipe Diameter: 0.0409 m. Orifice Diameter: 0.00476 m.

Orifice Number	Mass Flow Rate kg/s	Pressure Pa	Mass Flow Rate kg/s	Pressure Pa
1	0.01971	7264.5	0.02326	10040.4
2	0.01855		0.02789	
3	0.01782		0.02397	
4	0.01312		0.01463	
5	0.01432		0.01863	
6	0.00890		0.01363	
7	0.01262		0.02026	
8	0.00740		0.01674	
9	0.00269		0.01204	
10	0.00017	6573.8	0.00721	n. d.*
Total	0.11533		0.19888	

Pipe Diameter: 0.0409 m. Orifice Diameter: 0.00794 m.

Orifice Number	Mass Flow Rate kg/s	Pressure Pa	Mass Flow Rate kg/s	Pressure Pa
1	0.02531	470.9	0.03362	1942.7
2	0.01986		0.02630	
3	0.01300		0.01504	
4	0.00874		0.01344	
5	0.00734		0.01273	
6	0.00676		0.01092	
7	0.00644		0.00864	
8	0.00486		0.00808	
9	0.00450		0.00459	
10	0.00337	46.1	0.00470	981.2
Total	0.10022		0.13806	

<sup>\*</sup> no data.

Table B3. Cont'd.

Pipe Diameter: 0.0525 m. Orifice Diameter: 0.00318 m.

Orifice Number	Mass Flow Rate kg/s	Pressure Pa	Mass Flow Rate kg/s	Pressure Pa
1	0.00758	4611.5	0.01256	11647.4
2	0.00709		0.01192	
3	0.00863		0.01042	
4	0.00646		0.01018	
5	0.00652		0.01148	
6	0.00709		0.01138	
7	0.00547		0.00966	
8	0.00521		0.00924	
9	0.00498		0.00938	
10	0.00150	n. d.*	0.00363	n. d.*
Total	0.06055		0.09988	

Pipe Diameter: Orifice Diameter:

0.0525 m. 0.00476 m.

Orifice Number	Mass Flow Rate kg/s	Pressure Pa	Mass Flow Rate kg/s	Pressure Pa
1 2 3 4 5 6 7	0.01298 0.01238 0.00878 0.00800 0.00770 0.00840 0.00859 0.00507	3532.2	0.01908 0.00880 0.01610 0.01400 0.01402 0.01528 0.01243 0.01250	3612.2
9 10 Total	0.00791 0.00672 0.08657	4169.9	0.00446 0.00301 0.11968	7456.8

<sup>\*</sup> no data

Table B3. Cont'd.

Pipe Diameter: 0.0525 m. Orifice Diameter: 0.00794 m.

Orifice Number	Mass Flow Rate kg/s	Pressure Pa	Mass Flow Rate kg/s	Pressure Pa
1	0.01923	7358.4	0.02535	1226.4
2	0.01814		0.02296	
3	0.01171		0.0185	
4	0.00988		0.01206	
5	0.00798		0.01036	
6	0.00705		0.0199	
7	0.00933		0.01106	
8	0.00664		0.00957	
9	0.00669		0.00909	
10	0.00344	735.8	0.00608	245.2

### APPENDIX C

Energy Loss Coefficient Due to Turbulence and the Corrected Orifice Discharge Coefficient for 5, 7.5 and 10% Starch Solutions

Table C1. Results of the energy loss coefficient due to the turbulence and the corrected orifice discharge coefficient for a 5% starch solution.

Manifold Diameter: 0.0518 m. Orifice Diameter: 0.00318 m.

Orif	•						
Num.	Press.	k	Veloc.	С	e	C'	Reo
	Pa	f	m/s				
1 2 3 4 5 6 7 8	1363.8 855.6 758.0 698.6 652.9 616.0 589.9 570.9 560.2	635 74 0 0 0 0 0	1.00 0.89 0.64 0.63 0.37 0.41 0.31 0.25 0.19	0.455 0.437 0.381 0.377 0.279 0.298 0.245 0.210 0.171	1.329 1.544 1.341 1.381 1.132 1.212 1.116 1.064 1.001	0.605 0.675 0.511 0.521 0.316 0.361 0.273 0.223	140.33 121.60 81.45 79.42 42.54 48.09 33.91 26.52 19.37
10	556.4	0	0.07	0.070	1.000	0.070	5.72
1	2256.7	1042	1.29	0.484	1.257	0.608	190.86
2 3	1023.0	26	0.94	0.470	1.679	0.803	129.74
3	900.9	0	0.97	0.450	1.596	0.718	134.78
4	817.6	0	0.53	0.430	1.528	0.657	65.14
5	751.4	0	0.73	0.406	1.453 1.337	0.589	95.70 73.95
7	700.8 663.8	0	0.59 0.55	0.367 0.353	1.328	0.491 0.469	68.15
8	640.7	0	0.33	0.333	1.067	0.260	33.52
6 7 8 9	626.3	ŏ	0.27	0.221	1.037	0.229	28.75
10	620.8	Ŏ	0.11	0.108	1.000	0.108	10.09

Manifold Diameter: 0.0518 m. Orifice Diameter: 0.00476 m.

Orif. Num.	Press.	k	Veloc.	С	e	C'	Reo
	Pa	f	m/s				J
1	2904.2	0	1.86	0.588	1.312	0.771	404.52
2	2280.4	33	1.59	0.584	1.263	0.738	336.61
3	1969.4	9	1.41	0.581	1.224	0.711	291.02
4	1528.6	44	1.18	0.573	1.175	0.673	234.13
5	1109.0	77	0.93	0.554	1.123	0.622	176.08
6	794.7	96	0.72	0.523	1.089	0.569	129.88
7	576.5	120	0.55	0.478	1.074	0.513	93.86
8	381.9	215	0.39	0.407	1.080	0.439	61.89
9	246.8	414	0.25	0.310	1.111	0.344	35.87
10	178.6	509	0.16	0.224	1.142	0.256	21.00

Table Cl. Cont'd.

Manifold Diameter: 0.0518 m. Orifice Diameter: 0.00476 m.

Orif. Num.	Press.	k <sub>f</sub>	Veloc. m/s	С	e	c'	Reo
1	1775.9	0	1.32	0.578	1.213	0.701	269.19
2	1429.3	30	1.12	0.569	1.172	0.668	220.37
3	1108.3	48	0.93	0.554	1.123	0.622	175.91
4	836.4	68	0.75	0.528	1.093	0.577	136.25
5	615.6	97	0.59	0.490	1.076	0.527	101.75
6	319.7	544	0.33	0.370	1.090	0.403	50.33
7	247.5	23	0.28	0.336	1.102	0.370	41.49
8	183.6	607	0.17	0.232	1.141	0.265	22.18
9	136.9	1085	0.09	0.139	1.150	0.159	10.54
10	113.7	3714	0.05	0.060	1.048	0.063	5.03

Manifold Diameter: 0.0518 m.
Orifice Diameter: 0.0079375 m.

Orif. Num.	Press. Pa.	<sup>k</sup> f	Veloc. m/s	С	<b>e</b> ,	C'	Reo
1	1688.0	0	1.21	0.681	0.980	0.667	1366.21
2	1226.6	0	1.04	0.680	0.982	0.667	1266.43
3	871.2	0	0.88	0.680	0.990	0.673	1040.17
4	592.9	0	0.89	0.680	1.208	0.821	1053.20
5	398.8	0	0.66	0.674	1.092	0.736	728.10
6	272.0	0	0.53	0.664	1.087	0.721	567.07
7	209.0	0	0.29	0.591	0.770	0.456	274.70
8	134.2	185	0.10	0.331	0.572	0.189	72.29

Table C2. Results of the energy loss coefficient due to turbulence and the corrected orifice discharge coefficient for a 7.5% starch solution.

Manifold Diameter: 0.0158 m. Orifice Diameter: 0.00318 m.

Orif Num.	Press.	k <sub>f</sub>	Veloc.	С	e	C'	Reo
	Pa.		m/s				
1	13838.8	0	3.01	0.461	1.256	0.577	55.22
2	12443.9	0	2.76	0.459	1.228	0.563	50.23
3	8155.7	490	2.20	0.453	1.220	0.552	37.91
4	6221.8	11	1.87	0.445	1.199	0.533	30.75
5	5042.0	0	1.59	0.434	1.168	0.501	23.34
6	4771.2	0	1.52	0.430	1.158	0.498	23.93
7	4125.1	. 0	1.33	0.417	1.125	0.469	20.36
8	3315.0	104	1.04	0.389	1.064	0.413	15.17
9	2809.6	77	0.85	0.356	1.008	0.359	11.52
10	2171.2	1829	0.53	0.274	0.947	0.259	6.56

Manifold Diameter: 0.0525 m. Orifice Diameter: 0.00318 m.

Orif. Num.	Press.	<sup>k</sup> f	Veloc.	С	e	c <i>'</i>	Reo
	Pa.		m/s				
1	3246.9	0	1.06	0.389	1.077	0.418	15.39
2	3246.9	0	1.05	0.308	1.077	0.418	15.17
3	3246.9	0	0.86	0.355	0.961	0.331	11.94
4	3246.9	0	0.72	0.328	0.884	0.289	9.68
5	3246.9	0	0.80	0.344	0.928	0.319	10.90
6	3246.9	0	0.96	0.375	1.013	0.379	13.64
7	3246.9	0	0.96	0.377	1.019	0.384	13.64
8	3246.9	0	0.98	0.379	1.029	0.389	14.08
9	3246.9	·O	0.79	0.340	0.915	0.311	10.70
10	3246.9	0	1.02	0.384	1.054	0.405	14.73

Table C2. Cont'd

Manifold Diameter: 0.0409 m. Orifice Diameter: 0.00476 m.

Orif Num.	Press.	k <sub>f</sub>	Veloc.	С	e	c'	Reo
	Pa.		m/s				
1	3336.0	0	1.45	0.486	1.163	0.565	30.81
2	3252.2	0	1.33	0.485	1.092	0.530	27.79
3	3101.0	90	1.08	0.484	0.973	0.471	23.58
4	2993.4	0	0.93	0.482	0.900	0.435	20.85
5	2817.3	0	1.11	0.481	0.863	0.415	19.40
6	2726.6	50	0.90	0.479	0.805	0.386	17.36
7	2650.2	0	1.02	0.482	0.885	0.427	20.12
8	2591.1	171	0.86	0.477	0.787	0.371	16.40
9	2548.0	0	0.90	0.479	0.799	0.383	17.10
10	2523.5	970	0.82	0.476	0.750	0.357	15.35

Manifold Diameter: 0.0158 m. Orifice Diameter: 0.00476 m.

Orif	· .						
Num.		${f k_f}$	Veloc.	С	e	C'	$Re_{o}$
	Pa.	_	m/s				
1	6279.5	0	2.29	0.486	1.251	0.608	54.32
2	2207.3	260	1.39	0.486	1.381	0.671	29.38
3	1627.0	0	1.20	0.485	1.420	0.675	24.60
4	610.10	30	0.73	0.470	1.430	0.667	13.30
5	369.0	0	0.54	0.449	1.300	0.642	9.34
6	121.1	0	0.17	0.275	1.092	0.358	2.32
7	101.3	0	0.07	0.143	1.092	0.156	0.85
8	98.9	0	0.04	0.085	1.000	0.085	0.48
9	98.1	0	0.02	0.052	1.000	0.052	0.27
10	97.9	0	0.01	0.022	1.000	0.022	0.18

Table C2. Cont'd.

Manifold Diameter: 0.0525 m. Orifice Diameter: 0.00476 m.

Orif Num.	Press.	k <sub>f</sub>	Veloc.	С	e	C'	Reo
	Pa.		m/s				
1	1079.8	0	0.79	0.474	1.141	0.541	14.84
2	1129.9	0	0.76	0.472	1.092	0.515	14.15
3	1103.6	0	0.74	0.470	1.059	0.499	13.63
4	1103.6	0	0.74	0.470	1.058	0.497	13.58
5	1050.0	830	0.68	0.466	1.016	0.473	12.42
6	1093.5	0	0.73	0.470	1.050	0.494	13.36
7	1050.0	900	0.68	0.466	1.016	0.473	12.40
8	1002.5	1720	0.64	0.461	0.991	0.457	11.32
9	1023.2	0	0.66	0.463	1.000	0.463	11.79
10	997.1	1060	0.63	0.460	0.987	0.454	11.19

Manifold Diameter: 0.0409 m. Orifice Diameter: 0.0079375 m.

Orif. Num.	Press.	<sup>k</sup> f	Veloc. m/s	С	e	C'	Re <sub>o</sub>
1	461.1	0	0.72	0.517	1.467	0.616	19.38
2	710.9	0	0.66	0.514	1.084	0.628	17.44
3	530.0	240	0.58	0.508	1.111	0.626	14.93
4	347.2	520	0.39	0.494	1.137	0.578	9.31
5	257.0	90	0.39	0.476	1.135	0.548	9.08
6	177.3	280	0.30	0.437	1.108	0.470	6.59
7	141.9	0	0.23	0.399	1.076	0.429	4.76
8	124.4	0	0.19	0.366	1.053	0.401	3.84
9	102.0	0	0.14	0.307	1.009	0.335	2.63
10	90.8	0	0.11	0.261	1.000	0.280	1.94

Table C2. Cont'd.

Manifold Diameter: 0.0158 m.
Orifice Diameter: 0.0079375 m.

Orif.	Press.	<sup>k</sup> f	Veloc. m/s	С	e	C'	Re <sub>o</sub>
1	3385.0	0	2.07	0.522	1.544	0.806	71.04
2	2211.0	0	1.36	0.522	1.250	0.653	42.19
3	1114.6	0	0.68	0.515	1.000	0.515	18.24
4	275.6	441	0.17	0.343	0.679	0.235	3.37
5	55.6	2890	0.03	0.101	1.000	0.101	0.44

Table C3. Results of the corrected orifice discharge coefficient for a a 10% starch solution.

Manifold Diameter: 0.0409 m. Orifice Diameter: 0.00318 m.

Orif Num.	-	Flow Rate	Veloc.	С	e	C'	Reo
	Pa.	kg/s	m/s				•
1	10186.5	0.0114	1.39	0.270	1.051	0.284	12.76
2	9984.1	0.0088	1.07	0.230	1.051	0.242	9.35
3	9802.8	0.0095	1.15	0.234	1.064	0.249	10.01
4	9644.5	0.0054	0.66	0.162	0.962	0.156	4.81
5	9500.9	0.0092	1.12	0.237	1.088	0.258	9.62
6	9383.8	0.0053	0.64	0.158	0.969	0.153	4.61
7	9283.2	0.0069	0.85	0.195	1.007	0.196	6.65
8	9206.7	0.0072	0.88	0.201	1.024	0.206	7.04
9	9160.1	0.0055	0.67	0.164	0.989	0.162	4.89
10	9145.2	8000.0	0.10	0.029	0.901	0.026	0.38

Manifold Diameter: 0.0525 m. Orifice Diameter: 0.00318 m.

Orif	•						
Num.	Press.	Flow rate	Veloc.	С	e	C'	${\sf Re}_{\sf o}$
	Pa.	kg/s	m/s				
1	11647.4	0.0126	1.53	0.287	1.123	0.322	14.56
2	11522.9	0.0119	1.45	0.278	1.105	0.307	13.58
3	11410.1	0.0104	1.27	0.257	1.050	0.270	11.37
4	11308.1	0.0102	1.24	0.253	1.047	0.265	11.04
5	11217.3	0.0115	1.40	0.251	1.044	0.262	12.93
6	11138.0	0.0114	1.39	0.247	1.040	0.257	12.78
7	11070.9	0.0097	1.18	0.245	1.038	0.254	10.29
8	11016.9	0.0092	1.13	0.240	1.028	0.247	9.70
9	10977.3	0.0094	1.14	0.239	1.028	0.246	9.90
10	10954.9	0.0036	0.44	0.196	0.943	0.185	2.83

Table C3. Cont'd.

Manifold Diameter: 0.0409 m. Orifice Diameter: 0.00476 m.

Orif. Num.	Press.	Flow Rate	Veloc.	С	e	C'	Reo
	Pa.	kg/s	m/s				-
1	7264.5	0.0197	1.07	0.263	1.010	0.266	12.35
2	6863.4	0.0186	1.01	0.255	1.090	0.278	11.40
3	6494.5	0.0178	0.97	0.247	1.100	0.272	10.81
4	6157.8	0.0131	0.71	0.221	1.070	0.236	7.22
5	5849.3	0.0143	0.78	0.188	1.030	0.194	8.10
6	5564.5	0.0089	0.48	0.176	1.030	0.181	4.33
7	5302.0	0.0126	0.69	0.151	1.200	0.181	6.85
8	5058.6	0.0074	0.40	0.129	1.100	0.142	3.39
9	4831.4	0.0027	0.15	0.052	0.950	0.049	0.89
10	4610.2	0.0002	0.01	0.004	0.950	0.004	0.02

Manifold Diameter: 0.0525 m. Orifice Diameter: 0.00476 m.

Orif. Num.	Press.	Flow Rate	Veloc.	С	e	C′	Reo
	Pa.	kg/s	m/s				
1	3612.2	0.0191	1.04	0.258	1.520	0.392	11.82
2	3475.3	0.0880	4.78	0.148	1.246	0.184	88.95
3	3346.8	0.0161	0.88	0.232	1.485	0.345	9.45
4	3234.0	0.0140	0.76	0.217	1.465	0.318	7.86
5	3136.5	0.0140	0.76	0.211	1.468	0.310	7.87
6	3054.9	0.0153	0.83	0.224	1.528	0.342	8.82
7	2992.3	0.0124	0.68	0.193	1.554	0.300	6.72
8	2947.7	0.0125	0.68	0.194	1.466	0.284	6.77
9	2925.7	0.0045	0.24	0.083	1.232	0.102	1.74
10	2914.8	0.0030	0.16	0.058	1.195	0.069	1.03

Table C3. Cont'd.

Manifold Diameter: 0.0409 m.
Orifice Diameter: 0.0079375 m.

<b>^</b> ~	ŧ	£	
OT	1	т	

Num.	Press. Pa.	Flow Rate kg/s	Veloc. m/s	С	e	C'	Reo
1	1942.7	0.0336	0.66	0.323	1.010	0.326	28.57
2	1639.1	0.0263	0.51	0.284	1.020	0.290	25.14
3	1388.7	0.0150	0.29	0.215	0.940	0.202	12.64
4	1174.9	0.0134	0.26	0.181	0.960	0.174	11.01
5	995.0	0.0127	0.25	0.174	1.030	0.179	10.30
6	847.2	0.0109	0.21	0.154	1.080	0.166	8.53
7	730.7	0.0086	0.17	0.127	1.110	0.141	6.39
8	642.1	0.0081	0.16	0.120	1.170	0.140	5.89
9	584.3	0.0046	0.09	0.073	1.170	0.085	2.94
10	547.9	0.0047	0.09	0.074	1.180	0.087	3.02

Manifold Diameter: 0.0158 m. Orifice Diameter: 0.0079375 m.

#### Orif

Num.	Press.	Flow rate	Veloc.	C	e	C'	Reo
	Pa.	kg/s	m/s				_
1	8725.5	0.1083	2.12	0.434	1.188	0.515	129.78
2	4772.4	0.0392	0.77	0.346	0.730	0.253	33.96
3	2640.0	0.0173	0.34	0.218	0.691	0.151	11.53
4	1598.3	0.0062	0.12	0.096	0.711	0.068	2.99
5	1110.0	0.0026	0.05	0.043	0.779	0.033	0.96
6	985.2	0.0004	0.01	0.007	0.779	0.005	0.08

## APPENDIX D

Listing of the Computer Program Used to Simulate the Manifold Flow Distribution

```
MANIFOLD SYSTEM PROGRAM
 20 '
                          VERSION Sept 1988
                     By Walter F. Salas Valerio
                      Michigan State University
                 Department of Agricultural Egineering
          Language : Basic
    'THIS PROGRAM COMPUTES TTHE FLOW RATE AT EACH ORIFICE FROM A
    'MANIFOLD SYSTEM BASED ON THE CHARACTERISTIC OF THE FLUID (NON-
    'NEWTONIAN FLUID), MAIN PIPE
 30 'AND ORIFICE DIAMETER.
    'THE INPUT VARIABLES REQUIRED ARE: PIPE INSIDE DIAMETER, ORIFICE
     DIA., LENGTH OF THE PIPE. NUMBER OF ORIFICES, FLOW RATE AT THE
     ENTRANCE
 50 'CHARATERISTIC OF THE FLUID (CONSISTENCE COEFFICIENT, FLOW
     BEHAVIORAL INDEX AND DENSITY).
 60 *******************************
 70 CLS
 80 PRINT
100 LOCATE 2, 1: PRINT AH$: PRINT
 110 PRINT "
                       DETERMINATION OF THE DISCHARGE DISTRIBUTION":
 PRINT
                               IN A MANIFOLD SYSTEM": PRINT : PRINT
 120 PRINT "
 130 PRINT "
                            BY WALTER F. SALAS VALERIO": PRINT
 140 LOCATE 24. 1: INPUT "(PREES RETURN TO CONTINUE)". Z$: PRINT
 150 CLS
          MAIN MENU
 160 '
 170 PRINT "
                                       MAIN MENU ": PRINT : PRINT
 180 PRINT "
                              1) INPUT PIPE CHARACTERISTICS": PRINT
 190 PRINT "
                               2) INPUT FLUID CHARACTERISTICS": PRINT
                               3) INPUT EXPERIMENTAL DATA": PRINT
 200 PRINT "
 201 PRINT "
                               4) EXIT OF THIS PROGRAM": PRINT
 210 INPUT "(CHOOSE 1, 2, 3 OR 4)", IMM: PRINT
 211 IF IMM - 1 THEN GOTO 220
 212 IF IMM - 2 THEN GOTO 220
 213 IF IMM - 3 THEN GOTO 220
 214 IF IMM - 4 THEN GOTO 5000
 220 UPR$ - "N / m^2": ULE$ - "m": UVE$ - "m/s": UMF$ - "kg/s": UTE$ - "C": UCC$ - "N s^n / m^2": UDE$ - "kg / m^3": GC - 1: URS$ -
     "1/s": ULG$ - "m": UDI$ - "m": UEE$ - "m": DI$ - "m": ULK$ - "m":
     ULCH$ - "m": RH$ -
 230 UMFQ$ - "kg/s": UEE$ - "m": PR$ - "Pa": Q$ - "kg/s"
 240 CLS
 250 INPUT " FLUID NAME : ", FLNA$: LOCATE 2, 58
 270 PRINT "DATE: ": DATES
 290 PRINT " TEMPERATURE ("; UTE$; ") :";
 310 INPUT " ", TEMP$: LOCATE 3, 58: PRINT "TIME : "; TIME$
 320 PRINT
 340 PRINT " Manifold characteristic (manifold pipe)"
 360 PRINT " Length of the pipe ("; ULG$; ") :", ,
 380 INPUT ULG: LOCATE 6, 43: PRINT USING "######.##": ULG
 400 PRINT " Manifold diameter("; UDI$; ") :",
 420 INPUT UDI: LOCATE 7, 43: PRINT USING "######.###"; UDI
 440 PRINT " Number of orifices :", ,
 460 INPUT UNT: LOCATE 8, 43: PRINT USING "#####"; UNT
```

```
470 PRINT " Distance b. orifice ("; UEE$; ") :",
490 INPUT UEE: LOCATE 9. 43: PRINT USING "##### ###" UEE
500 PRINT
510 PRINT '
530 PRINT " Fluid characteristic "
550 PRINT " Flow behavior index :"
570 INPUT N: LOCATE 13, 43: PRINT USING "######.##"; N
590 PRINT " Consistency coefficient ("; UCC$; ") :";
610 INPUT K: LOCATE 14, 43: PRINT USING "######.###"; K
650 INPUT YS: LOCATE 15, 43: PRINT USING "######.###": YS
670 PRINT " Fluid density ("; UDE$; ") :",
690 INPUT DE: LOCATE 16, 43: PRINT USING "#####, .###"; DE
710 PRINT " Diameter of the orifice ("; ULE$; ") :"
730 INPUT DI: LOCATE 17, 43: PRINT USING "######.###"; DI
760 PRINT " Flow rate at the entrance ("; UMFQ$; ") :"
780 INPUT UMFQ: LOCATE 18, 43: PRINT USING "######.###"; UMFQ
800 PRINT " Pressure at the entrance ("; PR$; ") :", 820 INPUT PR: LOCATE 19, 43: PRINT USING "######.###"; PR
830 CLS
900
910 CLS
930 '
940 PRINT " COMPUTING..."
950 '
960 PRINT "Orifice
                      Ratio
                                Press.
                                            Flow rate
                                                          Total F.R
 E "
970 '
980 PRINT " No
                       (x/L)
                                 (Pa )
                                              Kg /s
                                                             Kg/s "
990 ULG - 1
1260 MAX - 10: ER - .000001: NOROOT - 1: PI - 3.141592
1270 QQ - UMFQ
1280 '*** PRELIMINARIES COMPUTATIONS ***
1290 '*** AREA OF THE PIPE ***
1300 AT = PI * UDI ^ 2 / 4
1310 '
1320 '*** AREA OF THE ORIFICE ***
1330 AP = PI * DI ^{2} / 4
1340 '
1345 ' *** FLUID VELOCITY IN THE ORIFICE ***
1348
1350 GOTO 1390
1360 CLS
1440 ' PE is specific weight in N/m<sup>3</sup>
1450 ' PR is pressure drop in the orifice in N/m^2.
1460 '
1461 '**** FLUID VELOCITY IN THE PIPE *****
     v = UMFQ / (AT * DE):
     **** CALCULATION OF THE ENERGY LOSS DUE TO THE FRICTION *** '
      GOSUB 2230
1465 EFP = 2 * FRI.FAC * v ^ 2 * UEE / UDI
     **** CALCULATION OF THE ENERGY LOSS DUE TO TURBLULENCE *****
      KF = 281.2 * RE ^ (-.97) + 148.4
      EFK - KF * (QQ / (AT * DE)) ^
1466 '*** PRESSURE AT THE ORIFICE *****
     PRP1 = (PRP / DE - EFP - EFK) * DE
1468 '*** FLUID VELOCITY IN THE ORIFICE ****
1469 vv = QQ / (AP * DE)
     *** CALCULATION OF THE C' VALUE ****
```

```
GOSUB 4110
     *** PRESSURE IN THE FIRST ORIFICE ***
      PR - (QQ / (AP * c * DE)) ^ 2 * DE / 2
LOCATE 23, 1: PRINT PR, PRP1, QQ, EFK
      IF PR - PRP1 < 5 THEN GOTO 1490
1470
1480
     QQ = QQ - .0001#: GOTO 1465
1490 PRP - PRP1
1540 '*** CALCULATE THE PRESSURE AT THE NEXT ORIFICES ***
1590 XX = UEE + .1
1610 000 - 00
1630 \ v0 - v
1650 FOR I - 2 TO UNT
1680 '*** MASS BALANCE IN THE ORIFICE ***
1700 v = v0 - QQ / (AT * DE)
1710 ' *** CALCULATION OF THE FRICTION FACTOR ***
1730 GOSUB 2230
1740 '*** CALCULATION OF THE ENERGY LOSS COEFFICIENT ****
1750 ' *** DUE TO TURBULENCE ****
1770 KF = 281.2 * RE ^ (-.97) + 148.4
1820 '*** CALCULATION OF THE ENERGY LOSSES DUE TO FRICTION ***
1840 EFP = 2 * FRI.FAC * UEE * v ^ 2 / UDI
1860 '**** CALCULATION OF THE ENERGY LOSS DUE TO THE TURBULENCE ***
1880 EKF - KF * (QQ / (AT * DE)) ^ 2 / 2
1900 '*** PRESSURE IN THE ORIFICE ***
1920 PRP1 - (PRP / DE - EFP - EFK) * DE
1950 '*** FLOW RATE IN THE NEXT ORIFICE ***
1960 vv = QQ / (AP * DE)
     *** CALCULATE THE CORRECTED ORIFICE DISCHARGE COEFFICIENT ***
1970 GOSUB 4110:
1980 '*** PRESSURE IN THE ORIFICE ***
      PR = (QQ / (DE * c * AP)) ^ 2 * DE
1995
2010 '*** COMPARE THE CALCULATED PRESSURES ****
2040 IF PR - PRP1 < 3 THEN GOTO 2090
2050
      QQ - QQ - .00001
2060
      GOTO 1870
2090
      QQQ = QQQ + QQ
2100
     PRP - PRP1
2110 'LPRINT I+1 .: LPRINT USING "##.###^^^ ":XX/ULG .: LPRINT USING
      "##.##"; PRP,: LPRINT USING "##.##"; QQ,:LPRINT USING
      "#.##";QQQ
2120 LOCATE I + 3, 2: PRINT I: LOCATE I + 3, 10: PRINT USING "# #"; XX
      / ULG, : LOCATE I + 3, 18: PRINT USING "######.#"; PRP, : LOCATE I + 3, 30: PRINT USING "#.###"; QQ,
      LOCATE I + 3, 40: PRINT USING "#.##"; QQQ, : LOCATE I + 3, 50:
      PRINT USING "#.###"; c: LOCATE I + 3, 60: PRINT USING "####.#";
      KF
2140
      XX - XX + UEE
2150
     v0 - v
2170
      NEXT I
      FOR I - 1 TO 500: NEXT I
2190
2220
2230 'SUBROUTINE
2250
     P1 = 1 + 3 * N: P2 = 1 + 2 * N: P3 = 1 + N: P4 = 2 + N
2260
      P5 - 2 / N - 1: P6 - 2 / N + 1: P7 - 2 / N - 2
      P8 - 16800 * SQR(1 / 27) * P4 ^ (P4 / P3) / N
2270
2310 '*** COMPUTE THE GENERALIZED REYNOLDS NUMBER AT ANY POINT ***
     LOCATE 18, 3: PRINT RE, v
RE = 8 * DE * (N / P1) ^ N * (UDI / 2) ^ N * v ^ (2 - N) / (K *
      GC)
```

```
2330 '*** COMPUTE THE GENERALIZED HEDSTROM NUMBER ***
2350 UNI - 2
2360 IF YS - 0 THEN HE - 0: UPR - 0: UPR.CR - 0 ELSE HE - DE * UDI ^ 2
      * (YS / K) '
                   (2 / N) / (YS * GC)
2370
     GOTO 2390
2380 '***COMPUTE THE CRITICAL UNSHEARED PLUG RADIUS THROUGH ITERATION
2390 X0 = 0: X1 = .999: m = 1
2400
     GOSUB 3230
2410
     IF NOROOT - 1 GOTO 2480
2420 LOCATE 14, 1
2430 PRINT " THE CRITICAL UNSHEARED PLUG RADIUS WAS NOT FOUND
                IN THE RANGE"; XO: "TO": X1
2440 PRINT "
               WHAT IS THE NEW RANGE (XO.X1):
                 WARNING: 0 < - x0.x1 < 1 "
              X0 - "; X0
2450 INPUT "
2460 INPUT " X1 - ": X1
2470 NOROOT - 1: GOTO 2400
2480 UPR.CR - X
2490 '*** CALCULATON OF THE FRICTION FACTOR ****
         *** COMPUTE CRITICAL PSI ***
2510 GOSUB 3740
2520 PSI.CR - LF
         *** COMPUTE THE CRITICAL REYNOLDS NUMBER ***
2540 REC1 = 2 * P8 * N ^ 2 * PSI.CR ^ P5
2550 REC2 - P1 ^ 2 * (1 - UPR.CR)
2560 RE.CR - REC1 / REC2
         *** COMPUTE THE CRITICAL FRICTION FACTOR ***
2580 FF.CR - 16 / (RE.CR + PSI.CR)
2590 '
2600 IF RE <> RE.CR GOTO 2660
        *** THE FLOW IS CRITICAL ***
2620 FLW.CON$ - " CRITICAL"
2630 FRI.FAC - FF.CR
2640 UPR - UPR.CR
2650 GOTO 3030
2660 IF RE > RE.CR GOTO 2900
         *** THE FLOW IS LAMINAR ***
2680 FLW.CON$ - " LAMINAR"
         *** COMPUTE THE UNSHEARED PLUG RADIUS TRHOUGH ITERATION ***
2700 IF HE - 0 THEN PSI - 1: GOTO 2860
2710 m - 2: X0 - UPR.CR: X1 - .999
2720 GOSUB 3230
2730 IF NOROOT - 1 GOTO 2800
2740 LOCATE 14, 1
2750 PRINT " THE UNSHEARED PLUG RADIUS WAS NOT FOUND
                 IN THE RANGE"; XO; "TO"; X1
              WHAT IS THE NEW RANGE (X0,X1):
2760 PRINT "
                WARNING: 0 <= X0, X1 < 1 "
             X0 - "; X0
2770 INPUT "
2780 INPUT " X1 - ": X1
2790 NOROOT - 1: GOTO 2720
2800 UPR - X
2820 '*** COMPUTE PSI ***
2830 GOSUB 3740
2840 PSI - LF
      *** COMPUTE THE LAMINAR FRICTION FACTOR ***
2860 FRI.FAC - 16 / (RE * PSI)
2870 GOTO 3030
2880 '*** THE FLOW IS TURBULENT ***
```

```
2900 FLW.CON$ - " TURBULENT"
2910 EO = 16 * (2 * HE) ^ (N / (2 - N)) * (N / P1) ^ <math>(2 * N / (2 - N))
2920 F0 = 2 * YS / (DE * v^2 2): m = 3: X0 = F0 + .00001: X1 = 1
2930 GOSUB 3230
2940 IF NOROOT - 1 GOTO 3010
2950 LOCATE 14, 1
2960 PRINT "
              THE TURBULENT FRICTION FACTOR WAS NOT FOUND
                 IN THE RANGE "; XO; "TO"; X1
               WHAT IS THE NEW RANGE (XO, X1):
2970 PRINT "
                  WARNING: "; F0; " < X0,X1 "
2980 INPUT " X0 - "; X0
2990 INPUT " X1 - "; X1
3000 NOROOT - 1: GOTO 2930
3010 FRI.FAC - X
3020 UPR - EO / FRI.FAC
3030 WSS - FRI.FAC * DE * v ^ 2 / (2 * GC)
3040 WSR - ((WSS / K) * (1 - UPR)) ^ (1 / N)
SUBROUTINE: ROOT FINDING-1. THIS SUBROUTINE IS A COMBINATION OF
                   THE BISECTION AND NEWTON ROOT FINDING ITERAION. THE
3190 '
                   MIDPOINT OF THE INITAL INTERVAL IS USED TO START THE
                   NEWYON ITERATION. THE PROGRAMS CONTINUES WITH THIS
                   METHOD UNTIL THE SOLUTION IS FOUND OR ONE OF THE
3200 '
                   FOLLOWING SITUATIONS OCCURS: THE DERIVATIVE OF THE
                   FUNCTION IS EQUAL TO ZERO; 2- X FALL OUTSIDE THE INTERVAL KNOWN TO CONTAIN THE SOLUTION; 3- THE
3210 '
                   DIFFERENCE IN SUCCESIVE APPROXIMATION DOES NOT
                   DECREASES:
                   4- THE NUMBER OF ITERATION EXCEEDS MAX. IF ANY OF THE
3220 '
                   ABOVE SITUATIONS HAPPEN, THE PROGRAM SWITCHS TO THE
                    BISECTION METHOD TO OBTAIN A SMALLER INTERVAL.
3230 XA - X0: XB - X1
3240 IF XA > XB THEN SWAP XA, XB
3250 X - XA
3260 ON m GOSUB 3640, 3800, 3950
3270 FA - Y
3280 IF FA - 0 THEN RETURN' ROOT HAS BEEN FOUND
3290 X - XB
3300 ON m GOSUB 3640, 3800, 3950
3310 \text{ FB} - Y
3320 IF FB - 0 THEN RETURN' ROOT HAS BEEN FOUND
3330 IF FA * FB > 0 THEN NOROOT - 0: RETURN' ROOT WAS NOT FOUND
3340 \text{ XM} - (\text{XA} + \text{XB}) / 2
3350 OLDDIF = ABS(XA - XB) / 2
3360 X - XM
        *** NEWTON ITERATION ***
3380 FOR J = 1 TO MAX
3390 \text{ OLDX} - X
3400 ON m GOSUB 3680, 3850, 4020
3410 YPRIME - Y
3420 IF YPRIME - 0 THEN GOTO 3510
3430 ON m GOSUB 3640, 3800, 3950
3440 X - X - Y / YPRIME
3450 DIFF = ABS(X - OLDX)
3460 IF DIFF <- ABS(X * ER) THEN RETURN' ROOT HAS BEEN FOUND
3470 IF DIFF >- OLDDIF THEN GOTO 3510
3480 OLDDIFF - DIFF
3490 NEXT
```

```
*** BISECTION ITERATION ***
3510 X - XM
3520 ON m GOSUB 3640, 3800, 3950
3530 \text{ FM} - Y
3540 IF FM = 0 THEN RETURN' ROOT HAS BEEN FOUND
3550 IF FA * FM <- 0 THEN GOTO 3590
3560 XA - XM
3570 FA - FM
3580 GOTO 3600
3590 \text{ XB} - \text{XM}
3600 \text{ XM} - (\text{XA} + \text{XB}) / 2
3610 IF ABS(XA - XB) > ABS(XM * ER) THEN GOTO 3350 ELSE X - XM:
                      RETURN
3220 *******************************
3630 ' FUNCTION SUBROUTINE : CRITICAL UNSHEARED PLUG RADIUS EQUATION
                              WRITEN AS Y-FUNC. (X)-0
3640 Y = HE - P8 * X ^ P5 / (1 - X) ^ P6
3650 RETURN
3660 '*********************************
     FUNCTION SUBROUTINE : DERIVATIVE OF THE CRITICAL UNSHEARED PLUG
                         RADIUS EQUATION WITH RESPECT TO THE
                          CRITICAL
3680 Y1 = (2 - N) * X ^ P7 / (1 - X) ^ P6
3690 Y2 = P4 * X ^ P5 / (1 - X) ^ (2 / N + 2)
3700 Y = -P8 * (Y1 + Y2) / N
3710 RETURN
3730 ' FUNCTION SUBROUTINE : LAMINAR FUNCTION PSI
3740 LF1 - 1 - X
3750 LF2 = 2 * X * LF1 * P1 / P2
3760 LF3 = X ^2 \times P1 / P3
3770 LF = LF1 ^{\circ} P3 ^{\star} (LF1 ^{\circ} 2 + LF2 + LF3) ^{\circ} N
3780 RETURN
3790 *******************************
     FUNCTION SUBROUTINE: UNSHEARED PLUG RADIUS EQUATION WRITEN AS
                    Y=FUNC.(X)=0
3800 GOSUB 3740
3810 Y = RE * X ^{\circ} P5 - 2 * HE * LF ^{\circ} P5 * (N / P1) ^{\circ} 2
3820 RETURN
3830
**********************
         FUNCTION SUBROUTINE: DERIVATIVE OF THE UNSHERED PLUG RADIUS
3840 '
                              EQUATION WITH RESPECT TO THE UNSHEARED
                              PLUG RADIUS
3850 Y1 - 1 - X
3860 Y2 = P1 * P3 * Y1 ^ 2 + 2 * P2 * P1 * Y1 * X + P1 * P2 * P3 * X ^
3870 Y3 = P2 * P3 * Y1 ^ 3 + 2 * P1 * P3 * Y1 ^ 2 * X + P1 * P2 * Y1 *
    X ^ 2
3880 SIGMMA - Y2 / Y3
3890 GOSUB 3740
3900 Y4 - 2 * HE * P5 * (N / P1) ^ 2 * SIGMMA * LF ^ P5
3910 Y5 = P5 * RE * X ^{\circ} P7
3920 Y - Y4 + Y5
3930 RETURN
3940
**********************************
```

FUNCTION SUBROUTINE: FRICTION FACTOR EQUATION FOR TURBULENT FLOW WRITEN AS Y-FUNC.(X)=0

```
3950 Y1 = .45 - 2.75 / N + 1.97 * LOG(1 - EO / X) / N
3960 Y2 = (P1 / (4 * N)) ^ N
3970 Y3 = 1.97 * LOG(RE * Y2 * X ^ (1 - N / 2)) / N
3980 Y - Y1 + Y3 - 1 / SQR(X)
3990 RETURN
4000
******************
4010 'FUNCTION SUBROUTINE : DERIVATIVE OF THE FRICTION FACTOR EQUATION
                         FOR TURBULENT FLOW WITH RESPECT TO THE
                         FRICTION FACTOR
4020 Y1 = 3.94 * E0 * SQR(X) / X + N * (1 - E0 / X)
4030 Y2 = 3.94 * (1 - N / 2) * (1 - E0 / X) * SQR(X)
4040 Y3 = 2 * N * (1 - E0 / X) * X ^ 1.5
4050 Y - (Y1 + Y2) / Y3
4060 RETURN
4070
4080 IF (Q1 - QQQ) > .002 THEN GOTO 1520
*<del>**************************</del>
4100 '
4110 ' FUNCTION SUBROUTINE : CALCULATE THE DISCHARGE COEFFICIENT AT
4120 '
                          THE ORIFICE
4130 REO = (DI ^ N * vv ^ (2 - N) * DE) / (8 ^ (N - 1) * K) * (4 * N /
     (1 + 3 * N))^N
4140 ' CALCULATE THE GENERALIZED REYNOLDS NUMBER IN THE
4150 ' IN THE ORIFICE
4160 ' IF DI - .00318 THEN GOTO 4170
    ' IF DI - .00476 THEN GOTO 4170
4170 c = .59 * (1 - EXP(-.071 * REO)) + .027: GOTO 4220
4220 RETURN
4230
*********************
5000 CLS
5001 FOR III - 1 TO 50
5002 PRINT "
                                        BYE!"
5003 NEXT III
```

5004 SYSTEM